الجمهورية الجزائرية الديمقراطية الشعبية
People's Democratic Republic of Algeria
وزارة التعليم العالي والبحث العلمي
Ministry of Higher Education and Scientific Research
جامعة الشهيد الشيخ العربي التبسي - تبسة

Dissertation

Submitted in partial fulfillment of the requirements for the degree of

Master

Specialty: Materials Engineering
Field: Mechanical Engineering

Influence of Heat Treatment on Recovery and Recrystallization Behavior of Cold Drawn Aluminum Wires

Presented by:

Islem ABBAS

Publicly defended on 08/06/2026 in front of the jury committee composed of

President: Lazhar TORCHANE	Prof	University of Tebessa
Supervisor: Abdallah DIHA	MCA	University of Tebessa
Examiner: Med Tahar HANNACHI	Prof	University of Tebessa

Academic Year: 2025/2026

Dedication



To my beloved parents, the architects of my character and the foundation of every success I have achieved. Your love, sacrifices, and unwavering faith in me have been the light that guided my path. This accomplishment belongs to you as much as it belongs to me. Words will never be enough to express the depth of my gratitude and appreciation.

To my sisters, thank you for being my strength, my shelter, and the only place where I could always be myself. You carried my burdens and celebrated my smallest victories as if they were your own. You are the reason behind my smiles. Having you by my side is life's greatest gift.

To all my friends and colleagues, thank you for your laughter, encouragement, and presence through moments of doubt. You stood by me and reminded me I was never walking this road alone.

To myself, for refusing to give up, for daring to rise every time I fell, and for remembering:

"IF NOT YOU, THEN WHO?"

Acknowledgments

First and foremost, I would like to express my deepest gratitude to **Dr. Abdallah DIHA**, my supervisor, whose guidance, patience, and unwavering support accompanied me throughout every stage of this research. His valuable insights, encouragement, and dedication greatly contributed to the successful completion of this work. I am truly grateful for having had the privilege of learning under his supervision.

I extend my sincere thanks to **Prof. Lazhar TORCHANE** for honoring me by presiding over the jury, and to **Prof. Med Tahar HANNACHI** for kindly accepting to examine this work. I deeply appreciate the time and attention they devoted to evaluate my research.

My sincere thanks also go to **Ms. Amal**, supervisor of the Heat Treatment Laboratory, for her kind assistance and support during the experimental work.

Finally, I wish to thank all the members of the Department of Mechanical Engineering at Cheikh Larbi Tebessi University, whose teaching and support throughout my academic journey have left a lasting mark.

ملخص

تهدف هذه الدراسة إلى تحليل تأثير المعالجة الحرارية على سلوك الاسترجاع وإعادة التبلور في أسلاك الألمنيوم النقي المسحوبة على البارد، المصنّعة من قِبَل المؤسسة الوطنية لصناعة الكوابل (EN.I.CA.B) ببسكرة. تم سحب الأسلاك انطلاقاً من قطر أولي قدره 9.5 مم إلى ثلاثة أقطار نهائية: 5.92 مم، 4.24 مم و3.33 مم، مما يقابل نسب تشوه تبلغ 61.17%، 80.08% و87.72% على التوالي. خُضعت العينات لمعالجتين حراريتين: معالجة استرجاع عند 160 °C لمدة 90 دقيقة، ومعالجة إعادة تبلور عند 290 °C لمدة 60 دقيقة. شملت تقنيات التوصيف اختبارات الشد، وقياسات صلادة فيكرز، والمراقبة بالمجهر الضوئي. أظهرت النتائج أن معالجة الاسترجاع تؤدي إلى انخفاض طفيف في الصلادة مع إعادة ترتيب الانخلاعات دون تغيير البنية الحبيبية، في حين تُفضي معالجة إعادة التبلور إلى انخفاض ملحوظ في المقاومة الميكانيكية وظهور حبيبات جديدة خالية من التشوه، مما يُحسّن ليونة المادة بشكل كبير.

الكلمات المفتاحية: الألمنيوم، السحب على البارد، الاسترجاع، إعادة التبلور، المعالجة الحرارية، الانخلاعات.

Résumé

Ce travail porte sur l'étude de l'influence du traitement thermique sur les phénomènes de restauration et de recristallisation de fils d'aluminium pur tréfilés à froid, produits par l'entreprise nationale de câblerie (EN.I.CA.B) de Biskra. Les fils ont été tréfilés à partir d'un diamètre initial de 9,5 mm jusqu'à trois diamètres finaux: 5,92 mm, 4,24 mm et 3,33 mm, correspondant respectivement à des taux de réduction de 61,17%, 80,08% et 87,72%. Deux traitements thermiques ont été appliqués: un recuit de restauration à 160°C pendant 90 minutes, et un recuit de recristallisation à 290°C pendant 60 minutes. Les techniques de caractérisation employées comprennent les essais de traction, la microdureté Vickers et la microscopie optique. Les résultats montrent que le recuit de restauration entraîne une légère diminution de la dureté par réarrangement des dislocations sans modification de la structure granulaire, tandis que le recuit de recristallisation provoque une chute significative de la résistance mécanique et l'apparition de nouveaux grains équiaxes sans déformation, conduisant à une amélioration notable de la ductilité.

Mots-clés: Aluminium, tréfilage à froid, restauration, recristallisation, traitement thermique, dislocations.

Abstract

This work investigates the influence of heat treatment on the recovery and recrystallisation behaviour of cold-drawn commercially pure aluminum wires, manufactured by the national cable enterprise EN.I.CA.B, Biskra. The wires were cold-drawn from an initial machine wire diameter of 9.5 mm to three final diameters: 5.92 mm, 4.24 mm, and 3.33 mm, corresponding to area reduction ratios of 61.17%, 80.08%, and 87.72%, respectively. Two annealing treatments were applied: a recovery annealing at 160°C for 90 minutes, and a recrystallisation annealing at 290°C for 60 minutes. The characterization techniques employed include tensile testing, Vickers microhardness measurements, and optical microscopy. The results indicate that recovery annealing induces a slight decrease in hardness through dislocation rearrangement and partial annihilation, without altering the grain structure. Recrystallisation annealing, on the other hand, leads to a significant reduction in mechanical strength and the formation of new strain-free equiaxed grains, resulting in a marked improvement in ductility.

Keywords: Aluminum, cold drawing, recovery, recrystallisation, heat treatment, dislocations.

List of Symbol

σ: Stress

ε: Strain / Reduction ratio

Δl: Absolute elongation

l_o: Initial length

R_e: Yield strength

σ_{Uts}: Ultimate tensile strength

A%: Percentage elongation after fracture

Z%: Reduction of area coefficient

E: Young's modulus

σ_y: Elastic limit / Yield point

b: Burger's vector

ρ: Dislocation density

G: Shear modulus

τ: Shear stress

F: Attractive force between dislocations / Drawing force

N: Number of new nuclei per unit time / Nucleation rate

G: Volumetric growth rate / Migration rate

$\bar{R}$: Mean grain size

V: Recrystallization rate

P_{dr}: Driving force for recrystallization

Q_G: Activation energy for grain growth

T_f : Melting temperature

List of Figures

Chapter I

Figure I.1: The principal aluminum alloys.....25
Figure I.2: Schematic stress-strain curve of a metallic material showing the elastic region (0–A–B) and plastic region (B–E). Point B indicates the elastic limit (yield point). The plastic region includes strain hardening (C–D), necking (D–E), and final fracture at point E ..29
Figure I.3: The slip mechanism. 31
Figure I.4: The twinning mechanism.....31
Figure I.5: Edge Dislocation. 32
Figure I.6: Screw Dislocation.....33
Figure I.7: Mixed Dislocation 33
Figure I.8: An indication of how the grain structure change during the cold rolling procedure 36
Figure I.9: An indication of how the grain structure change during the hot rolling procedure 37
Figure I.10: Evolution of dislocation density as a function of deformation at different temperatures (25℃, 200℃, and 250℃). The dislocation density increases with strain, but higher temperatures reduce the accumulation rate due to dynamic recovery.....39
Figure I.11: Principle of wire drawing 41
Figure I.12: Aluminum wire rod 41
Figure I.13: Continuous casting process at ENICAB Biskra 42
Figure I.14: Cross-sectional profile of a typical wire drawing die. 43
Figure I.15: Wire drawing lubrication system.....44
Figure I.16: Single-pass wire drawing device.....45
Figure I.17: Continuous multi-pass wire drawing machine 45
Figure I.18: Accumulation-type multi-Pass wire drawing machine 46
Figure I.19: Multi-pass slip-type wire drawing machine.....46

Chapter II

Figure II.1: Schematic representation of a typical heat treatment cycle, showing the successive stages of heating (A to B), holding (B to C), and cooling (C to D) 56
Figure II.2: Schematic illustration of the three stages of annealing: recovery, recrystallization, and grain growth 57
Figure II.3: An isothermal annealing curve for cold-worked nickel 59
Figure II.4: Deformed Microstructure (a); Recovered Microstructure (b).....60
Figure II.5: Schematic of successive dislocation annihilation mechanisms 61
Figure II.6: Polygonization of a bent single crystal.....62

Figure II.7: Schematics showing dislocation structure changes during recovery, random dislocation tangles through cell structures to sub-grains 63
Figure II.8: Evolution of electrical conductivity of a cold-rolled 1200 aluminum sheet during isothermal annealing at 250℃ as a function of annealing time.....64
Figure II.9: Microstructure and property change during cold-working and annealing (recover, recrystallization and grain growth) of material.....65
Figure II.10: Effect of cold work on recrystallization of aluminum.....70
Figure II.11: Schematic illustration of recrystallization nucleation by sub-grain rotation and coalescence: (a) sub-grains with similar orientation rotate to form a high-angle boundary and a viable nucleus, followed by (b) nucleus growth into the deformed matrix, resulting in a fully recrystallized structure 73
Figure II.12: Sequence of recrystallization in a cold-rolled sample: (a) deformed microstructure, (b) nucleation at shear bands and grain boundaries, (c) grain growth, and (d) fully recrystallized structure 74
Figure II.13: IPF maps of a TWIP steel sample showing the microstructural evolution from (a) 42% cold-rolled, to (b) recovered at 600℃, and partially recrystallized at (c) 700℃, (d) 750℃, (e) 775℃, and (f) 850℃ 75
Figure II.14: Hardness as a function of annealing time for cold-rolled aluminum (99.5% purity, true strain 5.5) at temperatures from 140℃ to 220℃. The arrow indicates the onset of recrystallization 76
Figure II.15: EBSD maps showing continuous recrystallization in Al-0.1 Mg deformed to a strain of 2.6 and then annealed for 1 h at 200℃, 225℃, 250℃ and 300℃ 78
Figure II.16: Grain structures of the 1050 aluminum cold-rolled sheet followed by final annealing 79
Figure II.17: Photomicrographs showing several stages of the recrystallization and grain growth of brass. (a) Cold-worked (33% CW) grain structure. (b) Initial stage of recrystallization after heating for 3 s at 580℃ (1075℉); the very small grains are those that have recrystallized. (c) Partial replacement of cold-worked grains by recrystallized ones (4 s at 580℃). (d) Complete recrystallization (8 s at 580℃). (e) Grain growth after 15 min at 580℃. (f) Grain growth after 10 min at 700℃ (1290℉) 83

Chapter III

Figure III. 1: General view of the wire drawing workshop at EN.I.CA.B, Biskra.....88
Figure III.2: Cold drawing machine at EN.I.CA.B, Biskra. 90
Figure III.3: Nabertherm programmable electric resistance furnace used for heat treatment (Heat Treatment Laboratory, University of Tebessa).....91

Figure III.4: Buehler Metaserv Grinder-Polisher used for mechanical grinding and polishing (Heat treatment Laboratory, University of Tebessa). 92
Figure III.5: (a) grinding papers. (b) diamond polishing compound (6 µm), (Heat Treatment Laboratory, University of Tebessa). 92
Figure III.6: Reagents used for chemical etching: distilled water, nitric acid (HNO_3 65%), hydrochloric acid (HCl 37%), and hydrofluoric acid (HF 40%) (Heat treatment Laboratory, University of Tebessa). 93
Figure III.7: Tensile test specimens of cold-drawn aluminum wires with diameters of 5.92 mm, 4.24 mm, and 3.33 mm (total length: 200 mm). 94
Figure III.8: Universal tensile testing machine (Materials Science Laboratory, University of Tebessa).....94
Figure III.9: KB 250 universal hardness testing machine (Materials Science Laboratory, University of Tebessa). 95
Figure III. 10: Optical microscope (Heat treatment Laboratory, University of Tebessa).....96

Chapter IV

Figure IV. 1: Stress-strain curves of cold-drawn aluminum wires (5.92 mm, and 3.33 mm) before heat treatment. 99
Figure IV. 2: Stress-strain curves of cold-drawn aluminum wires (5.92 mm, 4.24 mm, and 3.33 mm) after recovery annealing at 160°C for 90 minutes. 100
Figure IV. 3: Stress-strain curves of cold-drawn aluminum wires (5.92 mm, 4.24 mm, and 3.33 mm) after recrystallisation annealing at 290°C for 60 minutes. 101
Figure IV. 4: Evolution of ultimate tensile strength as a function of area reduction ratio for all annealing conditions. 102
Figure IV. 5: Vickers hardness indentations on cold-drawn aluminum wire surfaces in the as-drawn condition: (A) 9.5 mm machine wire, (B) 5.92 mm, (C) 4.24 mm, (D) 3.33 mm.103
Figure IV. 6: Evolution of Vickers hardness as a function of area reduction ratio for cold-drawn aluminum wires in the as-drawn condition.....104
Figure IV. 7: Vickers hardness indentations on cold-drawn aluminum wire surfaces after recovery annealing at 160°C for 90 minutes: (A) 5.92 mm, (B) 4.24 mm, (C) 3.33 mm.....105
Figure IV. 8: Evolution of Vickers hardness as a function of area reduction ratio after recovery annealing at 160°C for 90 minutes.....106
Figure IV. 9: Vickers hardness indentations on cold-drawn aluminum wire surfaces after recrystallisation annealing at 290°C for 60 minutes: (A) 5.92 mm, (B) 4.24 mm, (C) 3.33 mm.....107
Figure IV. 10: Evolution of Vickers hardness as a function of area reduction ratio after recrystallisation annealing at 290°C for 60 minutes. 107

Figure IV. 11: Comparative evolution of Vickers hardness as a function of area reduction ratio for all annealing conditions. 108
Figure IV. 12: Optical micrographs of cold-drawn aluminum wire specimens in the as-drawn condition: (A) 9.5 mm machine wire, (B) ε = 61.17%, (C) ε = 80.08%, (D) ε = 87.72%. 109
Figure IV. 13: Optical micrographs of cold-drawn aluminum wire specimens after recovery annealing at 160°C for 90 minutes: (E) ε = 61.17%, (F) ε = 80.08% and (G) ε = 87.72% 110
Figure IV. 14: Optical micrographs of cold-drawn aluminum wire specimens after recrystallisation annealing at 290°C for 60 minutes: (H) ε = 61.17%, (I) ε = 80.08% and (J) ε = 87.72% 111

List of Tables

Chapter I

Table I.1: Properties of pure aluminum (purity 99.990%) 22
Table I.2: The Various Degrees of Purity of Pure Aluminum. 24
Table I.3: Classification of aluminum alloys. 25

Chapter II

Table II.1: Summary of annealing stages for pure aluminum: temperature range, key mechanism, and property changes. 58
Table II.2: Approximate recrystallization temperatures for several metals and alloys 69

Chapter III

Table III.1: Chemical composition of the aluminum wire (wt.%). 89
Table III.2: Physical properties of the aluminum machine wire. 89
Table III.3: Reduction ratios for the studied aluminum wires. 89
Table III.4: Heat treatment conditions applied to the studied wire specimens. 91

Chapter IV

Table IV.1: Tensile properties of cold-drawn aluminum wires in the as-drawn condition. 99
Table IV. 2: Tensile properties of cold-drawn aluminum wires after recovery annealing (160°C / 90 min). 100
Table IV.3: Tensile properties of cold-drawn aluminum wires after recrystallisation annealing (290°C / 60 min). 102
Table IV. 4: Vickers hardness of cold-drawn aluminum wires in the as-drawn condition. 104
Table IV. 5: Vickers hardness of cold-drawn aluminum wires after recovery annealing (160°C / 90 min). 105
Table IV. 6: Vickers hardness of cold-drawn aluminum wires after recrystallisation annealing (290°C / 60 min). 107

Table of Contents

List of Symbol 6
List of Figures 7
List of Tables 11
General Introduction **17**
Chapter I: Generalities on Aluminum & Metal Deformation **19**
Part 1: Generalities on Aluminum **20**
I.1 Introduction 21
I.2 Definition of Aluminum 21
I.3 Production of Aluminum 21
I.4 Mechanical and Physical Properties of Aluminum 22
1.5 Characteristics of Aluminum and Its Alloys 22
I.6 Types and Classification of Aluminum 23
I.6.1 Pure Aluminum 23
I.6.1.1 Commercially purity aluminum (99.5–99.79%): 23
I.6.1.2 High purity aluminum (99.8–99.94%): 24
I.6.2 Aluminum Alloys 24
I.6.2.1 Wrought Aluminum Alloys 24
I.6.2.2 Cast Aluminum Alloys 25
I.7 Application Fields of Aluminum Electrical Wires 25
Part 2: Deformation Processes **27**
I.8 Introduction 28
I.9 Plastic Deformation 28
I.9.1 Elastic and Anelastic Deformation 28
I.9.2 Plastic Deformation 29
I.9.3 Mechanisms of Plastic Deformation 30
I.9.3.1 Slip 30
I.9.3.2 Twinning 31
I.9.4 Dislocations 32
I.9.4.1 Edge Dislocation 32
I.9.4.2 Screw Dislocation 32
I.9.4.3 Mixed Dislocation 33
I.9.4.4 Burgers Vector 33

I.9.4.5 Dislocation Interactions 34
I.9.4.6 Dislocation Climb 34
I.9.4.7 Dislocation Mobility and Deformation 34
I.9.5 Types of Deformation 35
I.9.5.1 Cold Deformation 35
I.9.5.2 Hot Deformation 37
I.9.6 Work Hardening 38
I.9.6.1 Hardening Mechanism 38
I.10 Cold Drawing Process 40
I.10.1 Introduction and Principle 40
I.10.2 Key Elements of Cold Drawing 41
I.10.2.1 The Wire Rod 41
I.10.2.2 The Die 42
I.10.2.3 The Lubricant 43
I.10.3 Wire Drawing Machines 44
I.10.3.1 Single-Pass Machine (Machine Mono-Passe) 45
I.10.3.2 Multi-Pass Machine (Machine Multi-Passe) 45
I.10.3.2.1 Continuous or Direct-Pass Machine 45
I.10.3.2.2 Accumulation Machine 46
I.10.3.2.3 Slip Machine 46
I.10.4 The Drawing Force 47
I.10.5 Drawing Defects 47
I.11 Metallurgical Effects of Cold Drawing 48
I.11.1 Microstructure of Cold-Drawn Wires 48
I.11.2 Deformation Textures 49
I.11.3 Residual Stresses 49
I.11.4 Tensile Behavior of Cold-Drawn Wires 50
I.12 Conclusion 51
Chapter II: Heat Treatment of Metals 54
II.1 Introduction 55
II.2 Heat Treatment 55
II.2.1 Heat Treatment Processes 55
II.3 Principles of Annealing 56
II.3.1 Definition of Annealing 57
II.3.2 Stages of Annealing (Recovery » Recrystallization »Grain growth) 57

II.3.3 Objectives of Annealing 58
II.4 Recovery 59
II.4.1 Definition of Recovery 59
II.4.2 Mechanisms of Recovery 60
II.4.2.1 Dislocation Annihilation 60
II.4.2.2 Polygonization 61
II.4.2.3 Sub-grain Coarsening 62
II.4.3 Effect of Recovery on Mechanical and Physical Properties 63
II.4.3.1 Effect on Electrical Resistivity 63
II.4.3.2 Effect on Mechanical Properties 64
II.4.3.3 Effect on Microstructure 65
II.5 Recrystallization 65
II.5.1 Definition of Recrystallization 65
II.5.2 Conditions for Recrystallization 67
II.5.2.1 Minimum Deformation Requirement 67
II.5.2.2 Temperature and Time 67
II.5.2.3 Degree of Cold Work 69
II.5.2.4 Purity of the Metal 70
II.5.2.5 Original Grain Size 70
II.5.2.6 Temperature of Deformation 71
II.5.3 Laws of Recrystallization 71
II.5.4 Mechanisms of Recrystallization 72
II.5.4.1 Classical Nucleation 72
II.5.4.2 Nucleation Sites 72
II.5.4.3 Strain Induced Boundary Migration (SIBM) 74
II.5.4.4 Growth of Recrystallized Grains 74
II.5.5 Effect of Recrystallization on Properties 75
II.5.5.1 Effect on Mechanical Properties 76
II.5.5.2 Effect on Electrical Conductivity 77
II.5.5.3 Effect on Grain Size 77
II.5.5.4 Effect on Crystallographic Texture 79
II.6 Grain Growth After Recrystallization 79
II.6.1 Definition and Nature of Grain Growth 79
II.6.2 Driving Force for Grain Growth 80
II.6.3 Kinetics of Grain Growth 80
II.6.4 Factors Affecting Grain Growth 81

II.6.4.1 Temperature 81
II.6.4.2 Solutes and Particles 81
II.6.4.3 Specimen Size 82
II.6.4.4 Texture 82
II.6.5 Secondary Recrystallization (Abnormal Grain Growth) 82
II.7 Conclusion 83
Chapter III: Materials & Experimental Methods 87
III.1 Introduction 88
III.2 Material Selection 88
III.3 Sample Preparation 89
III.4 Annealing Treatment 90
III.5 Metallographic Preparation 91
III.5.1 Grinding 92
III.5.2 Polishing 92
III.5.3 Chemical Etching 93
III.6 Characterization Techniques 93
III.6.1 Mechanical Testing 93
III.6.1.1 Tensile Testing 93
III.6.1.2 Microhardness Analysis 95
III.6.2 Optical Microscopy 96
Chapter IV: Results & Discussion 97
IV.1 Introduction 98
IV.2 Mechanical Testing 98
IV.2.1 Tensile Testing 98
IV.2.1.1 As-Drawn Condition 98
IV.2.1.2 Recovery-Annealed Condition 99
IV.2.1.3 Recrystallisation-Annealed Condition 100
IV.2.1.4 Comparative Analysis 102
IV.2.2 Hardness Testing 103
IV.2.2.1 Hardness As-Drawn Wires Condition 103
IV.2.2.2 Hardness of Recovery-Annealed Wires 104
IV.2.2.3 Hardness of Recrystallisation-Annealed Wires 106
IV.2.2.4 Comparative Analysis 108
IV.3 Micrographic Analysis 108
IV.3.1 As-Drawn Condition 108

IV.3.2 Effect of Recovery Annealing 110
IV.3.3 Effect of Recrystallisation Annealing 111
IV.4 Conclusion 112
General Conclusion **113**

General Introduction

Aluminum is the most abundant metallic element in nature and ranks as the second widely used metal after steel. Its characteristics of low density, good mechanical strength, high corrosion resistance, and its formability makes it an essential material that is widely used in industrial applications. One of the most challenging applications is the production of aluminum electrical wires. Its mechanical and physical properties require specific control [1-2].

The national enterprise of cable manufacturing EN.I.CA.B, located in Biskra, Algeria, centres its production on aluminum wires for electrical applications. A cold-drawing process is followed to form the wires. Pulling the wire rods through calibrated dies, diminishes the cross-section of it and introduces crucial plastic deformation. Cold drawing leads to a growth in dislocation density, work hardening, and the build-up the stored material's elastic energy. As a result, there will be an increase in tensile strength and hardness, with a reduction in ductility and electrical conductivity [3-4].

A heat treatment, which is known as annealing, is applied to reconstruct the initial properties and microstructure of the material. These properties were infused within the material before the cold deformation. Three successive and overlapping patterns occur during the process of annealing: recovery, recrystallisation, and grain growth. First, recovery involves the rearrangement and annihilation of dislocations without the migration of high-angle grain boundaries, which leads to a fractional resetting of the physical properties. The second phase is recrystallisation, which produces a thorough restructuring of the deformed microstructure. This happens through the genesis and expansion of new strain-free grains. A major reinstatement of the mechanical properties is driven by accumulated energy of deformation. The final pattern is the grain growth. The grain enlargement may take place if the annealing temperature is adequately high or the dwell time is extended enough [5-6].

the recovery and recrystallisation of the cold-drawn aluminum wire is important not only scientifically but also industrially. A well-examined relationship between the cold-drawing variables, the annealing conditions, and the evolving microstructural and mechanical results is essential for maximising production yields at EN.I.CA.B to ensure the efficiency of the aluminum wires in service.

This dissertation aims at investigating the influence of heat treatment on the recovery and recrystallisation of the commercially pure cold-drawn aluminum wires produced by EN.I.CA.B enterprise in Biskra. The wires were cold-drawn from an initial diameter of 9.5 mm to three final diameters: 5.92 mm, 4.24 mm, and 3.33 mm, equivalent to a reduction in area ratios of 61.17%, 80.08%, and 87.72% respectively. Two annealing conditions were employed: recovery treatment at 160°C for about 90 minutes and recrystallization treatment at 290°C for 60 minutes. The empirical characterisation revolves around optical microscopy, Vickers hardness testing and tensile testing, all conducted at Cheikh Larbi Tebessi University in Tebessa.

This research is organised in four chapters:

The first chapter outlines a comprehensive literature review covering the aluminum properties and classifications along its alloys. It also includes a thorough analysis of the cold wire drawing process, including the plastic deformation mechanisms, the core components of the drawing process, the wire drawing machines, the drawing force, and the metallurgical effects of cold drawing on the aluminum wires, microstructure and properties.

The second chapter sheds light on the heat treatment of metals, with a special focus on annealing and its three progressive mechanisms: recovery, recrystallisation, and grain growth. This chapter investigates the underlying mechanisms, governing conditions, the definitions and effects on the mechanical and physical properties of the materials.

The third chapter explores the material description, the cold drawing conditions, the procedures of the heat treatment, the experimental characterisation techniques, namely, metallographic preparation, optical microscopy, Vickers hardness testing and tensile testing.

The fourth chapter discusses the experimental findings from the characterisation techniques. It highlights the evolution of microstructure and mechanical properties as a function of wire diameter and annealing condition. It interprets the results of the recovery and recrystallisation phases of cold-drawn commercially pure aluminum wires.

This dissertation summarises the principal findings of the study and outlines perspectives for future research.

Chapter I: Generalities on Aluminum & Metal Deformation

Part 1: Generalities on Aluminum

I.1 Introduction

Aluminum is a material that has experienced many changes from the point of view of mechanical properties in recent years. Indeed, the development of research has led to the appearance of new aluminum alloys adapted to numerous special applications. This is the reason why this light metal finds its application in fields where it still seemed unsuitable a few years ago.

Aluminum and its alloys are present in the most varied forms, practically in all markets or fields of application.

Pure aluminum has very low mechanical properties, insufficient for its use in many applications.

For a long time, metallurgists have shown that by adding certain elements to aluminum, its properties change and that certain additions tend to increase, through different processes, their mechanical, electrical and structural properties.

One can consider that today, researchers have sufficient elements to obtain an optimal microstructure meeting precise requirements. This essentially depends on the addition to the aluminum matrix.

I.2 Definition of Aluminum

Aluminum is the most abundant metallic element in nature and ranks second among the most widely used metals after steel. It is characterized by its low density, good mechanical strength, ease of machining, economic viability, and high resistance to corrosion. Aluminum is a silvery-white metal with a slight bluish tint and can easily obtain a high-quality polished surface finish [1,6].

I.3 Production of Aluminum

Aluminum is currently produced worldwide by the process developed by Héroult and Hall in 1886, which consists of the electrolysis of alumina dissolved in molten cryolite at approximately 1000 °C, in a cell having an internal lining of carbon-cathode. The aluminum formed by electrolysis deposits at the bottom of the cell, and the oxygen from the alumina reacts with the carbon of the anode to form carbon monoxide and carbon dioxide gas [2].

I.4 Mechanical and Physical Properties of Aluminum

Aluminum is a Group III element with an atomic number of 13 and an atomic mass of 26.98 g/mol. It adopts a face-centred cubic (FCC) crystal structure with a lattice parameter of approximately 0.404 nm, a density of 2.7 g/cm³, and a melting point of around 660 °C. Its Young's modulus is approximately 69 GPa, and it exhibits a linear thermal expansion coefficient of 23×10^{-6} K^{-1}.

Commercially pure aluminum typically contains up to 0.5 wt.% of impurities, predominantly iron (Fe) and silicon (Si), which measurably affect its physical, mechanical, and chemical behaviour. Higher purity grades (≥ 99.99%) can be obtained via electrolytic refining. The properties of aluminum may be further enhanced through mechanical processing, heat treatment, or alloying with elements such as magnesium (Mg), silicon (Si), and manganese (Mn). Under ambient conditions, aluminum spontaneously develops a thin, adherent alumina (Al_2O_3) surface layer that confers excellent resistance to chemical corrosion and mechanical degradation [3,6].

Table I.1: Properties of pure aluminum (purity 99.990%) [3][6].

Symbol	Al
Atomic number	13
Atomic mass	26.98 g/mol
Melting point	660 °C
Boling point	2480 °C
Modulus of elasticity	10×10^6 lb/in^2
Crystallizes	Face-centered cubic (FCC)
Density at 20 °C	2.7 g/cm³
Young's modulus	69 GPa
Thermal expansion	23.86×10^{-6} K^{-1}
Tensile strength	80 to 100 MPa
Electrical resistance	$2{,}7\times10^{-8}$ Ω.m
Electrical resistivity at 20 °C	2.63 μΩ.cm

1.5 Characteristics of Aluminum and Its Alloys

The development of applications for aluminum and its alloys is explained by several properties, particularly those listed below [4]:

Electrical conductivity: The electrical conductivity of aluminum is approximately Two-thirds that of copper. Aluminum is widely used in connection stations for high voltage overhead power transmission.

Corrosion resistance: Aluminum and its alloys generally have good resistance to atmospheric corrosion, in marine, urban and industrial environments. Aluminum is commonly used by architects. While offering numerous possibilities for shapes and surface treatments, aluminum building structures resist well over time. This good corrosion resistance combined with its low density has allowed extensive development for applications in construction.

Lightness: This is the primary advantage of aluminum. It is the lightest of all common metals, with a density of 2.7 g/cm³, which is three times less than that of iron.

Thermal conductivity: Pure aluminum has excellent thermal conductivity, approximately 60% that copper. Applications of aluminum heat exchangers are very numerous: solar energy, automobiles, seawater desalination, etc.

Diversity of aluminum alloys: Aluminum alloys are very numerous and varied in terms of their composition, properties and uses.

Ease of processing: Aluminum alloys are well suited to assembly techniques such as welding, bolting, riveting, bonding, etc.

I.6 Types and Classification of Aluminum

Aluminum is commercially available in different forms depending on its purity level and alloying composition. It can be broadly classified into pure aluminum and alloys, each having distinct mechanical and physical characteristics [5].

I.6.1 Pure Aluminum

Aluminum of 99.0% or higher has many applications, especially in the electrical and chemical fields. These grades of aluminum are characterized by excellent corrosion resistance, high thermal and electrical conductivities, low mechanical properties, and excellent workability.

Pure aluminum is generally categorized according to its purity percentage [5]:

I.6.1.1 Commercially purity aluminum (99.5–99.79%): Commercially pure aluminum highly resistant to chemical attack and weathering. Low cost, ductile for deep drawing,

and easy to weld. Used for high-purity applications such as chemical processing equipment. Also for nameplates, electrical wires, fan blades, sheet metal work, and fin stock.

I.6.1.2 High purity aluminum (99.8–99.94%): High purity aluminum is mainly used in electrical conductors, capacitors, and scientific applications due to its superior conductivity and low impurity content.

Table I.2: The Various Degrees of Purity of Pure Aluminum [6].

Aluminum (%)	Designation	Grade
99.5000 to 99.7900	Commercial purity	A5E to A7
99.8000 to 99.9490	High purity	A8 to A85
99.9500 to 99.9959	Super purity	A95 to A995
99.9960 to 99.9990	Extreme purity	A99
>99.9990	Ultra purity	A999

The mechanical strength of pure aluminum is relatively low compared to alloys; however, it exhibits excellent ductility and formability, which make it ideal for cold working processes such as rolling and drawing.

I.6.2 Aluminum Alloys

To improve the properties of pure aluminum, it is often alloyed with element such as copper (Cu), manganese (Mn), silicon (Si), magnesium (Mg), zinc (Zn), and lithium (Li). Based on their processing method, aluminum alloys are convenient to divide into two major categories [5]:

I.6.2.1 Wrought Aluminum Alloys These alloys are mechanically worked by rolling, extrusion, or drawing. They are designated by a four-digit numbering system:

Table I.3: Classification of aluminum alloys [7].

Series	Designation	Main Alloying Element
1000	1xxx	99% Aluminum
2000	2xxx	Copper (Cu)
3000	3xxx	Manganese (Mn)
4000	4xxx	Silicon (Si)
5000	5xxx	Magnesium (Mg)
6000	6xxx	Magnesium (Mg) and Silicon (Si)
7000	7xxx	Zinc (Zn)
8000	8xxx	Lithium (Li) and others

I.6.2.2 Cast Aluminum Alloys: These are used mainly in casting processes and contain higher alloying content to improve fluidity and castability.

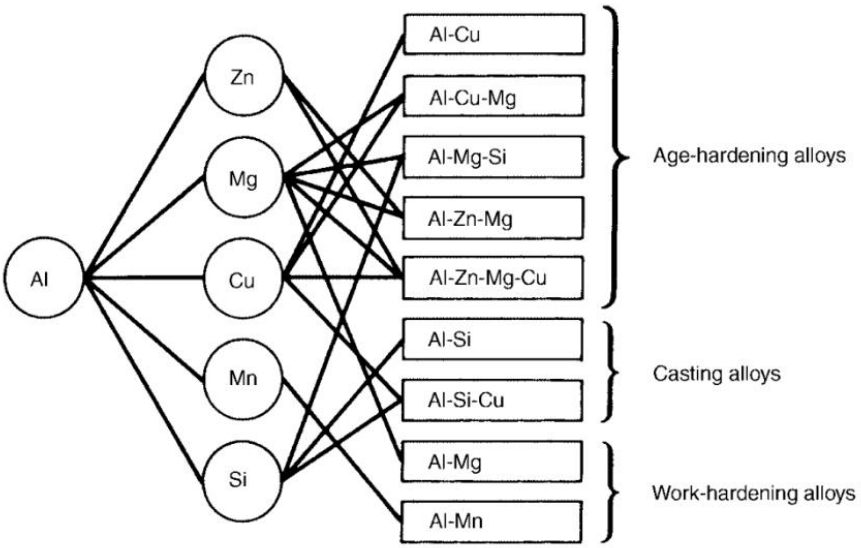


Figure I.1: The principal aluminum alloys [5].

I.7 Application Fields of Aluminum Electrical Wires

Aluminum is widely used in electrical applications due to its excellent electrical conductivity, low density and low cost. The electrical conductivity of pure aluminum is approximately 61% of that of copper on the International Annealed Copper Standard (IACS), which corresponds to about 35.7m/Ω.mm^2 at 20 °C. However, on weight basis, aluminum conducts nearly twice as much electricity as copper, making it advantageous for overhead power transmission cables where weight is a critical factor [6].

The main applications of aluminum in the electrical industry include:

- **Overhead Power Transmission Electrical Cables:** Aluminum cables are used for high-voltage overhead transmission lines, due to their lightweight and cost-effectiveness.
- **Transformer windings:** Aluminum is widely used as winding material in distribution transformers, particularly in regions where copper is expensive or in designs where weight reduction is priority.
- **Bus bars in electrical substations and switchgear:** the ease of fabrication, light weight and great conductivity this combination makes Aluminum a preferred material for solid bus bars used in power distribution systems.
- **Residential and industrial wiring:** in residential wiring Aluminum is used for main power distribution and service entrance cables, in industrial wiring aluminum is extensively used in power distribution systems, heavy duty cables and connections supplying electrical machines.

Despite these advantages, the application of aluminum in electrical systems is not without challenges. One significant limitation is its lower mechanical strength compared to copper. In its annealed condition.

Part 2: Deformation Processes

I.8 Introduction

This chapter addresses the theoretical foundations of cold wire drawing of aluminum, examining both the fundamental deformation mechanisms that govern the behaviour of metallic materials under cold working conditions and the industrial process of wire drawing itself. Cold wire drawing is the principal forming operation applied to aluminum wires in the present study, and a thorough understanding of its underlying physics is essential for interpreting the microstructural and mechanical changes observed following subsequent heat treatment.

The chapter begins with an examination of the mechanisms of plastic deformation, covering elastic and anelastic behaviour, the role of dislocations in mediating plastic flow, slip and twinning as the primary deformation modes, and the distinction between cold and hot deformation. The work hardening phenomenon, which results from the accumulation of dislocations during cold deformation, is then discussed, as it constitutes the principal driving force for the recovery and recrystallization phenomena examined in Chapter III.

The second part of the chapter is devoted to the cold drawing process itself. The principle of wire drawing is presented, followed by a detailed description of the key elements of the process: the wire rod, the die, and the lubricant. The different types of wire drawing machines are then described, along with the drawing force and the principal defects encountered in industrial practice. Finally, the metallurgical effects of cold drawing on aluminum wires are examined, including microstructural evolution, deformation texture, residual stresses, tensile behaviour, and stored energy all of which play a determining role in the response of the drawn wire to subsequent annealing treatments.

I.9 Plastic Deformation

I.9.1 Elastic and Anelastic Deformation

When a solid is subjected to external forces, it responds to this loading by deforming. Deformation is defined as the modification of the dimensions and shape of a substance under the action of applied forces [9]. Two distinct cases must be distinguished:

a) There is no dissipation of energy during the deformation process, meaning that all the energy expended is stored in the solid and is entirely restored when the constraint is removed: the deformation is then said to be elastic [10].

b) There is dissipation of energy during the deformation. The deformation is then said to be anelastic. This is reflected by the fact that the response is delayed relative to the

loading: if an instantaneous constraint is applied, the corresponding elastic deformation is not attained until a certain time has elapsed. It is therefore clear that the anelastic deformation is time-dependent [9].

The elastic deformation does not produce any permanent perceptible modification of structure and properties of the metal; the applied load produces only a relative and perfectly reversible displacement of atoms or pivoting of crystal blocks. In traction of a monocrystal, the atoms move apart from one another, and in compression, they draw closer together [8]. A typical stress-strain curve for a ductile metal is presented in Figure I.2. From 0 to point B, the material deforms elastically, and the deformation is fully reversible. Beyond point B (the elastic limit), the material enters the plastic region (B to E), where permanent deformation occurs. The plastic region includes strain hardening (C–D), necking (D–E), and finally fracture at point E.

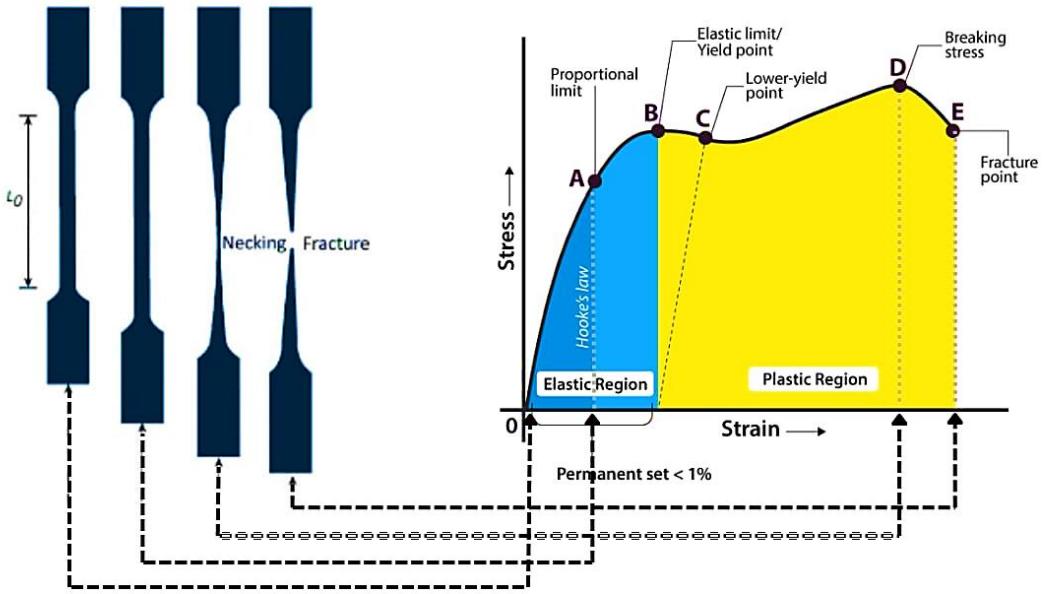


Figure I.2: Schematic stress-strain curve of a metallic material showing the elastic region (0–A–B) and plastic region (B–E). Point B indicates the elastic limit (yield point). The plastic region includes strain hardening (C–D), necking (D–E), and final fracture at point E [17].

I.9.2 Plastic Deformation

The plastic deformation of crystalline bodies can be produced through the movement of topological defects in the crystal arrangement, known as dislocations. These unidimensional perturbations of the arrangement of atoms permit the gliding of crystal planes: like the image of a carpet which is displaced by propagating a fold along its length, it is energetically more favorable for a crystal to deform by creating and propagating dislocations within it. Such a

displacement requires at each step only a few interatomic distances and demands much less effort than an instantaneous and rigid gliding of one half of the crystal over the other [8].

When the tangential constraints exceed a certain threshold (the elastic limit), the deformation becomes irreversible. The suppression of the constraint eliminates only the elastic component of the deformation, while the plastic deformation portion persists [10].

The plastic deformation of metals and alloys introduces into the crystal networks various supplementary defects, dislocations, vacancies, and occasionally twins. The work hardening material is characterized by a very elevated density of dislocation. The deformation leads to a heterogeneity of the microstructure and of the crystallographic texture within the grains [9].

I.9.3 Mechanisms of Plastic Deformation

In crystals, plastic deformation can be produced by slip or twinning with respect to a ratio b, also this mechanism is sensitive to the strain rate. This phenomenon is non-negligible on the metals and must be taken into account for elevated temperatures (T/Tf > 1/2) or for very large ranges of strain rates of deformation [11].

I.9.3.1 Slip

Plastic deformation by slip is the displacement (shear) of individual dislocations on the crystal planes which are filled most densely with atoms (which have the highest reticular density) and are respectively characterized by the largest interplane distances. The slip mechanism is schematically shown in Figure I.3. In F.C.C. metals and alloys, dislocation slip usually occurs on the {111} planes in the ⟨110⟩ directions [11].

Slip systems are defined by a slip plane (characterized by its normal unit vector) and a slip direction contained in that plane. The most direct method is then to measure the grain structure. The slip systems for the F.C.C. structure, as shown in the Table below, involve {111}{110}, which represents the ensemble of the slip plane de glissement system for the F.C.C. structure [12].

The constraint applied (F/S_0) is not a pure traction constraint. The more complex state of constraint which is present consists on one part of a traction (or normal) constraint σ which acts perpendicularly to the glide plane, and on the other part, of a shear constraint τ which acts parallel to this plane. A simple geometric reasoning allows finding that this shear is determined by [12]:

$$\tau = (F/S_0) \cdot \cos\theta \cdot \cos\lambda \qquad [I.1]$$

where S_0 is the cross-section of the specimen, λ the angle formed by the normal to the slip plane and the traction axis, and θ the angle formed by the slip direction and the traction axis.

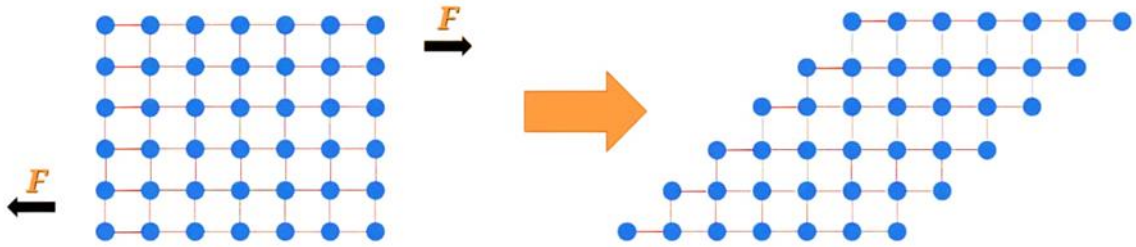


Figure I.3: The slip mechanism [18].

I.9.3.2 Twinning

Twinning is a much more complex deformation mode than slip. In this case, atoms of the materials move in such a manner that the deformed network is transformed and the twin network becomes symmetrical with respect to a twinning plane. Twinning exists as a complementary mode of plastic deformation to slip and this mode exists frequently in F.C.C. metals at temperatures below ordinary temperature [10]. The twinning mechanism is schematically shown in figure I.4.

The difference between deformation by twinning and by slip is that for slip, the orientation above and below the slip plane is the same after slip, while in twinning there is no orientation change across the twin plane. Unlike slip, the atomic movements in twinning are only a fraction of the interatomic spacing, and the shear is uniformly distributed over distinct planes [13].

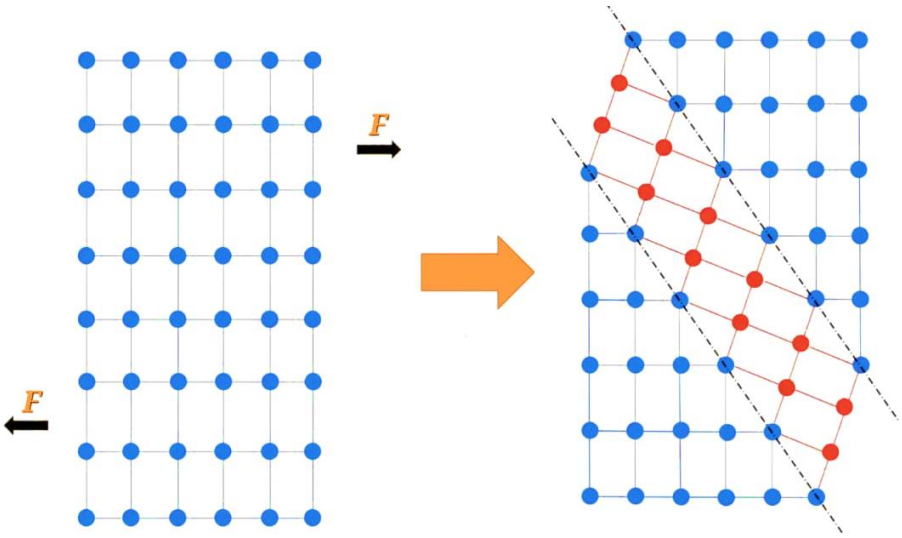


Figure I.4: The twinning mechanism [18].

I.9.4 Dislocations

Dislocations constitute in some sort the vectors of plastic deformation: when they move, the crystal deforms by shearing. The elementary deformation produced by the displacement of a dislocation can be represented by a vector b called the Burgers vector. This vector b is perpendicular to the dislocation line if the dislocation is of the edge type, and parallel to it if it is of the screw type, and mixed in all other cases [8].

The macroscopic constraint necessary to initiate the movement of dislocations is the elastic limit. However, the displacement of a dislocation depends directly on the local constraint, which is the result of the external constraint applied and the internal constraints due to the other defects of the material as well as the thermal agitation [8].

I.9.4.1 Edge Dislocation

An edge dislocation can be imagined as the introduction of a supplementary half-plane inside a perfect crystal. Its location is defined as the extremity of this half-plane. In the region surrounding this line, called the dislocation line, the structure of the crystal lattice is deformed. The dislocation line is perpendicular to the plane of the page [12].

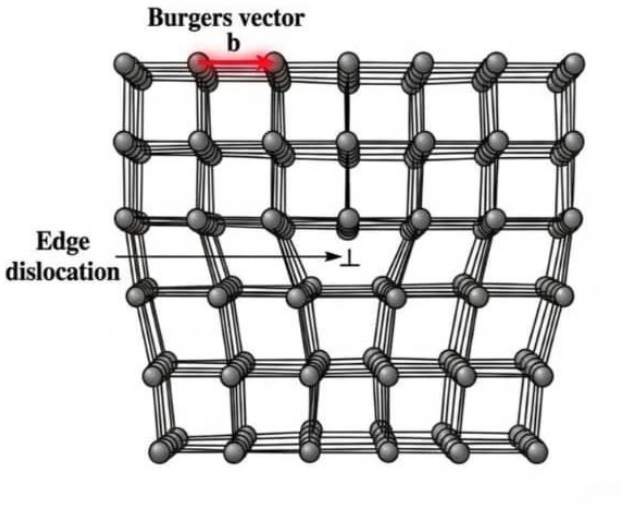


Figure I.5: Edge Dislocation [12].

I.9.4.2 Screw Dislocation

The screw dislocation can be seen as a notch of which one would have offset the edges. Its location corresponds to the extremity of the notch. Like the edge dislocation, one draws a Burgers circuit around the screw dislocation, and the missing vector to close the loop is the Burgers vector [12].

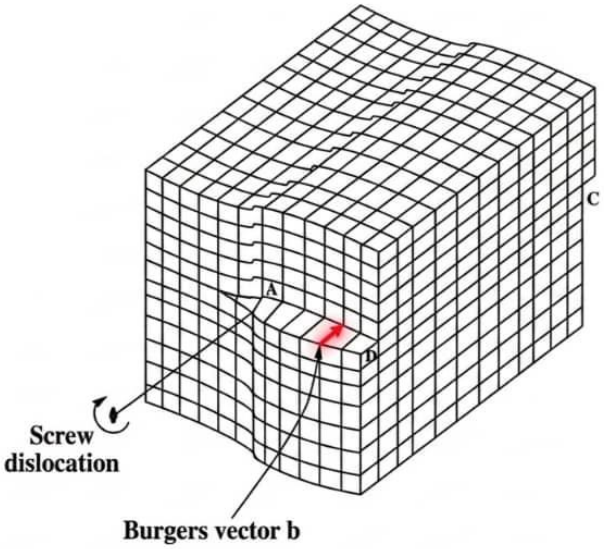


Figure I.6: Screw Dislocation [12].

I.9.4.3 Mixed Dislocation

In reality, dislocations are most often mixed; they may be of the edge type at certain points, and of the screw type at others or both at the same time. The dislocation line is defined by two vectors: the vector t which defines the direction of the line, and the Burgers vector b which specifies the height and the direction of the deformation [8].

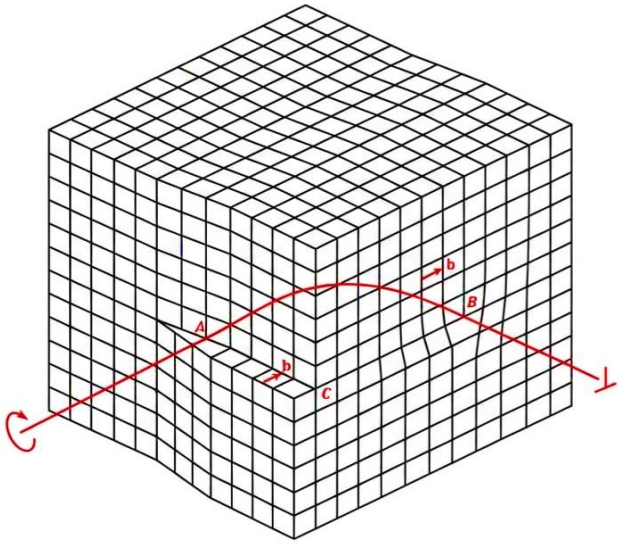


Figure I.7: Mixed Dislocation [13].

I.9.4.4 Burgers Vector

The dislocation is entirely described at each point by two vectors: the vector t which defines the direction of the line and the Burgers vector b which specifies the height and direction of deformation. One can construct the latter by making a Burgers circuit around

the dislocation and then copying this same circuit on a perfect portion of the crystal. The defect of closure of this circuit is filled by the Burgers vector. The Burgers vector is given by [8]:

$$\vec{b} = \oint \frac{\partial \vec{u}}{\partial l} dl \qquad [I.2]$$

I.9.4.5 Dislocation Interactions

The stress and deformation fields surrounding dislocation lines interact in a repulsive or attractive manner. To minimize the total internal energy of the system, two identical dislocations repel one another; two dislocations of opposite signs attract each other [8]:

- Two identical edge dislocations repel each other. If forced together, they may form a dipole, but annihilation only occurs between dislocations of opposite sign.
- Two edge dislocations of opposite signs that attract each other (bringing them closer causes their annihilation and the disappearance of all deformation energy) [8].

The elastic stress fields around dislocation lines also interact with other crystal defects (grain boundaries, precipitates, solute atoms, etc.), creating obstacles to their motion. This is the fundamental mechanism underlying work hardening: as dislocation density increases during plastic deformation, dislocations increasingly impede each other's motion, requiring progressively higher stresses to sustain further deformation [13].

I.9.4.6 Dislocation Climb

In addition to the gliding of a dislocation in a defined plane, another type of movement can be encountered: the climb. Climb is the operation which consists of displacing a dislocation out of its glide plane. The climb of a dislocation is effected by displacement of kinks along its line, by absorption or emission of vacancies. In fact, climb is a thermally activated process and is mainly active during hot loading when diffusion is significant [8].

I.9.4.7 Dislocation Mobility and Deformation

The distinguishing characteristic of dislocations, relative to grain boundaries and other crystalline defects, is that they are inherently mobile. Thus, if a crystal is subjected to stress starting from a defect-free state, a dislocation source can be activated and the defect propagates progressively [9].

Plastic deformation of a volume element is acquired when a dislocation reaches the surface of that element. Dislocations emerging at the surface may originate either from the exterior, traversing the volume from one part to another, or may be internally generated through a dislocation source. Plastic deformation therefore results from the flux of

dislocations across the boundaries of the representative volume element. As long as dislocations have not emerged at the surface, internal stresses exist within the volume element due to the distortion of the crystalline network around the stored mobile dislocations [9].

The macroscopic stress required to initiate dislocation motion is the elastic limit. The displacement of a dislocation depends directly on the local stress (resulting from the external applied stress and the internal stresses arising from other defects in the material) as well as on thermal agitation [8].

Among the various obstacles that can hinder or impede dislocation motion are grain boundaries, precipitates, the solid solution, and so on. It is also advisable to employ materials with complex structures in order to increase their resistance to plastic flow [8].

I.9.5 Types of Deformation

I.9.5.1 Cold Deformation

Cold deformation is that which is carried out at temperatures below the recrystallization temperature [10]. Cold plastic deformation leads to the work hardening of the material, hence to its hardening. This work hardening depends on the chemical composition of the material, the rate of applied deformation, and the conditions of deformation (temperature, strain rate, and deformation mode). In effect, cold deformation causes an important increase in dislocation density (i.e. stored elastic energy) within the material. It ensues a heterogeneity of the microstructure and of the crystallographic texture within the grains [8].

During cold deformation, the microstructure evolves as a function of the deformation rate. At the first stage of deformation, the grains subdivide, change shape, and elongate in the direction of loading. A sub-structure of dislocations appears inside the grains, depending on their crystallographic orientation. The subdivision of grains gives rise to a cellular configuration (blocks of cells) constituted of "walls" with a high dislocation density surrounding volumes with a low dislocation density [10].

When the deformation rate increases, the walls of the cells refine to form sub-joints. his transformation is accompanied by a decrease in the cell size as well as a progressive increase in their disorientation (1° to about 5°). The cell block joints are identified as being the dense dislocation walls (Dense Dislocations Walls DDW) [8]. The characteristic grain elongation during cold deformation is illustrated in figure I.8, where the initially equiaxed grains are transformed into a fibrous structure aligned with the deformation direction.

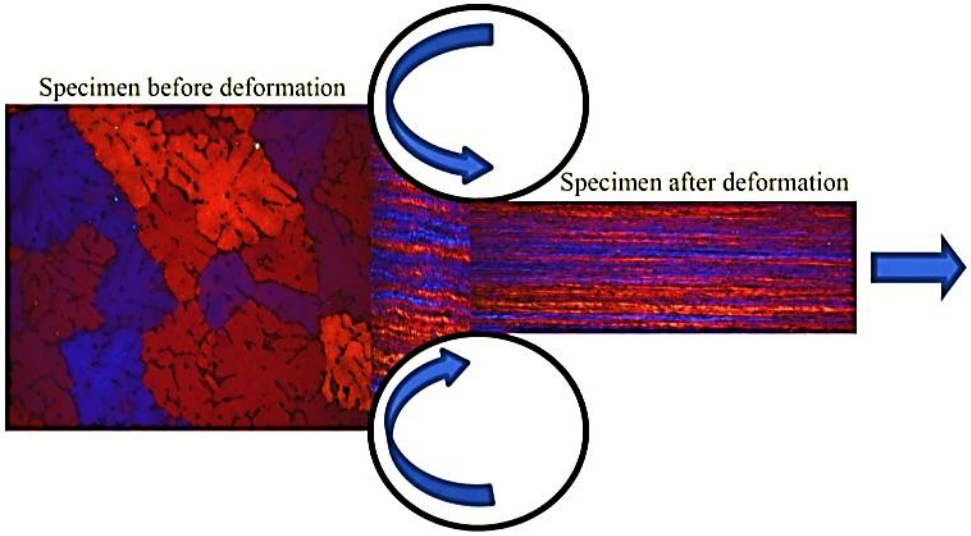


Figure I.8: An indication of how the grain structure change during the cold rolling procedure [19].

For heavy deformations, other forms of microstructural heterogeneity appear:

- **Microbands** composed of dislocation cells of smaller size than the average value of dislocation cells within the same material.
- **Shear bands**, typically oriented at 30° to 40° from the solicitation direction, in the form of elongated bands of thickness 0.1 to 2 μm and length 10 to 100 μm. The localization of deformation in these bands is all the more significant as the temperature and stacking fault energy are low.
- **Transition bands** that separate adjacent zones of strongly disoriented regions of the same grain. They are generally parallel to the principal deformation direction and accommodate misorientations greater than 20° over thicknesses of 1 to 2 μm. Plastic deformation also generates a significant quantity of point defects (vacancies and interstitials), which are largely eliminated either during deformation (dynamic recovery if $T \geq 0.2\ T_f$) or during subsequent annealing even at low temperatures [10].

I.9.5.2 Hot Deformation

Deformation is said to be hot if it is carried out at a temperature above the recrystallization temperature, in order to produce a completely recrystallized structure. At these temperatures, deformation also produces a hardening effect (hot work hardening), partially or completely eliminated by polygonization and recrystallization carried out at treatment temperatures and followed by cooling [10].

At homologous temperatures above 0.4 T_f, plastic deformation is strongly influenced by thermally activated processes so that the flow stress becomes temperature and strain rate dependent (viscoplastic). The processes involved are mostly controlled by local atomic diffusion and give rise to strong dynamic recovery of the dislocation substructure as the dislocations are continuously annihilated during deformation by climb and cross-slip mechanisms [14].

The limits between cold and hot deformation are conventional and depend on the strain rate, the deformation mode, and the treatment temperature, the cooling conditions, as well as the recrystallization rate of the metal [10]. The microstructural change during hot deformation is shown in figure I.9. In contrast to cold deformation, the high temperatures involved activate dynamic recrystallization, which produces a new population of fine, strain-free equiaxed grains.

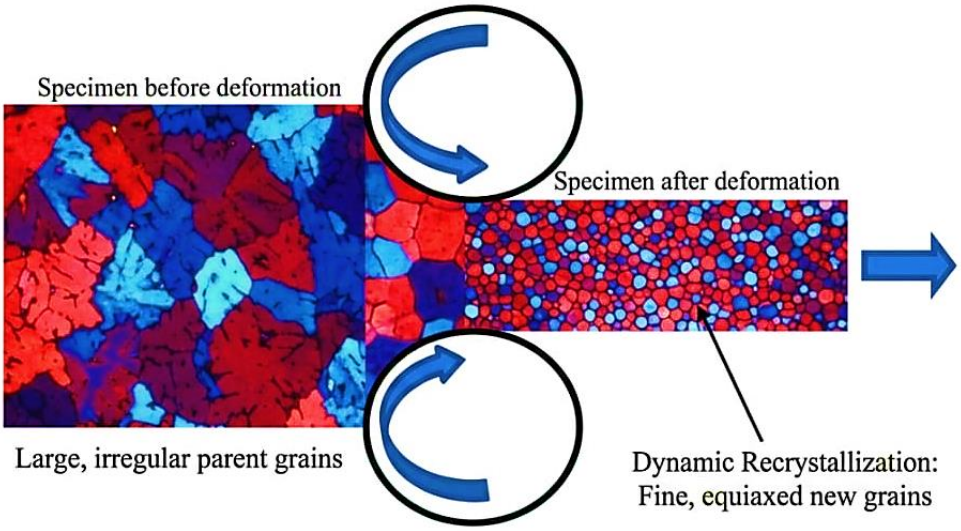


Figure I.9: An indication of how the grain structure change during the hot rolling procedure [19].

I.9.6 Work Hardening

I.9.6.1 Hardening Mechanism

Work hardening is among the most characteristic properties of metallic alloys; it is also the most practically useful since it represents the fundamental mechanism of strengthening metals during loading [14].

When force is applied such that it shears the crystal, dislocations in the slip plane above the dislocation line move to the right, while those in the lower plane move to the left, with the result that the dislocation advances one lattice spacing at a time. Note that only single bonds are broken at any one time, rather than the whole row. The movement is much like that of advancing a carpet along a floor by using a wrinkle that is easily propagated down its length. The stress required to cause plastic deformation is orders of magnitude lower when dislocations are present than in dislocation-free, perfect crystalline structures [13].

It is necessary to facilitate plastic deformation and therefore allow a metal to be formed into useful shapes; strengthening metals requires increasing the number of barriers to slip and reducing the ability to plastically deform. As a metal is plastically deformed, new dislocations are generated, so that the dislocation density becomes higher and higher. In addition to multiplying, dislocations become entangled and impede each other's motion. The result is increasing resistance to plastic deformation with increasing dislocation density. The number of dislocations is defined by the dislocation density ρ, which is the length of dislocations per unit volume of material; therefore, the units of ρ are cm/cm^3 or cm^{-2}. The dislocation density of an annealed metal may run as high as $10^6 cm^{-2}$, while that for a cold-worked metal may run as high as 10^{12} cm^{-2} [13]. The influence of deformation temperature on dislocation accumulation is illustrated in figure I.10. At room temperature (25°C), the dislocation density increases rapidly with strain, indicating significant work hardening. At elevated temperatures (200–250°C), dynamic recovery becomes active, reducing the rate of dislocation accumulation and lowering the stored energy available for subsequent recrystallization.

This continual increase in resistance to plastic deformation is referred to as work hardening, cold working, or strain hardening. Work hardening results in a simultaneous increase in strength and a decrease in ductility. Since the work-hardened condition increases the stored energy in the metal and is thermodynamically unstable, the deformed metal will attempt to attain a state of lower energy. This generally cannot be accomplished at room temperature; elevated temperatures, in the range of ½ to ¾ of the absolute melting point, are

necessary to allow mechanisms such as diffusion, to restore the lower-energy state. The process of heating a work-hardened metal to restore its original strength and ductility is called annealing [13].

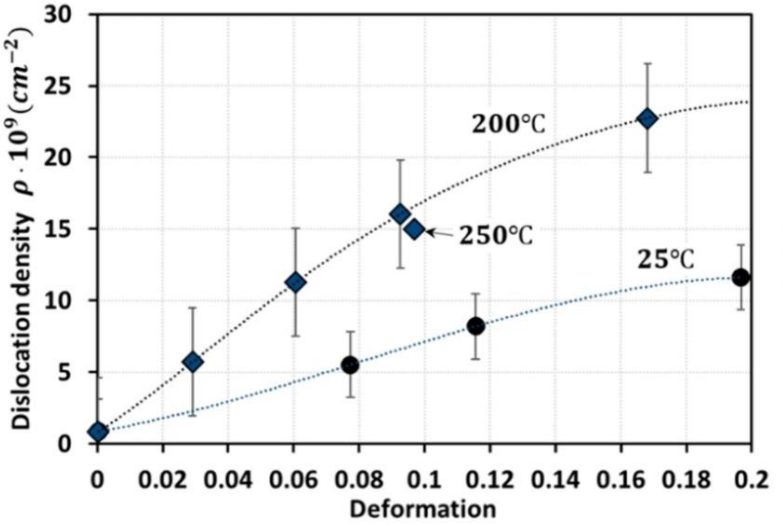


Figure I.10: Evolution of dislocation density as a function of deformation at different temperatures (25°C, 200°C, and 250°C). The dislocation density increases with strain, but higher temperatures reduce the accumulation rate due to dynamic recovery [20].

The dislocation density in crystalline materials is given by:

$$\rho = \frac{dN}{dA} \qquad [I.3]$$

- *dN*: the total number of dislocation lines
- *dA*: the cross-sectional area.

For polycrystalline metals, the dislocation density at the onset of plastic deformation is negligible since the movement of the first dislocations is restricted by the grain boundaries at which they are blocked and pile up. The more refined the grain size, the more pronounced is the Hall-Petch relationship [14]:

$$\sigma_y = \sigma_0 + k_y d^{-\frac{1}{2}} \qquad [I.4]$$

- k_y*:* the Hall-Petch coefficient,
- *d:* the grain diameter
- σ_0*:* the yield strength of an imaginary polycrystalline material having an infinite grain size [13].

The widely accepted square-root law of dislocation hardening shows that the flow stress is inversely proportional to the spacing of the obstacles, i.e. [14]:

$$\tau = \tau_0 + \alpha \times G \times B \times \sqrt{\rho} \qquad [I.5]$$

- τ_0: the flow stress of the material at zero strain
- α: the material constant of about 0.2–0.5
- G: the shear modulus
- b: the Burgers vector
- ρ: the dislocation density.

The stored energy of cold work serves as the driving force for the recovery and recrystallization phenomena that occur during subsequent annealing, which are the subject of the present dissertation [11].

I.10 Cold Drawing Process

I.10.1 Introduction and Principle

Wire drawing is a multifaceted manufacturing technique with several parameters interplaying. Known since the highest antiquity, wire drawing permits obtaining metallic wires of defined shape and form. The principle of the term derives from two notions: that of "traction" and that of "wire." It is a cold transformation process consisting of forcing the metal to pass through a calibrated orifice, called a die, under the action of a continuous traction force, this technique utilizes the aptitude for plastic deformation of the metal [8].

Wire drawing is a cold forming process by plastic deformation. It permits reducing the diameter of a wire by successive passes through dies of decreasing diameters in the presence of a lubricant. This technique permits obtaining wires of diameters less than 5 mm and to free oneself from the technological and economic limits of a hot deformation process, while respecting tight tolerances on diameters and conferring, where applicable, the mechanical characteristics adapted by work hardening [15].

The principle of wire drawing is based on the utilization of the plasticity of the material with the objective of reducing the cross-section of the wire by forcing its passage through successive calibrated orifices, the dies, of decreasing diameters, so that it is said to elongate and its section diminishes. The wire is constrained to pass through the dies by two different procedures: one imposes a displacement on it by applying a push on the back face (Back), it is the drawing (figure II.11) [8].

The deformation rate by wire drawing is defined by the following relation:

$$\varepsilon = \frac{(D_i^2 - D_f^2)}{D_i^2} \times 100 \qquad [I.6]$$

- D_i: the initial diameters of the wire
- D_f: the final diameters of the wire [8].

The wire drawing process capacity depends on three principal parameters such as the properties of the material of the wire, the geometries of the dies such as the length, the die angle, the wire drawing speed, and the friction at the interface between the die and the wire [15].

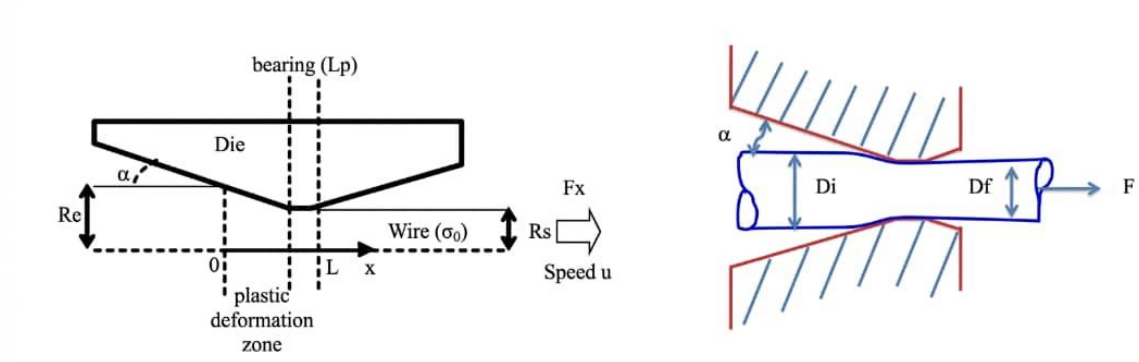


Figure I.11: Principle of wire drawing [15].

I.10.2 Key Elements of Cold Drawing

I.10.2.1 The Wire Rod

Wire drawing utilizes as its starting product the wire rod whose diameter varies from 7.5 to 20 mm. It is obtained from liquid metal according to two different procedures. The conventional procedure and the CLC procedure (continuous casting and rolling). The wire rod is generally in the form of coils or boxes [8].



Figure I.12: Aluminum wire rod [21].

The starting material utilized for wire drawing is called wire rod, of diameter 9.5 mm for aluminum and its alloys. It is generally presented, in the form of coils or boxes. The continuous casting permits a metallurgical process of controlling the transformation of a metal, from the liquid state to the solid state, in order to directly obtain semi-finished products (wire rod) [12]. The continuous casting process used to produce aluminum wire rods at ENICAB Biskra is illustrated in figure I.13.

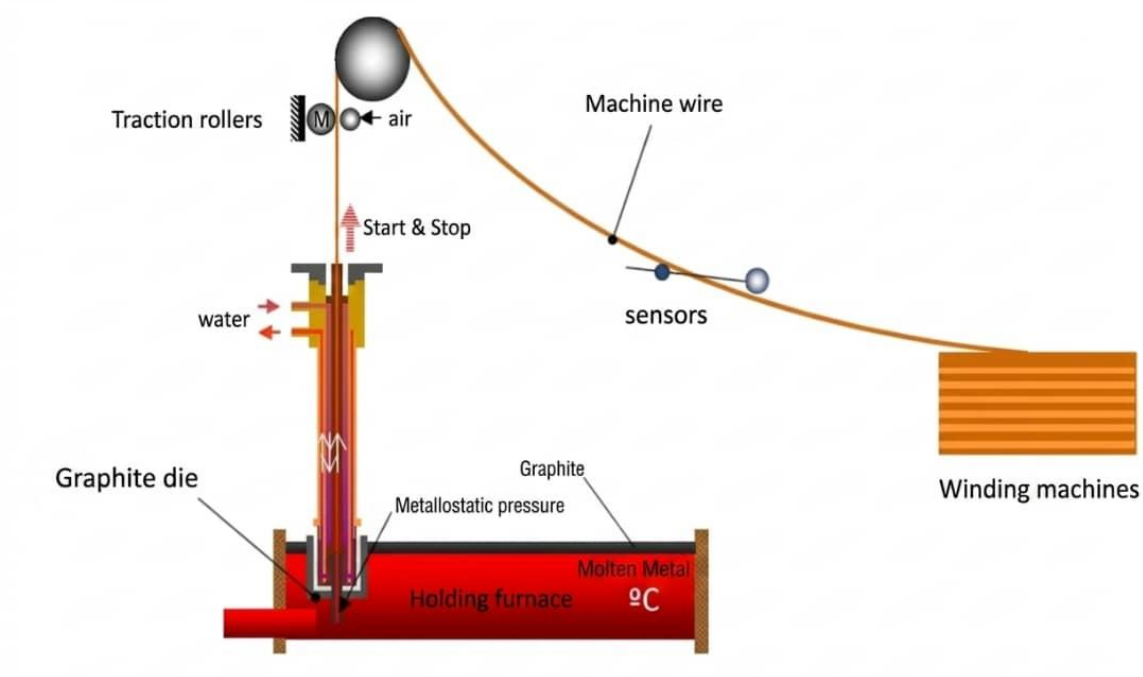


Figure I.13: Continuous casting process at ENICAB Biskra [12].

I.10.2.2 The Die

A wire drawing die is constituted of a hard core in tungsten carbide bonded with cobalt ensuring the reduction of the section of the wire. In certain cases, to limit the wear of the dies and their heating during the passage of the wire, diamond dies can be used. Their investment is much more expensive but their service life is greatly increased. The diamond is either natural (used exclusively for small diameters), or synthetic [15].

The geometry of the recommended dies is composed, in general, of [8]:

- A work cone sufficiently long to serve as a lubricant reservoir, with a very open entry angle (90° for example), which plays the role of disengagement and permits also distributing and driving the lubricant.
- A work cone angle of 16° to 12°.
- A bearing length of lower or equal to 1/4 the exit diameter (for carbide dies, largely the most used).

- A calibration zone, which as its name indicates, permits calibrating the diameter of the wire.
- A exit cone, of angle β, which permits a progressive disengagement of the die and the evacuation of the lubricant.

The die is composed of two parts: a very hard core, which ensures the reduction of the wire diameter, and a casing in steel which maintains the core and permits it to resist the strong pressures developed during wire drawing [12]. The geometry of a typical wire drawing die is shown in figure I.14, including the approach angle (α), the bearing surface (land), and the back relief zone.

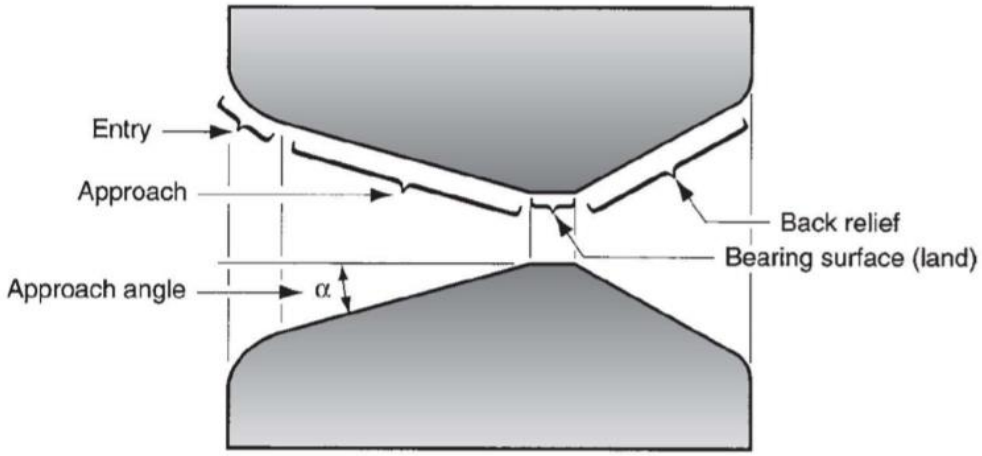


Figure I.14: Cross-sectional profile of a typical wire drawing die [16].

I.10.2.3 The Lubricant

The lubricant serves a dual purpose [15]:

- Reducing friction between the wire and the die in order to retard the wear of the latter.
- Giving the wire a surface condition adapted to its subsequent utilization.

The ensemble of the dies is immersed in a bath of aqueous lubricant in order to ensure the maintenance of a good state of the metallic wire surface and to limit the heating provoked by the work hardening of the metal. The diameter is thus reduced from 1.8 to 0.3 mm for the larger wires and from 1.4 to 0.2 mm for the fine wires, in 18 to 20 passes through the dies [15].

A good wire drawing lubricant must therefore possess the following properties [8]:

- A sufficient viscosity.
- A good resistance to pressure.
- A good resistance to temperature.

- A good resistance to shearing.
- A good chemical stability over time.

The lubrication regime depends on [15]:

- The applied load.
- The sliding speed.
- The viscosity of the lubricant.
- The contact geometry.
- The surface roughness.

Three lubrication regimes can be distinguished: the hydrodynamic regime, the mixed regime, and the limit regime [15].

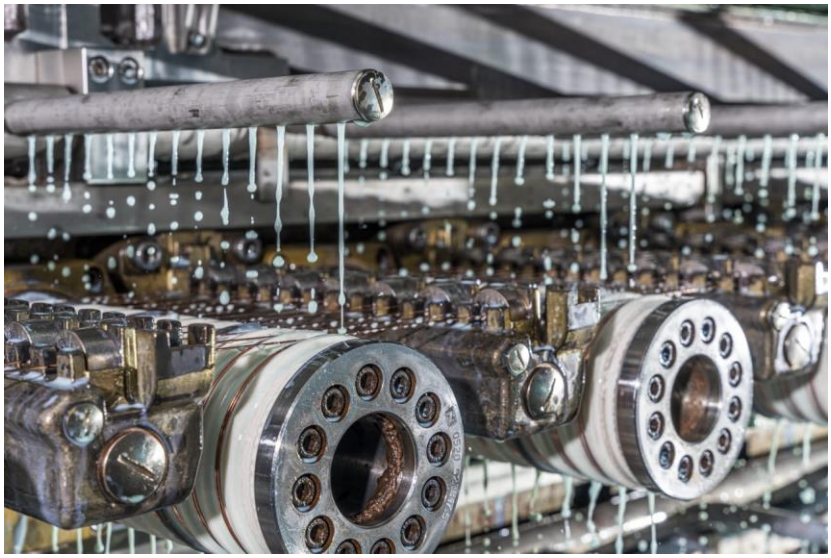


Figure I.15: Wire drawing lubrication system [22].

I.10.3 Wire Drawing Machines

The ensemble of wire drawing material permitting the transformation of the wire rod into wire is called drawing bench and comprises three elements [8]:

- Wire unwinding device.
- Wire drawing machine.
- Device for recovering the drawn wire.

The choice of the machine to draw depends on the alloy and the section reduction sought. Among all the devices, we distinguish [15]:

I.10.3.1 Single-Pass Machine (Machine Mono-Passe)

The single machine or single-pass machine is advisable for hard alloys requiring intermediate annealing during wire drawing (series 2000 and 7000) or for low section reductions. It consists of a system of wire unwinding, a wire drawing block, and a traction/recovery device. One distinguishes [8]:

- Simple blocks, with vertical coil axis.
- Lying benches, with horizontal coil axis.

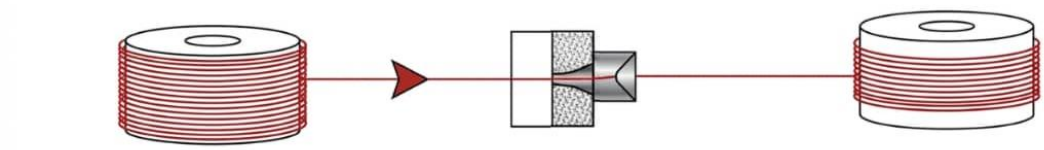


Figure I.16: Single-pass wire drawing device [23].

I.10.3.2 Multi-Pass Machine (Machine Multi-Passe)

On these machines, important section reductions are obtained by successive reductions carried out by the same apparatus. In this case, the wire passes from one coil to another by traversing a die, and it undergoes each time a section reduction and an increase in speed (conservation of material flow law). Three types of multi-pass machines are distinguished [15]:

I.10.3.2.1 Continuous or Direct-Pass Machine

These are the most modern and most widespread equipment. In them the speeds of the coils are automatically balanced so that each coil processes the quantity of wire necessary at the following: each coil behaves like a simple coil without it being necessary to have an accumulation of wire. The sliding of the wire on the coils compensates for speed differences [15].

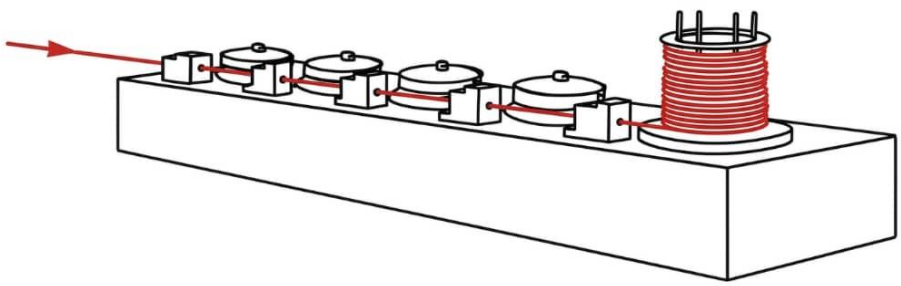


Figure I.17: Continuous multi-pass wire drawing machine [23].

I.10.3.2.2 Accumulation Machine

In these machines, there is no automatic balancing of speeds. The series of dies, or passes, are calculated so that each die processes more wire than what is necessary for the following one, so what creates an accumulation of wire on each coil. The accumulation machine permits [15]:

- Cooling the wire.
- Not interrupting the production of downstream coils in case of a stoppage of upstream coils.

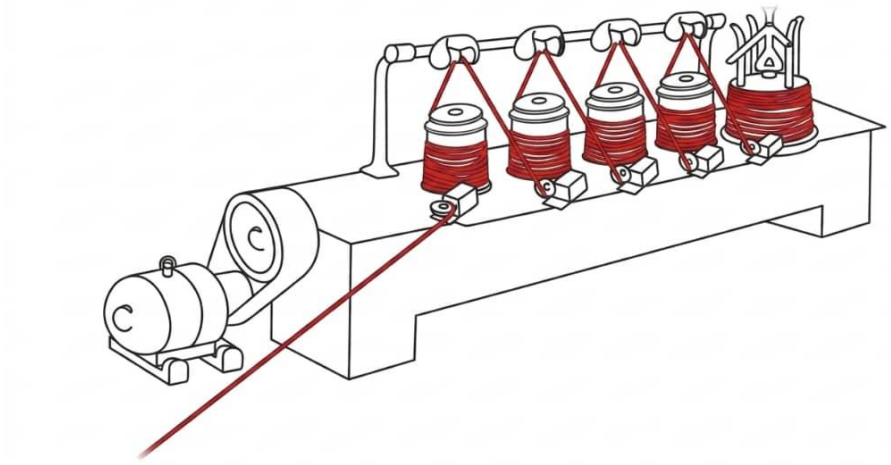


Figure I.18: Accumulation-type multi-Pass wire drawing machine [23].

I.10.3.2.3 Slip Machine

On these machines dedicated to wet wire drawing, there is neither balancing of speeds, nor accumulation of wire. The sliding of the wire on the coils compensates for speed differences. This type of machine is used above all for wet wire drawing of fine wires (diameters < 1 mm), the coil and die ensemble being sprinkled or immersed in the lubricant liquid which also plays the role of cooling agent for the wire [15].

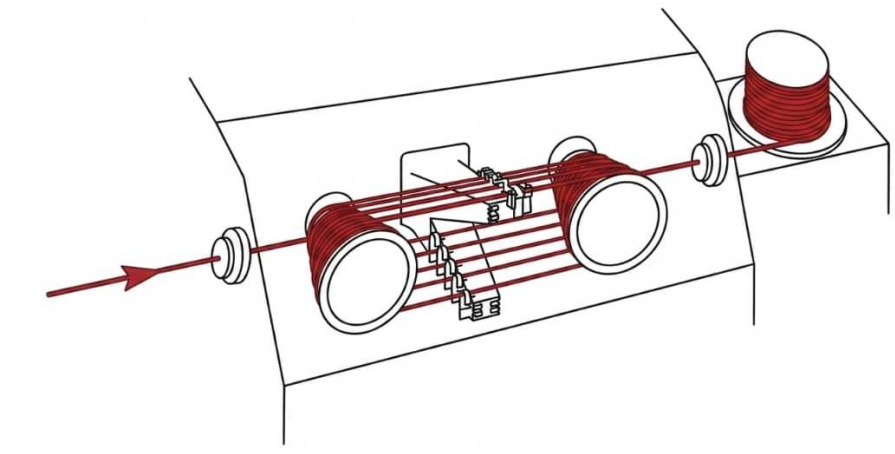


Figure I.19: Multi-pass slip-type wire drawing machine [23].

I.10.4 The Drawing Force

Although wire drawing seems to be a rather simple deformation, a precise calculation of the drawing force is not an easy task. In the simplest approach, factors such as friction, redundant deformation, and work hardening are neglected. If the effective strain is considered to be a pure uniaxial elongation *($\varepsilon = ln(D_i/Df)^2$)* and the material is rigid-plastic (with constant flow stress *σf*), the drawing force F can be estimated from [14]:

$$F = \sigma f \times ln(\frac{D_i}{D_f})^2 \quad [I.7]$$

The formula of Siebel adds a friction term, and a correction coefficient Φ which, according to Hosford and Caddell, can be expressed as a function of the Δ-factor [14]:

$$\sigma d = \Phi \times \sigma f(1 + \frac{\mu}{\tan \alpha}) \times ln(\frac{A_i}{A_f}) \quad [I.8]$$

- α: the die angle
- μ: the friction coefficient
- Φ: the redundant deformation factor
- A_i: the initial cross-sectional areas.
- *Af*: the final cross-sectional areas.

The reduction r and the true strain ε in wire drawing are defined as [14]:

$$r = \frac{(D_i^2 - D_f^2)}{D_i^2} \; and \; \varepsilon = ln(\frac{D_i}{D_f})^2 \quad [I.9]$$

I.10.5 Drawing Defects

At wire drawing, a certain number of defects on the wire can be due to the drawing operation itself [8]:

- **Cup and cone fracture:** This is primarily due to an excessively open work cone angle. These ruptures are mainly initiated on internal metallurgical defects of the type "cup and cone" [8].
- **Surface cracks:** These surface cracks are essentially attributable to an asymmetric deformation of the wire; the wire-die alignment must be controlled [8].
- **Wire scratches:** One of the origins of these scratches is the jamming of the die with metal chips. Such jamming causes locally poor lubrication of the wire [8].

Other defects can originate from the state of the metal. For instance, coarse inclusions lead to wire fractures, metal incrustations on the surface cause surface defects [8].

There are two major families of fracture that can be encountered at wire drawing [8]:

- **Internally initiated fractures:** except when the wire drawing scheme is too severe, the majority of these fractures are of the "cup and cone" metallurgical type.
- **Surface initiated fractures:** in this case, two types of defects can provoke fractures.

I.11 Metallurgical Effects of Cold Drawing

I.11.1 Microstructure of Cold-Drawn Wires

As any other manufacturing process, the plastic deformation involved in wire drawing brings about microstructures with specific characteristics. Cold drawn pearlitic wires develop a ⟨110⟩ texture, especially in the fibrous phase, with the texture intensity increasing with the combined use of transmission electron microscopy and x-ray diffraction techniques [16].

In polycrystals, which are encountered most often in practice, the nature of structural changes with deformation and the shape of the τ-ε curve, especially at the initial stage of hardening, greatly differ from those in single crystals. The main changes result from the fact that every crystallite in a polycrystal is oriented in space in a different manner than the surrounding adjacent crystallites from which the crystallite in question is separated by grain boundaries [11].

Therefore, even when a polycrystal is subjected to external stresses of the simplest anisotropic nature, for instance to uniaxial tension, slip begins in individual crystallites not at the same time and proceeds along differently oriented slip systems. Consequently, dimensional changes of various crystallites will be different in various directions [11].

During cold deformation, the microstructure evolves as a function of the deformation rate. At the first stage of deformation, the grains subdivide, change shape, and elongate in the direction of loading. A sub-structure of dislocations appears inside the grains. The subdivision of grains gives rise to a cellular configuration constituted of walls with a high dislocation density surrounding volumes with a low dislocation density. When the deformation rate increases, the walls of the cells refine to form sub-joints [11].

Fine-grained materials undergo a more intensive work-hardening than coarse-grained ones. Besides, core volumes of grains in coarse-grained materials become work-hardened to

a smaller degree than boundary regions. These phenomena are important for understanding recrystallization [11].

In addition to intragranular inhomogeneity, deformed polycrystals are characterized by an important intergranular inhomogeneity, i.e. by non-uniform deformation of adjacent grains. This feature makes itself felt heavily at relatively low strains and substantially influences the nature of subsequent recrystallization. The elongation in some grains of coarse-grained aluminum may vary from 2 to 14% or even more, with average elongation of a specimen of 5% [11].

I.11.2 Deformation Textures

One of the most significant consequences of plastic deformation in polycrystals is that their properties become anisotropic to some extent or other, i.e. grains which have been randomly oriented prior to deformation acquire a preferable crystallographic orientation which is called the texture [11].

During deformation of a metal specimen, its crystallites also change their shape and tend to orientate themselves definitely according to the external deforming forces. In polycrystals, such rotations, though of a more complicated nature, occur in individual crystallites. The orientation changes gradually as the deformation increases [11].

Drawing produces what is called an axial texture in which all crystallites show a definite crystal direction ⟨uvw⟩ along the axis of drawing, but occupy random positions around the ⟨uvw⟩ axis. In F.C.C. metals (aluminum), the texture formed with the {111} direction is established parallel to the drawing direction. In aluminum, for instance, only the {111} orientation can be formed with the (100) orientation, and of these (where the stacking fault energy is low), both orientations are possible [11].

When the wire is deformed sufficiently, most of the grains come to have at least one microband. Owing to sharp misorientations, microbands, like grain boundaries, become the preferable sites of formation of recrystallization nuclei [11].

I.11.3 Residual Stresses

Residual stresses, also referred to as internal stresses, exist in the material independent of any external load. A key feature of these stresses is their quality of being self-equilibrating, meaning that their compressive and tensile components sum to zero net force and moment within the whole volume. Various mechanisms can create residual stresses [16]:

- Non-uniform plastic deformation during manufacturing processes such as forging or rolling.
- Surface modification treatments, like plating or peening.
- Material phase and/or density changes throughout processes with large thermal gradients.

There are three length scale-based categories of residual stresses. Type I macro-stresses, either residual or applied, can cause Type II micro-stresses. Type III residual stresses are on the atomic scale around dislocations and crystal interfaces [16].

Cold drawing also causes a characteristic axial RS pattern with tensile components near the surface and compressive components in the center. The gradient and magnitude of the residual stress profile in cold-drawn wires and bars, however, depends on the die geometry [16].

Residual stresses can cause undesirable effects in other ways as well. For example, where dimensional precision is required, distortions occurring due to a redistribution of residual stresses after cutting or machining can pose problems. Heat treatment or incremental machining are common solutions to reduce residual stresses and preserve dimensional accuracy [16].

I.11.4 Tensile Behavior of Cold-Drawn Wires

It is known that the plastic deformation associated with the different forming methods brings about higher strength at the expense of ductility. This is the common trend observed in various techniques such as rolling, extrusion, and drawing. For instance, larger plastic deformation leads to higher yield strength but reduced elongation to failure (ductility) in Cu and Al [16].

The flow stress of cold-drawn materials at high strains approaches a saturation value σ_{sat}, at high strains induced by metal forming processes. This illustrates for pure copper and pure aluminum samples processed by equal channel angular pressing (ECAP) [16].

The deformation rate by wire drawing leads to a modification of the general properties of the wire. The variation of mechanical characteristics (hardness, elongation, and tensile strength...) or physical characteristics (resistivity, density...) by plastic deformation through wire drawing causes a work hardening which is expressed by [12]:

- An increase in tensile strength and hardness.

- A decrease in the ductility of drawn wires.
- An increase in electrical resistivity.

The heat treatment of metallic alloys by annealing is used to eliminate residual stresses, reduce hardness, improve ductility, and produce a particular microstructure [12].

I.12 Conclusion

This chapter has presented the theoretical framework governing the cold drawing of aluminum wires, from the fundamental mechanisms of plastic deformation to the metallurgical consequences of the drawing process.

It has been established that plastic deformation of metallic materials is mediated by the movement of dislocations on preferential slip planes and directions. In aluminum, which possesses an F.C.C. crystal structure and a relatively high stacking fault energy, slip occurs predominantly on the {111}⟨110⟩ system, and cross-slip is readily activated. Twinning, while possible, plays a secondary role in F.C.C. metals at room temperature. Cold deformation leads to a progressive increase in dislocation density, from approximately 10^6 cm^{-2} in the annealed state to values as high as 10^{10}–10^{11} cm^{-2} after heavy cold work, giving rise to work hardening and the accumulation of stored elastic energy within the material.

The cold drawing process has been described in detail, including its key elements — the wire rod, the die, and the lubricant as well as the different types of wire drawing machines used in industrial practice. The drawing force, which depends on the die geometry, the friction conditions, and the degree of redundant deformation, has been expressed through the analytical formulations of Siebel and Hosford-Caddell.

- The metallurgical effects of cold drawing on aluminum wires have been examined. Cold drawing produces a characteristic elongated grain structure, a pronounced axial deformation texture of the ⟨111⟩ type in F.C.C. aluminum, residual stresses with a tensile surface and compressive core profile, and a significant increase in tensile strength at the expense of ductility. The stored energy accumulated during cold drawing, in the form of dislocations and lattice defects, constitutes the thermodynamic driving force for the recovery and recrystallization phenomena that are the central subject of the present dissertation, and which are examined in detail in the following chapter.

References

[1] A. Sverdlin, "Introduction to Aluminum", in Handbook of Aluminum, Vol. 1, Physical Metallurgy and Processes, Edition: G.E. Totten and D.S. MacKenzie, Marcel Dekker Inc., New York, pp. 1–32, (2003).

[2] M. Colombié, Matériaux industriels, Matériaux Métalliques, DUNOD, Paris, (2000).

[3] H. Leiris, Métaux et alliages autres que les aciers et les fontes, Tome II, Masson et Cie Éditeurs, pp. 71–92, (1971).

[4] M. Guy, Aide-mémoire de métallurgie : Métaux, Alliages, Propriétés, Dunod, Paris, p. 330, (2004).

[5] J.R. Davis (Ed.), Aluminum and Aluminum Alloys, ASM International, Materials Park, Ohio, (1993).

[6] G.E. Totten and D.S. MacKenzie (Eds.), Handbook of Aluminum, Vol. 1: Physical Metallurgy and Processes, Marcel Dekker Inc., New York, (2003).

[7] S. Ouallam, Etude du soudage TIG et laser Nd-YAG de l'alliage d'aluminium 2024 T3, Master's Thesis, ENP, (2009).

[8] H. Dekhli and R. Farhani, Influence de la déformation à froid sur les propriétés mécaniques et microstructurales des fils d'aluminium tréfilés à l'ENICAB Biskra, Master's Thesis, University of Mohamed Khider, Biskra, (2015).

[9] A. Diha, Etude du fluage des fils d'aluminium tréfilés, Doctoral Dissertation, University of Mohamed Khider, Biskra, (2014).

[10] Y. Benlahbib and K. Maabed, Étude du comportement mécanique d'aluminium déformé par tréfilage, Master's Thesis, University of Larbi Tébessi, Tébessa, (2022).

[11] S.S. Gorelik, Recrystallization in Metals and Alloys, Mir Publishers, Moscow, pp. 90–93, (1981).

[12] L. Bessais, Etude et caractérisation de la réaction de recristallisation des fils d'aluminium tréfilés industriellement à E.N.I.CA. BISKRA, Doctoral Dissertation, University of Mohamed Khider, Biskra, (2017).

[13] F.C. Campbell, Elements of Metallurgy and Engineering Alloys, ASM International, (2008).

[14] B. Verlinden, J. Driver, I. Samajdar and R.D. Doherty, Thermo-Mechanical Processing of Metallic Materials, Pergamon (Elsevier), Oxford, (2007).

[15] A. Ourabi, Étude de l'influence du traitement de recuit sur le comportement au tréfilage et l'évolution des propriétés des fils en acier mi-dur, Doctoral Dissertation, University of Mohamed Khider, Biskra, (2024).

[16] A. Dashti, Influence of the Cold Drawing Process on the Mechanical Behavior of Cu-Al Composite Wires, Doctoral Dissertation, Normandie University, (2023).

[17] L.J.M. Tan, MDB: Mechanical Properties of Materials 2nd Year, University of Eastern Philippines, (2024).

[18] W.D. Callister and D.G. Rethwisch, Materials Science and Engineering: An Introduction, 10th ed., Wiley, (2018).

[19] J.E.M. Flatøy, Process and Alloy Development of Recyclable Aluminium Alloys: Recovery and Recrystallization Behavior of a Selection of AlMn-model Alloys, Master's Thesis, Norwegian University of Science and Technology, (2011).

[20] Y. Song, D. Garcia Gonzalez and A. Rusinek, "Constitutive Models for Dynamic Strain Aging in Metals: Strain Rate and Temperature Dependences on the Flow Stress", MDPI Materials, (2020). https://doi.org/10.3390/ma13071794. Accessed 9 Apr. 2026

[21] Jesada, Decadent Bare Aluminum Cable Isolated on White Background, Adobe Stock, id=347763019. https://stock.adobe.com/ Accessed 10 May 2026.

[22] Metalube, Wire Industry Lubricants and Solutions for Wire Drawing Applications. https://metalube.co.uk/industries/wire-industry/. Accessed 1 May 2026.

[23] S. Bellal and A. Mebarek Azzem, Effets du taux de tréfilage et des traitements de recuits sur les caractéristiques mécaniques et électriques des fils de cuivre, Final Year Project, Ecole Nationale Polytechnique, (2018).

[24] K. Huang (Ed.), Recrystallization: Types, Techniques and Applications, Nova Science Publishers (Materials Science and Technologies), New York, (2020).

Chapter II: Heat Treatment of Metals

II.1 Introduction

This chapter focuses on heat treatment processes for cold-deformed aluminum wires, specifically the annealing phenomena that restore their microstructure and properties. Cold wire drawing alters the material's physical and mechanical characteristics, including increased dislocation density, work hardening, and reduced electrical conductivity and ductility. Annealing reverses these modifications, allowing the material to return to its equilibrium state.

Annealing of cold-deformed metals occurs in three stages: recovery, recrystallization, and grain growth. During recovery, dislocations rearrange and annihilate without grain boundary migration, restoring some physical properties. Recrystallization involves new strain-free grains nucleating and growing at the expense of the deformed matrix, driven by stored deformation energy, restoring mechanical properties. Grain growth occurs if temperature or holding time is sufficient, coarsening the recrystallized grain structure.

In this chapter, we first present the general principles of heat treatment and the objectives of annealing. Then, we examine each annealing stage in detail: definitions, mechanisms, governing conditions, and effects on material properties. Particular attention is given to aluminum, which recovers readily at 100–150°C and recrystallizes at 200–350°C, depending on prior cold work.

II.2 Heat Treatment

The microstructural modifications induced by cold deformation, which is wire drawing, modify the physical and mechanical properties of metals. However, one can generally restore the properties and the microstructure that the metal possessed before deformation [1].

It is a heat treatment which aims to bring the alloy back to an equilibrium structure. It comprises three stages:

- Heating to a certain temperature called the annealing temperature.
- The holding time.
- Slow cooling which can be done in air.

II.2.1 Heat Treatment Processes

Heat treatment processes consist of [2]:

a) AB: Heating to temperatures above transformation temperatures (for example: AC3).

b) BC: Holding at a defined temperature.

c) CD: Cooling at a given speed:

- Slow (in the furnace, in air).
- Quite fast (in oil).
- Very fast (in water).

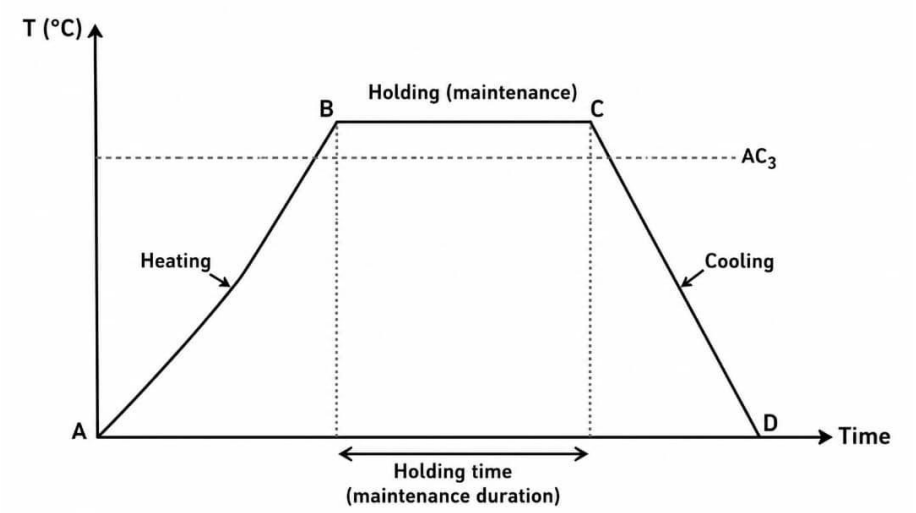


Figure II.1: Schematic representation of a typical heat treatment cycle, showing the successive stages of heating (A to B), holding (B to C), and cooling (C to D) [2].

The main types of heat treatment which modify in various ways the structure and properties of an alloy by operations of heating to a certain temperature, holding at this temperature, followed by cooling at a more or less accelerated speed are:

- Annealing.
- Normalizing.
- Quenching.
- Tempering and aging.

The main factors that allow distinguishing between the different types of heat treatments are the holding temperature and the cooling rate.

II.3 Principles of Annealing

In this study, we are interested in one type of heat treatment: annealing.

Annealing is a process involving heating and cooling, generally applied to produce softening. The term also refers to treatments intended to modify mechanical or physical properties, produce a defined microstructure, or eliminate gases. The temperature of the

operation and the cooling rate depend on the annealed material and the purpose of the treatment [3].

II.3.1 Definition of Annealing

by means of annealing: the thermal agitation of atoms due to the energy absorbed during this annealing activates the phenomena of return to the initial state "recovery", and increases the speed of these phenomena, this indeed allows a return towards the equilibrium state. This return, more or less complete, occurs essentially according to three processes: **recovery**, **recrystallization**, and **grain growth** or secondary recrystallization [2].

II.3.2 Stages of Annealing (Recovery » Recrystallization »Grain growth)

The annealing of deformed metals goes through three successive stages [4].

Recovery: Movement, rearrangement, and annihilation of dislocations, leading to the recovery of some properties without high-angle grain boundary migration.

Recrystallization: Nucleation and growth of new strain-free grains, leading to the occurrence of most mechanical property changes in this stage by high-angle grain boundary migration.

Grain growth: The further coarsening of the recrystallized structure by the reduction of grain boundary area and energy.

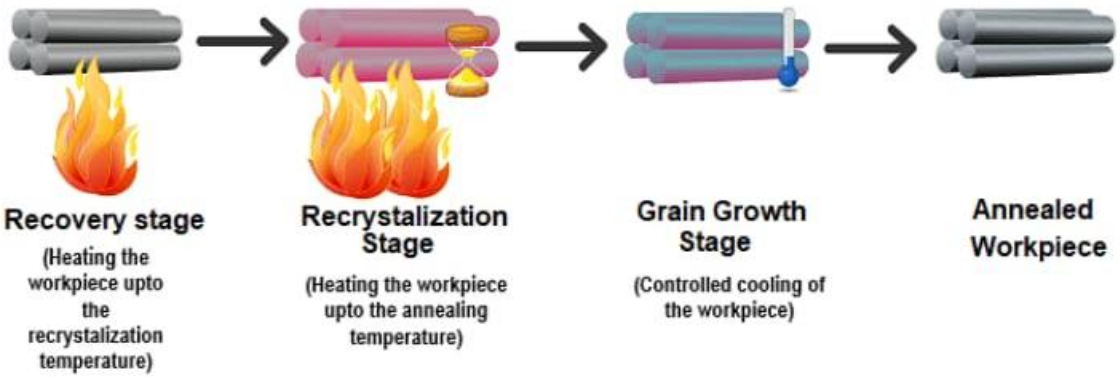


Figure II.2: Schematic illustration of the three stages of annealing: recovery, recrystallization, and grain growth [14].

These three stages are summarized in Table II.1 for pure aluminum, including temperature range, key mechanism, and property changes.

Table II.1: Summary of annealing stages for pure aluminum: temperature range, key mechanism, and property changes [7,11].

Stage	Temperature range (Al)	Key Mechanism	Property Change
Recovery	**100-250 °C**	**Dislocation rearrangement & annihilation, polygonization**	**Decrease in hardness and increase in conductivity**
Recrystallization	**200-350 °C**	**Nucleation & growth of strain-free grains**	**Major strength drop, ductility and conductivity recovery**
Grain Growth	**≥300 °C**	**Grain boundary migration**	**Slight strength and ductility increase**

As shown in the table, recovery occurs at low temperatures and only partially restores the original properties, while recrystallization occurs at higher temperatures and completely replaces the deformed structure. Finally, grain growth may occur if the temperature is sufficiently high or the holding time is long enough.

II.3.3 Objectives of Annealing

Annealed metallic components have advantages over untreated ones. The main objectives of the annealing process are [5]:

- **Restores the mechanical and physical properties:** Annealing restores the physical characteristics of the metal, particularly its ductility. The thermal energy during heating allows atomic migration within the metal's structure, and this eliminates work hardening and brittleness that may have developed during forming.
- **Improve machinability:** This is a product of the homogenized microstructure, with relief of work hardening and internal stresses.
- **Relief of internal stresses:** Stresses that accumulate within a component after forming or working are reduced. By that, annealing significantly lowers the risk of cracking in the finished component.
- **Rectification of dislocations:** Dislocations within the crystal lattice are reorganized, leading to improved electrical conductivity and magnetic properties.

- **Control over grain structure:** Some types of annealing can control the grain structure by selecting heating temperature and cooling rates. This control allows one to influence the physical and mechanical properties of the alloy.

II.4 Recovery

II.4.1 Definition of Recovery

Recovery is a thermal process that occurs in deformed materials without the migration of high-angle grain boundaries. During this stage, no new grains are created; instead, there is only a reduction in the number of atomic defects, vacancies and dislocations, and their rearrangement into more stable configurations. Recovery allows a partial restoration of the physical and mechanical properties of the work-hardened material [6].

Because of the high stored energy, the deformed aluminum is in an unstable state. On annealing, this stored energy is progressively released due to thermodynamic activation. At the beginning of annealing, the recovery process starts immediately with no incubation period. The dislocation density is drastically reduced from $10^{15}/m^2$ down to $1.5\times10^{14}/m^2$, but the basic deformed microstructure is retained [7]. The stored energy released during recovery is entirely caused by dislocation rearrangement and reduction, since vacancies produced by deformation have migrated out of the lattice structure at room temperature.

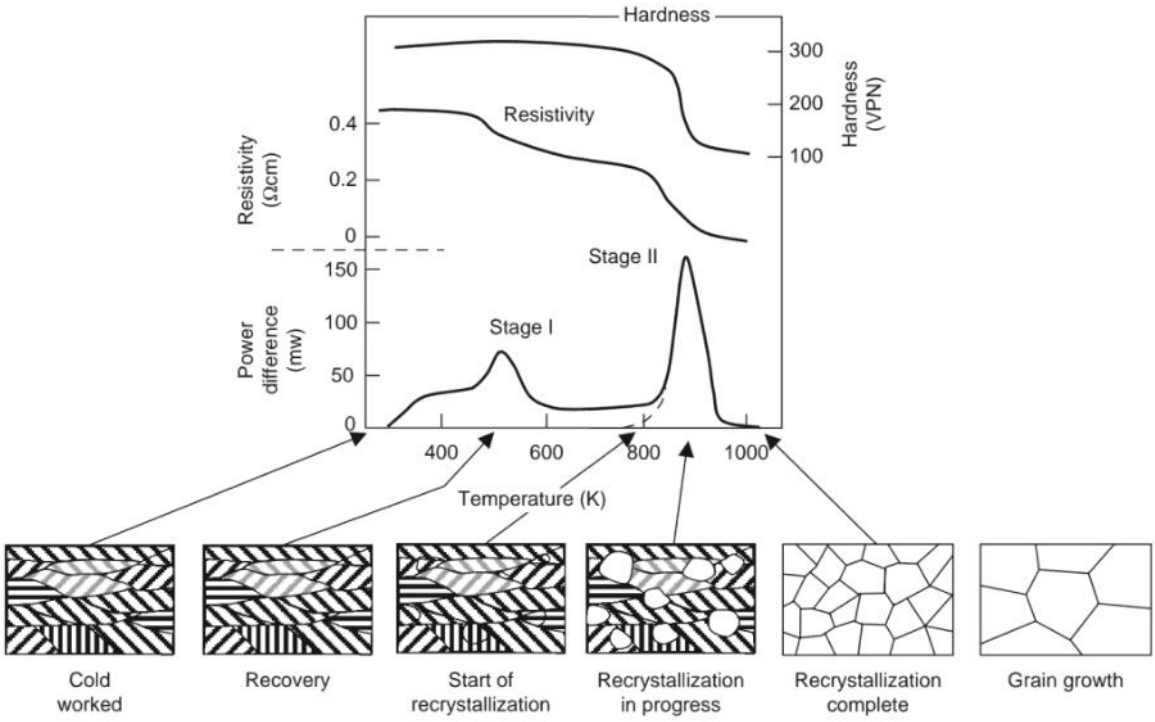


Figure II.3: An isothermal annealing curve for cold-worked nickel [11].

Recovery proceeds through several steps. First, dislocations group and condense into cell walls, within which the dislocation density is lower. Then, dislocations of opposite signs in the walls are annihilated and reorganized into two-dimensional networks forming sub-boundaries, this is the polygonization stage. Finally, some of these sub-grains evolve through sub-boundary movement to reach a structure that minimizes stored energy.

After recovery, the deformation texture remains unchanged, the electrical resistivity is slightly decreased, and 40% of the hardness induced by work hardening can be recovered in deformed pure aluminum [7].

II.4.2 Mechanisms of Recovery

During recovery, the stored energy of the material is reduced by dislocation movement. There are two primary processes: the annihilation of dislocations and the rearrangement of dislocations into lower energy configurations. Both processes are achieved by glide, climb and cross-slip of dislocations.

Figures II.4 (a) and (b) show the difference between deformed and recovered microstructures. The deformed microstructure (fig.II.4 a) contains a high density of dislocations and significant internal stresses. After recovery (fig.II.4 b), the dislocations have rearranged into lower energy configurations, resulting in a more stable structure without the formation of new grains.

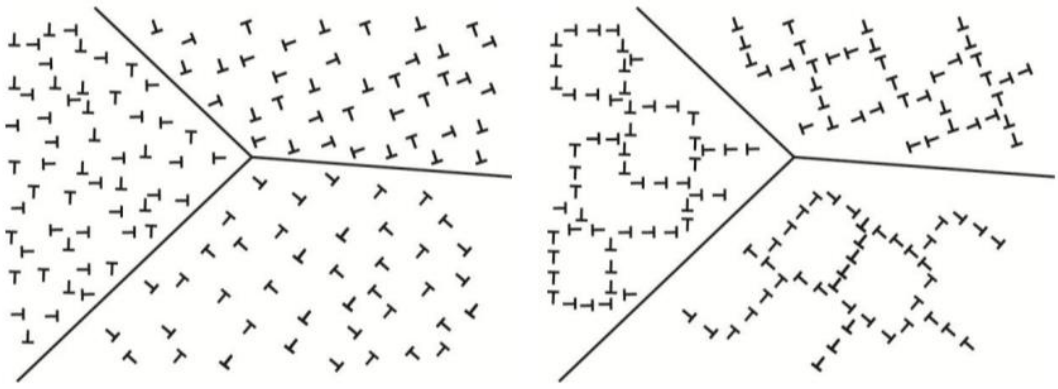


Figure II.4: Deformed Microstructure (a); Recovered Microstructure (b) [16].

II.4.2.1 Dislocation Annihilation

Dislocations of opposite sign on the same glide plane may annihilate by gliding towards each other. Such processes can take place even at low temperatures, reducing the dislocation density and leading to dynamic recovery. Dislocations of opposite sign on

different glide planes can annihilate by a combination of glide and climb. Since climb requires thermal activation, this can only occur at elevated temperatures.

Screw dislocations recover by annihilation through cross-slip, which occurs at low temperatures in aluminum due to its high stacking fault energy [8]. Figure II.5 illustrates the successive dislocation annihilation mechanisms during annealing. In a bent crystal containing both edge and screw dislocations that accommodate the orientation gradient, opposite sign dislocation segments (encircled in the figure) annihilate by climb.

The attractive force between two opposite screw dislocations is given by:

$$F = \frac{Gb^2}{2\pi x} \qquad \text{[II.1]}$$

- *F:* attractive force.
- *G:* the shear modulus.
- *b:* the Burgers vector.
- *x:* the separation distance.

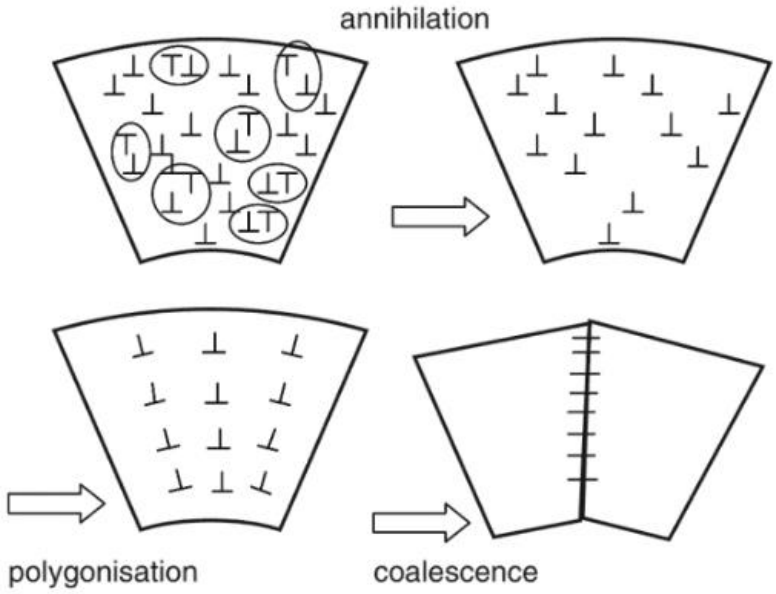


Figure II.5: Schematic of successive dislocation annihilation mechanisms [8].

II.4.2.2 Polygonization

When unequal numbers of dislocations of two signs are produced during deformation, the excess dislocations cannot be eliminated by annihilation. On annealing, these excess dislocations arrange into lower energy configurations in the form of regular arrays or low angle grain boundaries (LAGBs). The simplest case involves dislocations of only one

Burgers vector, producing a structure known as polygonization [4]. Figure II.6 also shows the remaining dislocations rearranging into sub-grain boundaries through polygonization and coalescence.

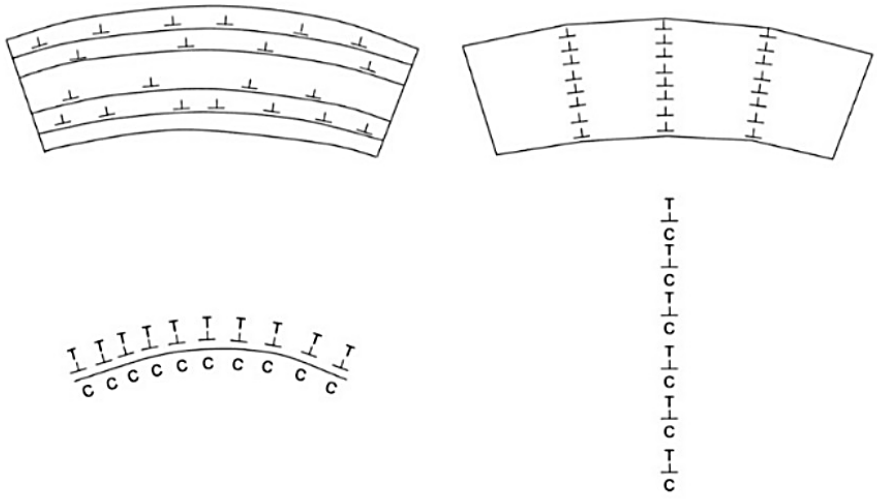


Figure II.6: Polygonization of a bent single crystal [11].

The dislocation walls formed are known as tilt boundaries, a simple type of low angle grain boundary. The energy of a tilt boundary increases with increasing misorientation, while the energy per dislocation decreases with increasing misorientation. Therefore, there is a driving force to form fewer, more highly misoriented boundaries as recovery proceeds [8].

II.4.2.3 Sub-grain Coarsening

The stored energy of a recovered substructure remains high compared to fully recrystallized material. It can be reduced further by substructure coarsening, which decreases the total area of low angle boundaries. The driving force for sub-grain growth arises from the energy stored in the sub-grain structure [4].

Many measurements of sub-grain size change with time at constant temperature reveal kinetics of the form:

$$D^n - D_0^n = c_1\, t \qquad \text{[II.2]}$$

- *D:* the sub-grain size at time t
- D_0*:* the initial sub-grain size at t=0.
- *n:* constant (≈2).
- c_1*:* temperature dependent rate constant

An alternative mechanism for sub-grain coarsening is rotation and coalescence, in which adjacent sub-grains of similar orientation rotate until they merge into one larger sub-grain. Figure II.4 illustrates this mechanism as well, where adjacent sub-grains coalesce into a larger structure [4].

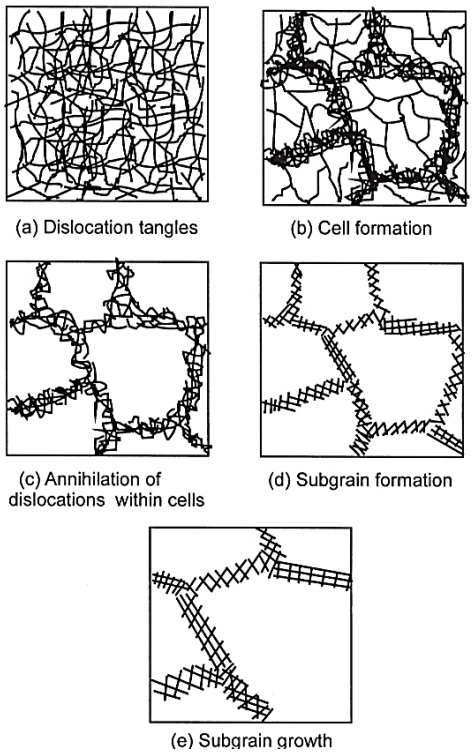


Figure II.7: Schematics showing dislocation structure changes during recovery, random dislocation tangles through cell structures to sub-grains [8].

II.4.3 Effect of Recovery on Mechanical and Physical Properties

The microstructural changes taking place during recovery influence both the physical and mechanical properties of the material. It should be noted that the kinetics of recovery are entirely characteristic and distinct from those of recrystallization. The rate of recovery increases with annealing temperature.

II.4.3.1 Effect on Electrical Resistivity

During heating from a sufficiently low temperature, equal to or below room temperature, the migration of point defects can be observed. This gives rise to one or several stages of reduction in electrical resistivity. When a metal is heated after deformation, point defects such as vacancies and interstitial atoms generated by cold working disappear rapidly. The principal consequence of this reduction in point defects is a decrease in resistivity, since this property is highly sensitive to the presence of such defects. Subsequently, a new redistribution of dislocations into networks of lower energy takes place, without any notable reduction in their density. The electrical resistivity is thus progressively restored toward its

original pre-deformation level, and is completely recovered before the onset of recrystallization [4]. As illustrated in figure II.8, the electrical conductivity increases progressively with annealing time at 250°C, reflecting the reduction in dislocation density and point defects during recovery.

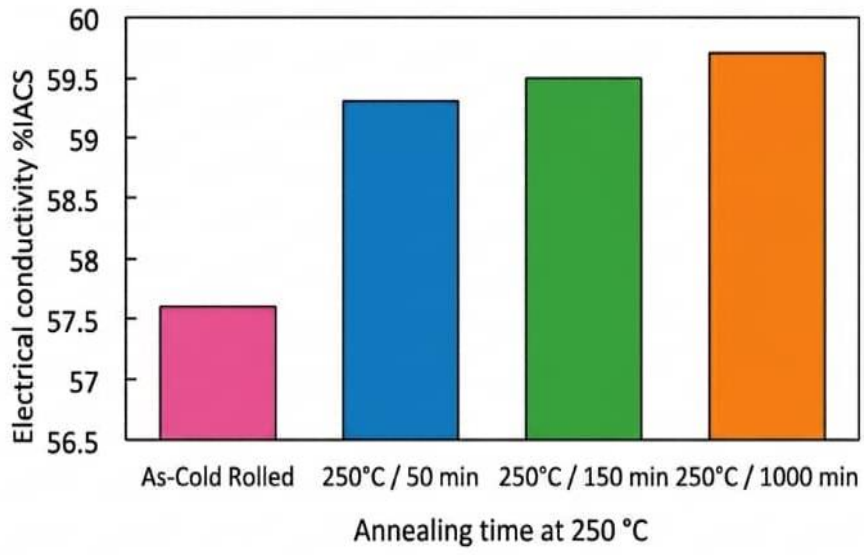


Figure II.8: Evolution of electrical conductivity of a cold-rolled 1200 aluminum sheet during isothermal annealing at 250°C as a function of annealing time [19].

II.4.3.2 Effect on Mechanical Properties

The simplest method to monitor this evolution is hardness measurement, which allows the temperature interval over which recovery occurs to be identified. The restoration of mechanical properties only begins to manifest at a relatively elevated temperature. A distinction must be made between two categories of metals [4]:

- Metals with high stacking fault energy, such as α-iron and aluminum: dislocation rearrangement by glide and climb is straightforward. A recovery stage is clearly observed well before recrystallization begins.
- Metals with low or medium stacking fault energy, such as copper and its alloys: dislocation climb is more difficult due to dissociation. In these materials, it is recrystallization that governs the evolution of mechanical properties.

As dislocation density decreases during recovery, the flow stress and hardness are progressively reduced, while ductility increases.

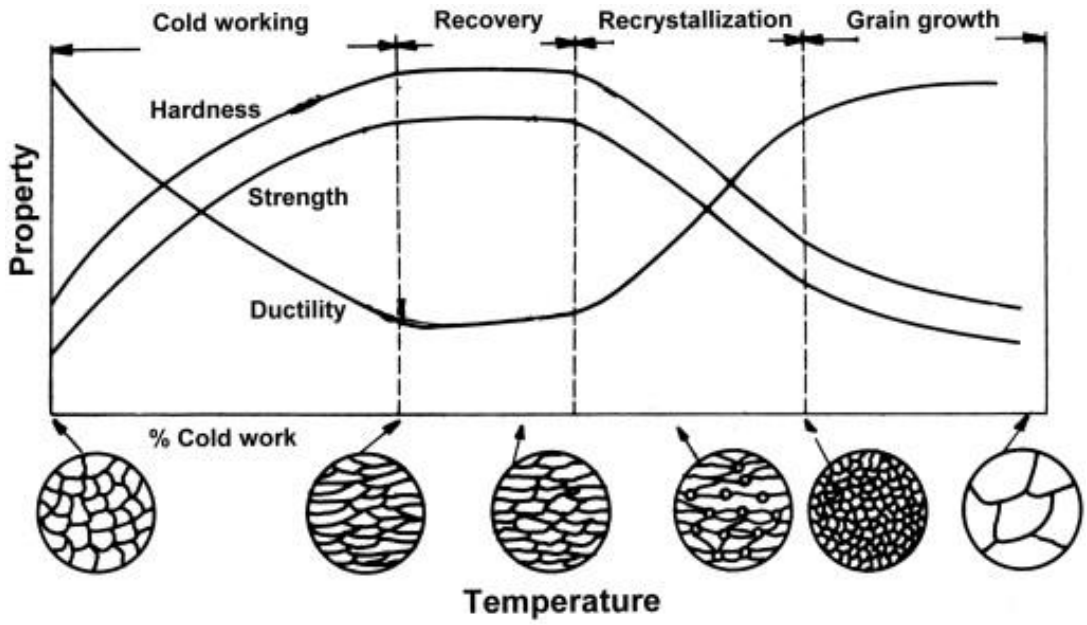


Figure II.9: Microstructure and property change during cold-working and annealing (recover, recrystallization and grain growth) of material [15].

II.4.3.3 Effect on Microstructure

During recovery, dislocations align to form tilt boundaries, such that the regions of the crystal bordered by these boundaries become free of dislocations. This dislocation rearrangement is driven by a reduction in the total energy of the system under the effect of temperature. The dislocations migrate toward more stable configurations of lower total energy, forming the walls of polygonal cells hence the name polygonization. A stress relief heat treatment applied to eliminate residual stresses introduced by prior forming operations is termed stress relief annealing [4].

II.5 Recrystallization

II.5.1 Definition of Recrystallization

Even after recovery is complete, the grains remain in a relatively elevated strain energy state. Recrystallization is the formation of a new set of strain-free and equiaxed grains having approximately equal dimensions in all directions, which possess low dislocation densities and are characteristic of the pre-cold-worked condition. The driving force to produce this new grain structure is the difference in internal energy between the strained and unstrained material. The new grains nucleate as very small embryos and expand until they completely consume the parent material, through processes that involve short-range diffusion [4].

Primary recrystallization reduces most radically the volume energy of deformed crystallites, principally by diminishing the number of structural defects caused by prior

deformation, and restores the structure and properties the metal possessed before deformation. The essence of the process is that recrystallization nuclei form in the deformed matrix and develop at the expense of that matrix. These nuclei are matrix portions having an undistorted lattice and are separated from the deformed matrix by large-angle boundaries. Cold-worked grains having a high dislocation density are replaced by new grains having a much lower dislocation density, which decreases from approximately 10^8–10^{11} cm^{-2} down to 10^6–10^7 cm^{-2}. New orientations, new grain sizes, and new grain shapes form during this process. Primary recrystallization comes to an end as soon as the deformed matrix disappears [11].

Primary recrystallization is commonly divided into two stages: nucleation and growth of nuclei in the cold-worked matrix. Nucleation takes place preferentially at locations of high dislocation density and elevated strain energy, such as original grain boundaries, grain-boundary triple points, and sub-grains formed during polygonization. Nuclei will not form until the driving force provided by thermal energy becomes sufficiently large. The recrystallization rate, expressed as the volume recrystallized per unit time, is written as [9]:

$$V = N \cdot G \qquad \text{[II.3]}$$

- *N:* the number of new nuclei per unit time
- *G:* their volumetric growth rate.

Since both quantities are time-dependent, the kinetics of recrystallization is not a simple function of time. Accordingly, isothermal recrystallization curves are typically sigmoidal in shape, where there is an incubation period during which no visible recrystallization occurs. During incubation, stable nuclei are formed by the coalescence of sub-grains, leading to the formation of high-angle grain boundaries.

The reduction of the volume energy of the deformed material constitutes the principal driving force of primary recrystallization. In a rough approximation, if ΔN_d is the difference of dislocation densities in the deformed material and in a recrystallization nucleus, the driving force is [10]:

$$P_{dr} \approx k \cdot \Delta N_d \cdot Gb^2 \qquad \text{[II.4]}$$

- *k:* factor that accounts for the nature of dislocation distribution.
- *G:* the shear modulus.
- *B:* the Burgers vector.

The gain in free energy per mole is denoted P_{dr}, and in the general case:

$$P_{dr} = \sum P_i = P_v + P_b + P_s \quad [II.5]$$

- P_v: the gain in volume energy
- P_b: the gain in grain-boundary energy.
- P_s: the gain in surface energy.

Also, during recrystallization, the mechanical properties that were altered as a result of cold working are restored toward their pre-cold-worked values that is, the metal becomes softer and less resistant, yet more ductile. Recovery and recrystallization are two distinctly different processes: at a constant temperature, recovery starts rapidly and then decreases with time, while recrystallization starts slowly and then builds up to a maximum rate before rapidly leveling off.

II.5.2 Conditions for Recrystallization

Recrystallization is not a spontaneous process; it requires specific conditions related to both the material and the thermal treatment applied. The main factors that govern the occurrence and rate of recrystallization are:

- Temperature and time.
- Degree of cold work.
- Purity of the metal.
- Original grain size.
- Temperature of deformation.

II.5.2.1 Minimum Deformation Requirement

A minimum deformation is needed to initiate recrystallization. The deformation must be sufficient to produce a nucleus for recrystallization and to provide the necessary driving force to sustain its growth. There is a minimum amount of strain, generally 1–5%, below which recrystallization will not occur. Above this strain the rate of recrystallization increases, levelling out to a maximum value at true strains of approximately 2–4. At small deformations, sub-grains form on heating and grow, but the boundaries between them remain low-angle boundaries, and recrystallization does not take place [8].

II.5.2.2 Temperature and Time

The temperature required for recrystallization is not fixed; it depends on the composition of the alloy and, in particular, on the amount of prior cold work performed. Recrystallization temperatures for metals of commercial purity are in the range of 0.3 to 0.5

of their absolute melting temperature. The temperature at which recrystallization occurs decreases as the time of anneal increases, since the microscopic mechanisms controlling recrystallization are thermally activated and the relationship between the recrystallization rate and the temperature follows the Arrhenius equation:

$$Rate = \left(\frac{1}{t}\right) = A \times e^{\left(-\frac{B}{T}\right)} \quad [II.6]$$

- *A* and *B* are constants
- *t:* the time for 50% recrystallization.

If we consider the transformation as a whole and take the time for 50% recrystallization ($t_{0.5}$) to be a measure of the rate of recrystallization, then we might expect a relationship of the type [8]:

$$Rate = \left(\frac{1}{t_{0.5}}\right) = C \times e^{\left(-\frac{Q}{KT}\right)} \quad [II.7]$$

Table II.2 presents approximate recrystallization temperatures for several metals. For pure aluminum (99.999%), recrystallization occurs at approximately 80°C, while commercially pure aluminum (99.9%) requires about 290°C. Aluminum alloys recrystallize at approximately 320°C [11].

The activation energy for recrystallization in pure aluminum is about 60 kJ/mol. However, the addition of only 0.0068 atomic percent of copper raises this energy to approximately 120 kJ/mol, significantly retarding the recrystallization process [8].

Table II.2: Approximate recrystallization temperatures for several metals and alloys [11].

Metal	Recrystallization temperature (°C)
Aluminum (99.999%)	80
Aluminum (99.9%)	290
Aluminum alloys	320
Copper (99.999%)	120
Copper (5% Al)	250
Copper (5% Zn)	320
Nickel (99.99%)	370
Low-carbon steel	540
Magnesium (99.99%)	65
Zinc	10
Tin	-5
Lead	-5

II.5.2.3 Degree of Cold Work

As the amount of cold work increases, recrystallization takes place at lower temperatures and in shorter durations. A certain minimum amount of cold work, often called the recrystallization threshold, is necessary. If the degree of cold work is too low, there will not be sufficient stored energy to initiate recrystallization. As the deformation is reduced to smaller values, the nucleation rate falls much faster than the growth rate. Thus, there is a critical amount of cold work required to form the nuclei needed for recrystallization. By increasing the degree of cold work, more stored energy is available for the nucleation of new grains with a resultant finer grain size.

For recrystallization to occur, a certain amount of deformation, called the recrystallization threshold, is necessary. If the degree of cold work is too low, there will not be a sufficient amount of stored energy to initiate recrystallization. At small deformations, which can range from as low as 2% to as much as 20%, recrystallization does not occur at temperatures even approaching the melting point. The critical degree of deformation can vary with the type of deformation [11]. Figure II.10 shows the effect of cold work on the recrystallization of aluminum at a constant annealing temperature of 350°C. As the amount of cold work increases, the time required for recrystallization is drastically reduced. Additionally, the incubation period becomes shorter for more highly cold-worked metal.

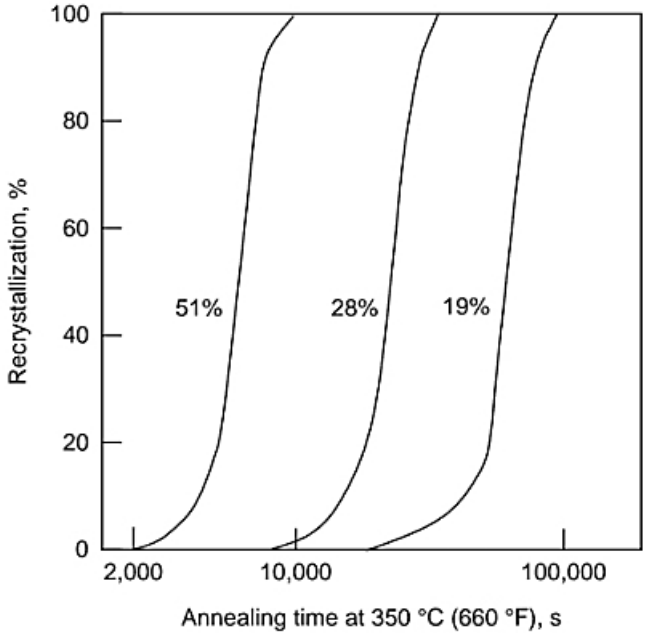


Figure II.10: Effect of cold work on recrystallization of aluminum [11].

II.5.2.4 Purity of the Metal

Very pure metals exhibit lower recrystallization temperatures compared to their alloys. Impurities, solutes, or fine second-phase particles slow down grain-boundary migration; therefore, their presence retards recrystallization. Solid-solution impurities tend to migrate to dislocations and grain boundaries and slow their motion, thus raising the recrystallization temperature. The usual effect of solutes is to hinder recrystallization. Very small concentrations of iron in solid solution in high purity aluminum may increase the recrystallization temperature by approximately 100°C. The addition of alloying elements is one method used in cold-work-hardened alloys to prevent them from softening in service [8].

The addition of a small amount of alloying elements usually sharply increases the temperature required for recrystallization. However, with further increases, the recrystallization temperature usually reaches a maximum value and then decreases. Some elements are more effective than others. For aluminum, the optimal addition of magnesium is 1%, and zirconium is also very effective in raising the recrystallization temperature of aluminum [11].

II.5.2.5 Original Grain Size

Smaller initial grain sizes yield smaller recrystallized grain sizes. Since grain boundaries stop dislocation movement during deformation, they become highly strained and smaller, and thus more numerous grain boundaries provide more active sites for nucleation

during recrystallization. A fine-grained material will recrystallize more rapidly than a coarse-grained material. The larger the original grain size of the material, the greater the amount of cold work required to achieve an equivalent recrystallization for a given temperature and time. For a given amount of work hardening, a higher working temperature is accompanied by a coarser grain size and requires a higher temperature to cause recrystallization [11].

II.5.2.6 Temperature of Deformation

As the temperature of cold working is raised above room temperature, a greater amount of cold working is required to obtain an equivalent amount of recrystallization at a given time and temperature. When the cold working temperature increases, dynamic recovery begins to occur during the deformation process. Therefore, there is less stored energy in the metal to serve as a driving force for recrystallization [11].

II.5.3 Laws of Recrystallization

The laws of recrystallization can be summarized as follows [6]:

1) Recrystallization occurs only after a certain minimum deformation, known as critical strain hardening.
2) The larger the initial grain size, the higher the deformation required to produce recrystallization, under given temperature and time conditions.
3) The recrystallization temperature is lower the longer the annealing time (for the same deformation).
4) At a given temperature, the recrystallization speed (recrystallized volume per unit time) starts from zero, increases and passes through a maximum: hence the characteristic shape of recrystallization kinetics curves, which begin with an "incubation period".
5) The grain size after recrystallization decreases when the deformation rate increases or when the annealing temperature decreases.
6) The new grains do not grow at the expense of deformed grains of neighboring orientation.
7) The lower the deformation, the higher the recrystallization temperature: the recrystallization temperature is the minimum temperature at which the metal must be annealed for recrystallization to occur in a given time.
8) The recrystallization temperature is lower the higher the purity of the metal.

II.5.4 Mechanisms of Recrystallization

Recrystallization nucleation is a critical factor in determining both the size and orientation of the resulting grains. In order to control recrystallization effectively, it is necessary to understand the mechanisms of nucleation and the parameters which govern it. The mechanism of formation of recrystallization nuclei is the key problem in the theory of recrystallization. Since nuclei are very small at the early stage of their formation and appear in microvolumes of the highest dislocation density, understanding their origin requires advanced characterization techniques.

It is now accepted that the "nuclei" from which recrystallization originates are not nuclei in the strict thermodynamic sense, but rather small volumes which pre-exist in the deformed microstructure [8].

II.5.4.1 Classical Nucleation

The possibility that classical nucleation theory might be applicable to recrystallization was examined by Burke and Turnbull (1952). In this situation, nucleation would be accomplished by random atomic fluctuations leading to the formation of a small crystallite with a high angle grain boundary. Such a nucleus would be stable if the difference in energy between the local deformed state and the recrystallized state were larger than the energy of the high energy interface produced in forming the nucleus. However, this mechanism is considered highly unlikely for two principal reasons [8]:

The driving force is low: in comparison with phase transformations, the energy which drives the recrystallization process is very small.

The interfacial energy is large: the energy of a high angle grain boundary, which is an essential factor in the recrystallization process, is large.

Calculations based on nucleation theory indicate that the radius of the critical nucleus is greater than 0.1 μm, so large that the rate of nucleation will be negligible. Classical nucleation is therefore not a viable mechanism for the origin of recrystallization.

II.5.4.2 Nucleation Sites

Recrystallization nuclei develop in regions of the highest distortion of a crystal lattice due to plastic deformation, mainly in local areas of substantial misorientation relative to the surroundings. When deformation is sufficient to initiate recrystallization, new grains nucleate not uniformly over the whole volume but only in some preferable locations, mainly on grain boundaries and triple joints, and less frequently on twin boundaries. The least size

of a recrystallization nucleus formed during heating of a deformed metal, i.e. the size of a region separated from the deformed matrix by large-angle boundaries, is of an order of 1 to 3 micrometers [10]. Figure II.11 (b) illustrates the nucleation and growth of recrystallized grains in a cold-rolled sample. As shown in the figure, nucleation occurs preferentially at shear bands and grain boundaries. The sequence from (a) to (d) shows the progressive transformation from the cold-rolled deformed structure to the fully recrystallized state [11].

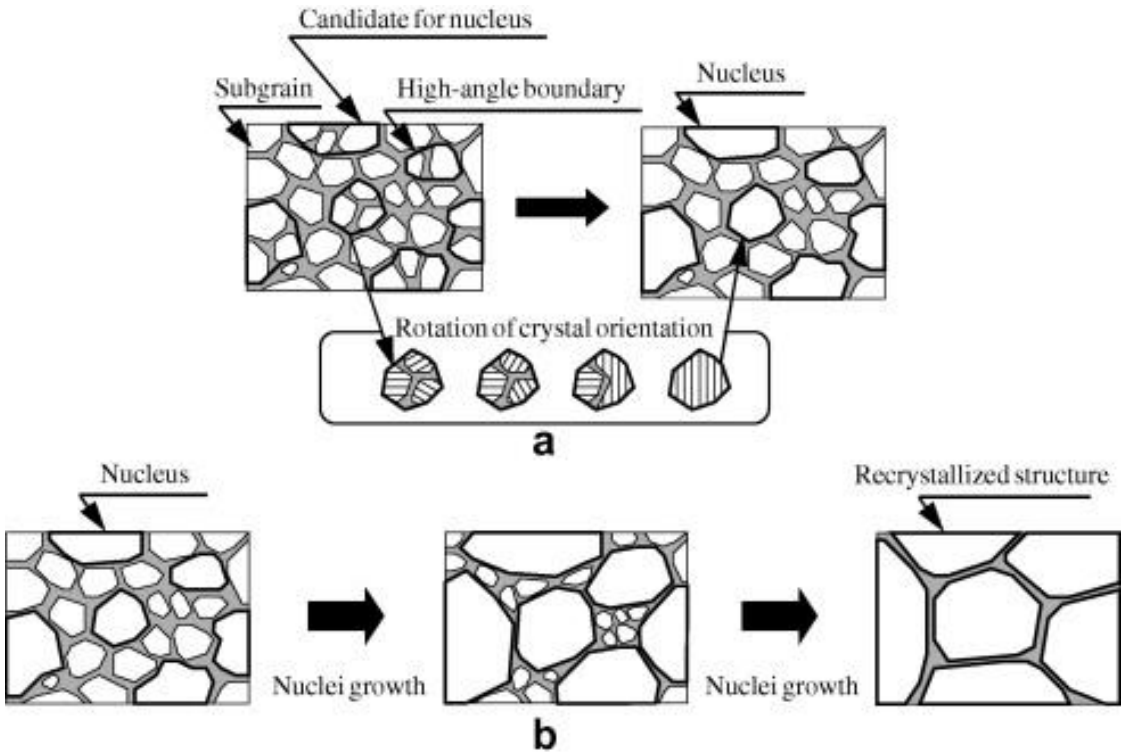


Figure II.11: Schematic illustration of recrystallization nucleation by sub-grain rotation and coalescence: (a) sub-grains with similar orientation rotate to form a high-angle boundary and a viable nucleus, followed by (b) nucleus growth into the deformed matrix, resulting in a fully recrystallized structure [17].

Nucleation takes place preferentially at locations of high dislocation density that possess elevated strain energies, such as at the original grain boundaries, grain-boundary triple points, and at the sub-grains formed during polygonization. Nuclei will not form until the driving force provided by thermal energy becomes sufficiently large. The incubation period corresponds to the irreversible growth of embryos unlike solidification, where an embryo that does not reach a critical size will redissolve in the melt, during annealing the embryo cannot redissolve and simply remains until it attracts enough atoms to become an active nucleus.

II.5.4.3 Strain Induced Boundary Migration (SIBM)

SIBM is the dominant nucleation mechanism in aluminum due to its high stacking fault energy. It involves the bulging of a pre-existing grain boundary into an adjacent grain with higher dislocation density. The driving force is the difference in stored energy across the boundary. When the bulging boundary reaches a critical radius, it detaches and forms a new strain-free recrystallization nucleus. [8]. Figure II.12 illustrates this mechanism, showing the transition from sub-grain to high-angle boundary to fully recrystallized structure.

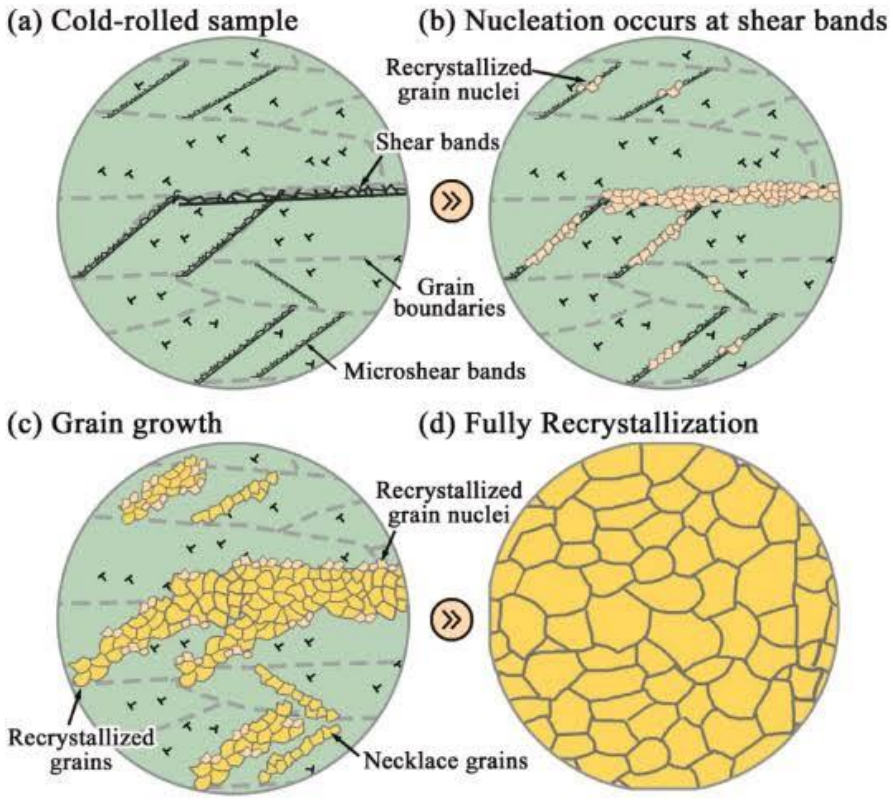


Figure II.12: Sequence of recrystallization in a cold-rolled sample: (a) deformed microstructure, (b) nucleation at shear bands and grain boundaries, (c) grain growth, and (d) fully recrystallized structure [18].

II.5.4.4 Growth of Recrystallized Grains

The nucleation of new grains at grain boundaries and sub-boundaries involves the formation and expansion of strain-free grains at the expense of the polygonized matrix, accomplished by the displacement of high-angle grain boundaries away from the center of boundary curvature. The strain-free nuclei develop into the deformed metal and gradually consume the whole of the deformed matrix. The growth of new grains proceeds rapidly because of the high mobility of the new high-angle grain boundaries, which have grain-boundary angles in the range of 30 to 40°.

The rate of recrystallization eventually diminishes as stored energy in the matrix is depleted and more of the new grains start impinging on each other. If the nucleation rate N is high and the growth rate G is low, then a fine grain size will result; conversely, if the nucleation rate is low and the growth rate is high, the microstructure will develop a large grain size. The ratio N/G is often used to interpret recrystallization behavior and predict the final grain size [11].

II.5.5 Effect of Recrystallization on Properties

Recrystallization produces significant modifications in both the mechanical and physical characteristics of cold-worked materials. The mechanical properties that were altered as a consequence of cold working are restored toward their pre-cold-worked values that is, the metal becomes softer and weaker, yet more ductile. The resulting mechanical softening completely eliminates the effects of cold working [9] [11]. The progressive transformation of the deformed microstructure through recovery to complete recrystallization is illustrated in figure II.13 In the cold-rolled state (a), the microstructure consists of highly deformed elongated grains. After recovery at 600°C (b), the structure remains deformed but internal stresses are partially relieved. As the annealing temperature increases from 700°C to 850°C (c–f), new strain-free grains nucleate and grow, gradually consuming the deformed matrix until a fully recrystallized equiaxed grain structure is obtained.

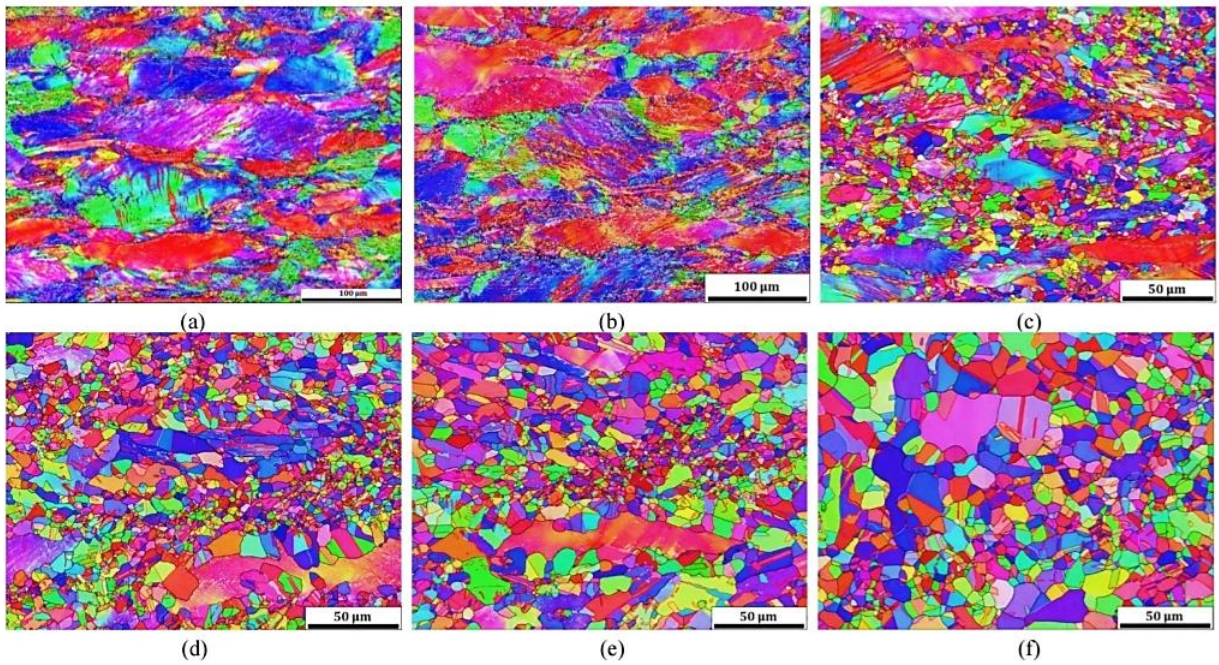


Figure II.13: IPF maps of a TWIP steel sample showing the microstructural evolution from (a) 42% cold-rolled, to (b) recovered at 600°C, and partially recrystallized at (c) 700°C, (d) 750°C, (e) 775°C, and (f) 850°C [19].

II.5.5.1 Effect on Mechanical Properties

Recrystallization is regarded as complete when the mechanical characteristics of the recrystallized metal approach those of the metal prior to cold working. Mechanical properties such as hardness, yield strength, tensile strength, percent elongation, and reduction in area change drastically over a very narrow temperature interval to become characteristic of the fully annealed material [11].

The influence of annealing temperature on tensile strength and ductility demonstrates that both quantities vary sharply during recrystallization: tensile strength and yield strength diminish rapidly, while ductility rises considerably. Recrystallization sharply reduces the tensile strength Rm and particularly the yield strength Re, while plasticity A improves considerably. This thermodynamic benefit of primary recrystallization eliminates practically all work hardening, and the metal recovers nearly all of its initial characteristics [12]. The effect of annealing temperature and time on the mechanical properties of cold-rolled aluminum is illustrated in figure II.14. At lower temperatures (140–180°C), hardness decreases slightly with time due to recovery processes. At higher temperatures (200–220°C), a sharp drop in hardness is observed, marking the onset of recrystallization. The arrow indicates the recrystallized states where new strain-free grains have formed, significantly softening the material.

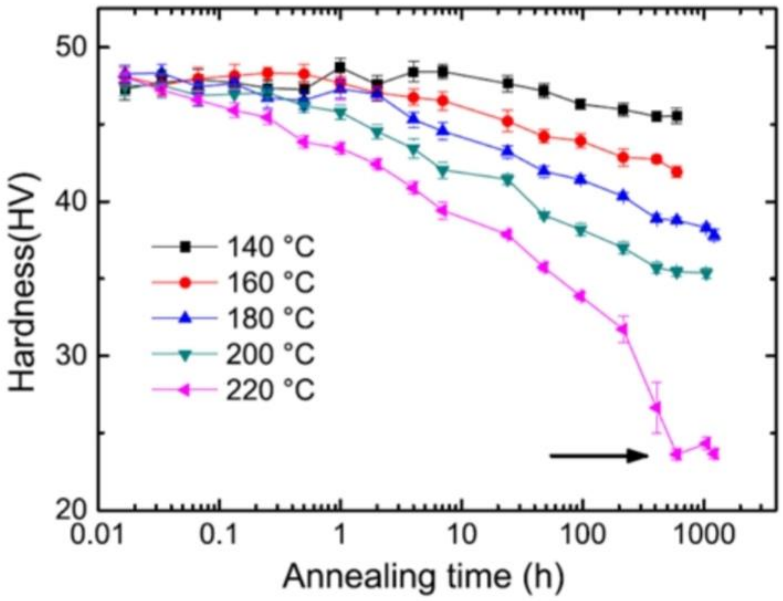


Figure II.14: Hardness as a function of annealing time for cold-rolled aluminum (99.5% purity, true strain 5.5) at temperatures from 140°C to 220°C. The arrow indicates the onset of recrystallization [19].

II.5.5.2 Effect on Electrical Conductivity

Although physical properties such as electrical conductivity undergo considerable increases during recovery, they also continue to rise during recrystallization. The formation of new strain-free grains with low dislocation densities diminishes the scattering of conduction electrons, thereby restoring the electrical conductivity of the material toward its pre-deformation level. The electrical resistivity ρ decreases progressively through recovery and continues to diminish during recrystallization, as the point defects and dislocation density are further reduced by the formation and advancement of high-angle grain boundaries [13].

II.5.5.3 Effect on Grain Size

The grain size following recrystallization is strongly influenced by both the annealing temperature and the degree of prior deformation. The type of structure that develops at the end of primary recrystallization is governed by the ratio of the nucleation rate N to the growth rate G. The final grain size is smaller at higher values of N and lower values of G. Both parameters and their ratio depend on a great number of factors; for an alloy of a particular composition, they primarily depend on the amount of cold deformation and, to a lesser extent, on the temperature of heating [10].

At deformations slightly exceeding the critical value, the value of N increases sharply from zero while G remains more moderate, resulting in a finer final grain size. At higher deformation levels, however, the grain structure after recrystallization becomes progressively coarser with further increases in annealing temperature.

The rate of recrystallization eventually diminishes as stored energy in the matrix is depleted and more of the new grains begin impinging on each other [11].

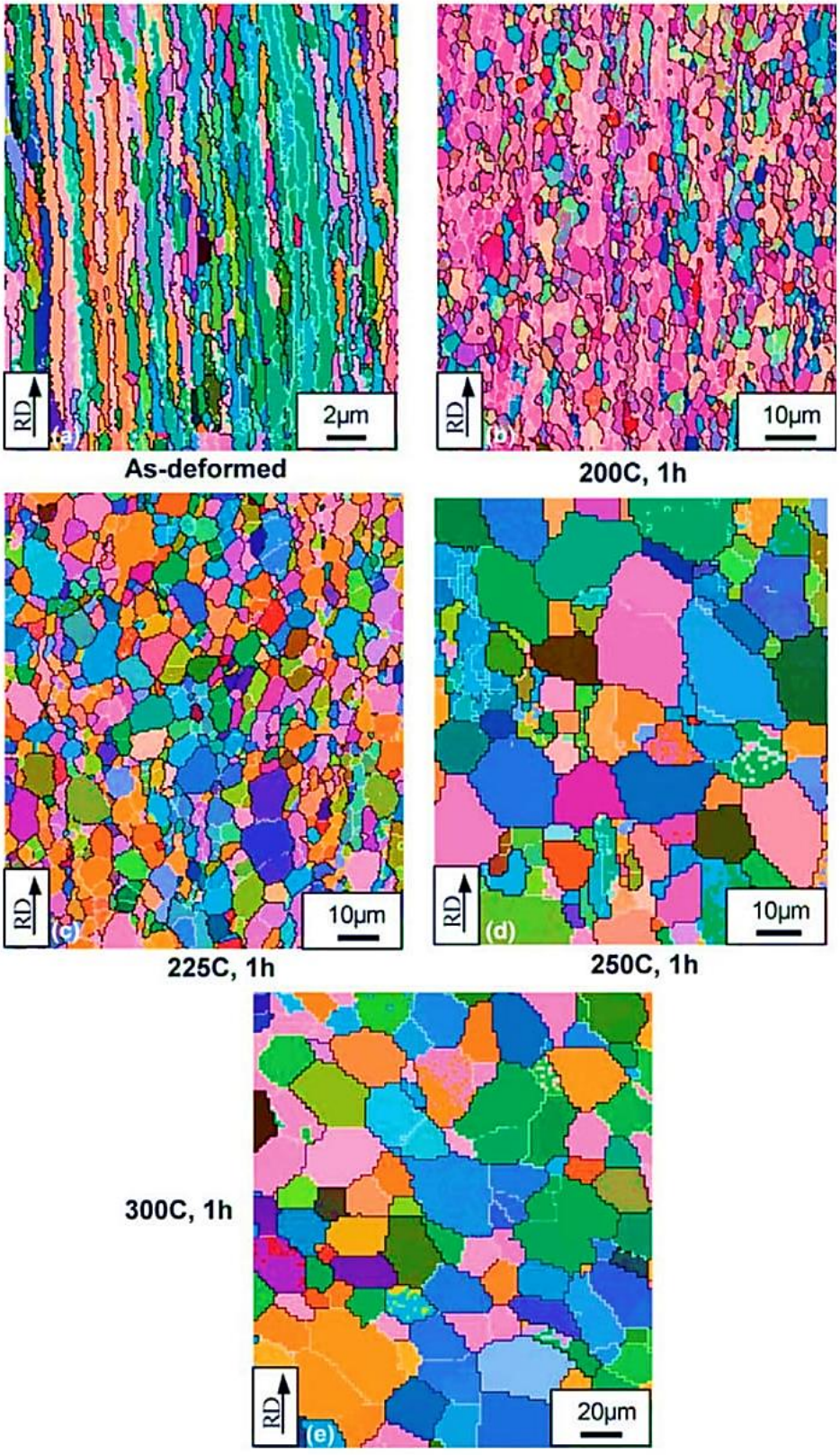


Figure II.15: EBSD maps showing continuous recrystallization in Al-0.1 Mg deformed to a strain of 2.6 and then annealed for 1 h at 200°C, 225°C, 250°C and 300°C [19].

II.5.5.4 Effect on Crystallographic Texture

Recrystallization generally produces a more isotropic grain arrangement compared to that obtained following deformation. After recrystallization, the newly formed grains are equiaxed and in general randomly oriented, which yields a more isotropic structure than that resulting from cold working. Recrystallization thus proceeds by nucleation and growth, eliminating the crystallographic texture introduced by cold working and replacing it with a recrystallization texture that is dependent on the material composition and processing history [8].

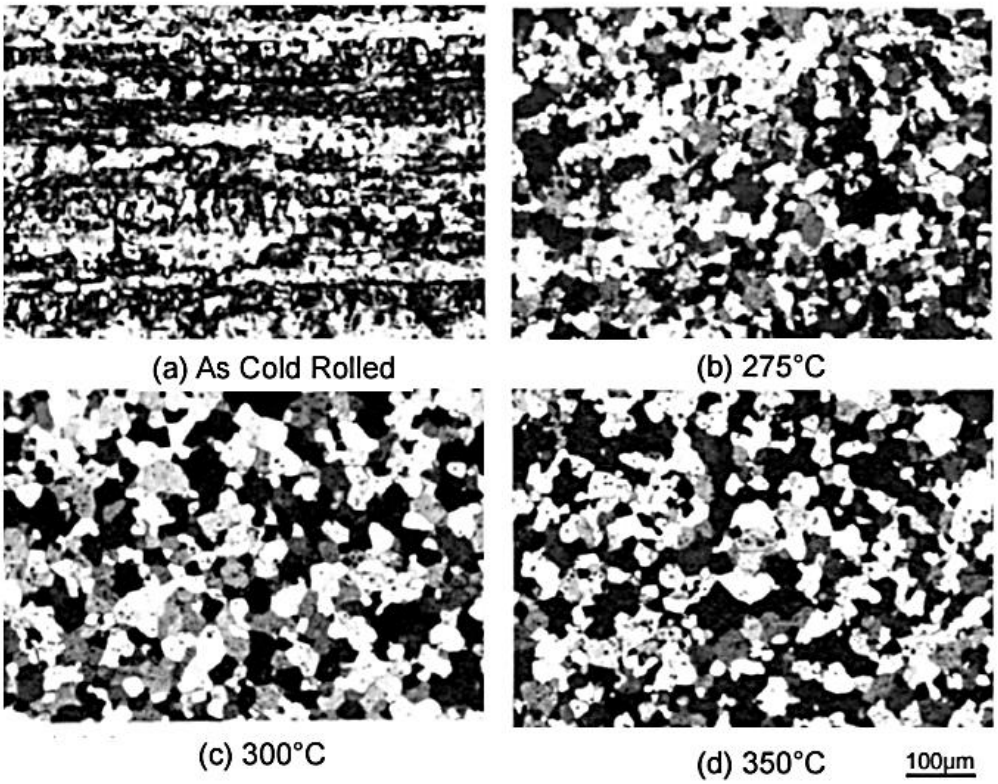


Figure II.16: Grain structures of the 1050 aluminum cold-rolled sheet followed by final annealing [19].

II.6 Grain Growth After Recrystallization

II.6.1 Definition and Nature of Grain Growth

Grain growth sets in after primary recrystallization, more strictly as the growing recrystallization nuclei begin to collide with one another. Grain growth is defined as the development of some new grains at the expense of other grains under conditions at which individual grains cannot grow preferably and exaggeratedly. Although primary recrystallization often precedes grain growth, it is of course not a necessary precursor [10].

Grain growth may be divided into two types: normal grain growth and abnormal grain growth. During normal grain growth, the microstructure changes in a rather uniform way; there is a relatively narrow range of grain sizes and shapes, and the form of the grain size distribution is usually independent of time and hence of scale. During abnormal grain growth, a few grains in the microstructure grow and consume the matrix of smaller grains and a bimodal grain size distribution develops. However, eventually these large grains impinge and normal grain growth may then resume [8].

The driving pressure for grain growth is some two orders of magnitude less than that for primary recrystallization. Consequently, grain boundary velocities will be slower than during primary recrystallization [8].

II.6.2 Driving Force for Grain Growth

It is generally adopted that the principal thermodynamic driving force of grain growth is the tendency to diminish the grain-boundary energy and counterbalance the grain-boundary tension of adjoining boundaries, which is realized through shortening of the boundaries as they migrate until an equilibrium configuration of grain boundaries is established. The following facts have been established [10]:

- Boundaries move toward the centers of their curvature.
- Boundaries tend to migrate so as to have the angles at grain joints close to 120°. This occurs through preferable consumption of grains which form sharper corners in triple joints.
- As the grains diminish in size, the rate of their consumption by neighbours grows.

If adjacent grains are not equal in size, the difference in unit energies of grain boundaries will represent the driving force of the process. So, the driving force grows with the difference in grain size. Thus, only at a very small grain size, which is commensurable with the size of primary recrystallization nuclei, the driving force of grain growth is of the same order of magnitude as it is in primary recrystallization. With larger grains, the driving force is one or two orders of magnitude smaller than would be the case for primary recrystallization [10].

II.6.3 Kinetics of Grain Growth

Burke and Turnbull (1952) deduced the kinetics of grain growth on the assumption that the driving pressure on a boundary arises only from the curvature of the boundary. Based on these assumptions, the grain growth kinetics follow a parabolic law of the general form [8]:

$$\bar{R}^n - \bar{R}_0^n = c_1 \times t \qquad \text{[II.8]}$$

- $\bar{R}$: the mean grain size at time t
- $\bar{R}_0$: the initial mean grain size
- c_1: the temperature dependent rate constant, and n is the grain growth exponent.

In the Burke and Turnbull analysis n is theoretically equal to 2. However, experimentally measured values of n are generally higher than 2, with aluminum exhibiting an exponent of approximately 4.

The dependence of the rate of grain boundary migration on temperature follows an Arrhenius-type relationship [10]:

$$G = G_0 \times e^{(-\frac{Q_G}{RT})} \qquad \text{[II.9]}$$

where Q_G is the activation energy for grain growth, which depends strongly on the purity of the metal and in some cases on the temperature interval of annealing. For commercial-purity brass, Q_G = 63 kcal/g-atom in the interval from 500 to 750°C.

II.6.4 Factors Affecting Grain Growth

II.6.4.1 Temperature

Grain growth involves the migration of high angle grain boundaries and the kinetics will therefore be strongly influenced by the temperature dependence of boundary mobility. As the driving force for grain growth is usually very small, significant grain growth is often found only at very high temperatures [8].

II.6.4.2 Solutes and Particles

Impurity atoms in a solid solution decrease the rate of boundary migration during grain growth much more sharply than they do in primary recrystallization. This is explained by the fact that, for the same resisting force, the driving force of grain growth is lower than that of primary recrystallization. An addition of 0.01% Mn to highest-purity aluminum decreases the boundary mobility by a factor of 10^{22}. Minor additions of magnesium sharply diminish the rate of grain growth in aluminum, as also do additions of molybdenum and tantalum in nickel [10].

Disperse particles of excess phases can sharply retard or even stop further grain growth. As the size of grains increases and the difference in grain-boundary tension at grain joints decreases, the effect of disperse particles becomes more and more pronounced, with the result that grain growth ceases [10].

II.6.4.3 Specimen Size

The rate of grain growth diminishes when the grain size becomes greater than the thickness of a sheet specimen. In this situation the grains are curved only in one direction rather than two, and thus the driving pressure is diminished. The grains may also develop grooves by thermal etching, and these will impede grain growth. In aluminum sheets of 99.997% purity of thickness 0.508 mm, in annealing below 600°C, grain growth obeyed the parabolic equation until D remained less than 0.35 mm [10].

II.6.4.4 Texture

A strongly textured material inevitably contains many low angle boundaries, and there is therefore a reduced driving force for grain growth [8].

II.6.5 Secondary Recrystallization (Abnormal Grain Growth)

Secondary recrystallization takes place when a material, in which primary recrystallization has occurred, is heated to higher temperatures, but differs from normal grain growth in that the grains grow not uniformly, but exaggeratedly a portion of grains which have preferable conditions for growth increase in their size at the expense of the main portion of grains whose growth is impeded for some reason or other [10].

The process is similar to primary recrystallization in that the growth of secondary nuclei also begins after a definite incubation period and that the size of the growing grains before collisions begin is linearly dependent on the time of heating. A feature typical of secondary recrystallization is a peculiar pattern of grain size distribution, characterized by two groups of grains of sharply different dimensions. The size of the growing grains and the area occupied by them increase continuously, whereas the size of the other grains remains unchanged and the area occupied by them diminishes owing to their consumption by the growing ones [10].

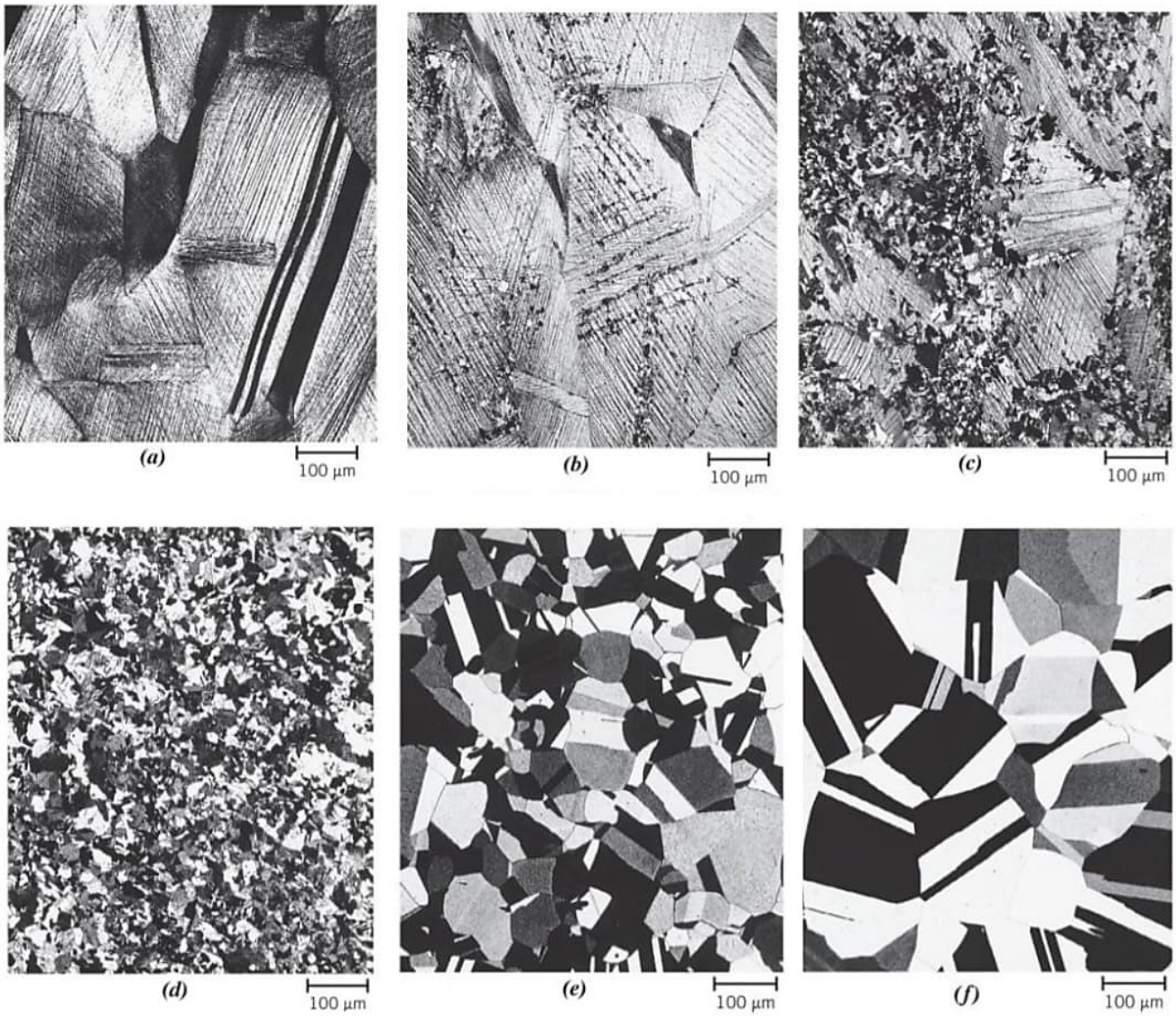


Figure II.17: Photomicrographs showing several stages of the recrystallization and grain growth of brass. (a) Cold-worked (33% CW) grain structure. (b) Initial stage of recrystallization after heating for 3 s at 580°C (1075°F); the very small grains are those that have recrystallized. (c) Partial replacement of cold-worked grains by recrystallized ones (4 s at 580°C). (d) Complete recrystallization (8 s at 580°C). (e) Grain growth after 15 min at 580°C. (f) Grain growth after 10 min at 700°C (1290°F) [9].

II.7 Conclusion

The objective of this chapter was to present the theoretical framework governing heat treatment of cold-drawn aluminum wires, focusing on annealing phenomena of recovery, recrystallization, and grain growth.

It has been established that the microstructural modifications induced by cold wire drawing primarily the accumulation of dislocations, work hardening, and the development of a deformation texture can be progressively eliminated through controlled annealing. Recovery, occurring at low temperatures, restores physical properties, particularly electrical

resistivity, by rearranging and annihilating dislocations and forming low-angle sub-grain boundaries through polygonization.

Recrystallization, occurring at higher temperatures, transforms the deformed microstructure through new strain-free grain nucleation and growth. The driving force is the stored energy of deformation. Conditions governing recrystallization, including minimum deformation, annealing temperature and time, metal purity, original grain size, and deformation temperature, have been discussed in detail, along with recrystallization laws and nucleation mechanisms: strain-induced boundary migration and sub-grain coalescence.

Grain growth follows recrystallization, leading to further grain coarsening driven by grain boundary energy reduction. Solute atoms, disperse particles, and specimen geometry all retard grain boundary migration and limit final grain size.

Analysis of these stages' effects on mechanical and physical properties confirms that annealing restores ductility and electrical conductivity while reducing hardness, tensile strength, and yield strength to pre-cold-worked values. These findings provide the theoretical basis for the experimental investigation of cold-drawn aluminum wire annealing behaviour in the following chapters.

References

[1] M. Zaoui, Influence des traitements thermiques sur la rupture fragile des constructions soudées cas des soudures épaisses, Doctoral Dissertation, University Mentouri, Constantine, (2009).

[2] A. Ourabi, Étude de l'influence de traitement de recuit sur le comportement au tréfilage et l'évolution des propriétés des fils en acier mi-dur, Doctoral Dissertation, University of Mohamed Khider, Biskra, (2024).

[3] G.T. Digges, S.J. Rosenberg and G.W. Geil, Heat Treatment and Properties of Iron and Steel, National Bureau of Standards Monograph 88, pp. 10, (1966).

[4] B. Verlinden, J. Driver, I. Samajdar and R.D. Doherty, Thermo-Mechanical Processing of Metallic Materials, Pergamon (Elsevier), Oxford, (2007).

[5] R.E. Smallman, Modern Physical Metallurgy, 4th ed., Butterworth Heinemann, Oxford, pp. 362–372, (1985).

[6] G. Benchabane, Les mécanismes de recristallisation et de croissance des grains dans les métaux et alliages métalliques légers, Doctoral Dissertation, University of Mohamed Khider, Biskra, (2009).

[7] G.E. Totten and D.S. MacKenzie (Eds.), Handbook of Aluminum, Vol. 1: Physical Metallurgy and Processes, Marcel Dekker Inc., New York, (2003).

[8] F.J. Humphreys and M. Hatherly, Recrystallization and Related Annealing Phenomena, 1st ed., Pergamon, Oxford, pp. 136–186, (1995).

[9] W.D. Callister and D.G. Rethwisch, Materials Science and Engineering: An Introduction, 10th ed., Wiley, (2018).

[10] S.S. Gorelik, Recrystallization in Metals and Alloys, Mir Publishers, Moscow, (1981).

[11] F.C. Campbell, Elements of Metallurgy and Engineering Alloys, ASM International, (2008).

[12] Y. Helal, Etude du mouvement des joints de grains lors de la réaction de recristallisation dans les alliages légers, Master's Thesis, University of Mohamed Khider, Biskra, (2006).

[13] R. Zhao et al., "Effect of Dislocation Characteristics on Electrical Conductivity and Mechanical Properties of AA 6201 Wires", Journal of Alloys and Compounds, ScienceDirect, (2021).

[14] E. Chen, "What is Annealing: All You Should Know", Dekmake, 30 Dec. 2024. www.dekmake.com/de/what-is-annealing/. Accessed 29 Apr. 2026.

[15] J. Sarkar, Sputtering Materials for VLSI and Thin Film Devices, Elsevier, Oxford, (2014).

[16] J.E.M. Flatøy, Process and Alloy Development of Recyclable Aluminium Alloys: Recovery and Recrystallization Behavior of a Selection of AlMn-model Alloys, Master's Thesis, Norwegian University of Science and Technology, (2011).

[17] M. Muramatsu, Y. Aoyagi, Y. Tadano and K. Shizawa, "Phase-Field Simulation of Static Recrystallization Considering Nucleation from Subgrains and Nucleus Growth with Incubation Period", Computational Materials Science, Elsevier, (2014). https://doi.org/10.1016/j.commatsci.2014.02.003. Accessed 29 Apr. 2026.

[18] P. Zhou, J. Tong, W. He, H. Chen, W. Xie, H. Wang and B. Yang, "Static Recrystallization Behavior and Strengthening Mechanism of a Single-Phase Cu–18Ni–17Zn Alloy", Materials Science and Engineering: A, Vol. 909, (2024).

[19] K. Huang (Ed.), Recrystallization: Types, Techniques and Applications, Nova Science Publishers (Materials Science and Technologies), New York, (2020).

Chapter III: Materials & Experimental Methods

III.1 Introduction

This chapter describes the material used in this study and the experimental procedures applied to investigate the recovery and recrystallisation behaviour of cold-drawn commercially pure aluminum wires. The material was supplied by the national cable manufacturing enterprise EN.I.CA.B, located in Biskra, Algeria (figures III.1). The wires were received in the cold-drawn state, with an initial machine wire diameter of 9.5 mm, and were subsequently cold-drawn to three final diameters: 5.92 mm, 4.24 mm, and 3.33 mm, corresponding to area reduction ratios of 61.17%, 80.08%, and 87.72%, respectively. To examine the influence of heat treatment on microstructural evolution and mechanical properties, two annealing conditions were applied: a recovery treatment at 160°C for 90 minutes, and a recrystallisation treatment at 290°C for 60 minutes. The characterization techniques employed include optical microscopy, Vickers hardness testing, and tensile testing, all carried out at the University of Tebessa.



Figure III. 1: General view of the wire drawing workshop at EN.I.CA.B, Biskra.

III.2 Material Selection

The material investigated in this study is commercially pure aluminum wire, supplied by the national cable manufacturing enterprise EN.I.CA.B (Entreprise Nationale des Industries du Câble), located in Biskra, Algeria. The wire is received in the form of a machine wire coil with an initial diameter of 9.5 ± 0.5 mm, produced by a cold drawing process through a series of dies, which progressively reduces the cross-section and introduces significant plastic deformation through work hardening.

The chemical composition of the aluminum wire, as provided by the manufacturer, is given in Table III.1, and its main physical properties are summarized in Table III.2.

Table III.1: Chemical composition of the aluminum wire (wt.%).

Al	Cu	Fe	Si	Zn	Cr+Mn+Ti+V	Others
99.5	0.01	0.2	0.08	0.05	0.01	0.02

Table III.2: Physical properties of the aluminum machine wire.

Machine Wire Diameter (mm)	R_m (MPa)	A (%)	Electrical Conductivity ($m^{-1} \cdot mm$) at 20°C
9.5±0.5	70-90	18	35.7

The section reduction ratio ε (%) for each wire diameter was calculated using the following equation:

$$\varepsilon = \frac{S_0 - S}{S_0} \times (100) \qquad \text{[III.1]}$$

- *ε (%):* reduction ratio
- S_0 *(mm²):* initial cross-sectional area of the wire machine (d_0= 9.5 mm)
- *S (mm²):* Final cross-sectional area after drawing the wire

The calculated reduction ratios are presented in Table III.3.

Table III.3: Reduction ratios for the studied aluminum wires.

Wire Diameter (mm)	ε (%)
3.33	87.72
4.24	80.08
5.92	61.17

III.3 Sample Preparation

The aluminum wires were received in the cold-drawn state directly from EN.I.CA.B, as shown in figure III.2. For each wire diameter (5.92 mm, 4.24 mm, and 3.33 mm), as well as

for the as-received machine wire (9.5 mm), specimens were cut to the dimensions required by each characterization technique.

For tensile testing, specimens were cut to a total length of 200 mm. For hardness testing and metallographic observation, specimens were cut into small cylinders of approximately 1 cm in height, in both longitudinal and transverse orientations.

For each wire diameter, three conditions were prepared and tested:

- **As-drawn,** no heat treatment applied
- **Recovery,** annealed at 160°C for 90 minutes
- **Recrystallisation,** annealed at 290°C for 60 minutes

It should be noted that for the as-received machine wire (9.5 mm), only hardness testing and optical microscopy were performed, serving as a reference state prior to cold drawing.



Figure III.2: Cold drawing machine at EN.I.CA.B, Biskra.

III.4 Annealing Treatment

To investigate the thermal softening behaviour of cold-drawn aluminum wires, heat treatments were carried out in a Nabertherm programmable electric resistance furnace (figure III.3), available at the Materials Science Laboratory of the University of Tebessa. The furnace temperature was controlled with an accuracy of ±5°C, and it was preheated to the target temperature before placing the specimens inside. After annealing, all samples were air-cooled to room temperature.

Two annealing temperatures were selected, corresponding to distinct metallurgical regimes:

- 160°C for 90 minutes: This low-temperature treatment is expected to promote recovery mechanisms.
- 290°C for 60 minutes: This higher temperature is sufficient to initiate recrystallisation.



Figure III.3: Nabertherm programmable electric resistance furnace used for heat treatment (Heat Treatment Laboratory, University of Tebessa).

The selection of these temperatures was guided by published data on the annealing behaviour of commercially pure aluminum, for which recrystallisation typically occurs between 250°C and 350°C depending on the degree of prior cold deformation. The holding times were chosen to allow sufficient thermal activation for each metallurgical process without inducing excessive grain growth. The annealing conditions applied to each wire diameter are summarized in Table III.4.

Table III.4: Heat treatment conditions applied to the studied wire specimens.

Wire diameter (mm)	Annealing temperature (°C) (1)	Holding time (min) (1)	Annealing temperature (°C) (2)	Holding time (min) (2)
3.33	160	90	290	60
4.24	160	90	290	60
5.92	160	90	290	60

III.5 Metallographic Preparation

Metallographic preparation was carried out on the cut specimens in order to obtain flat, scratch-free, and chemically reactive surfaces suitable for optical microscopic observation.

The preparation procedure followed the standard sequence of grinding, polishing, and chemical etching.

III.5.1 Grinding

The mounted specimens were ground on a mechanical polishing machine using a series of silicon carbide abrasive papers of progressively increasing fineness, ranging from 80 to 4000 grit. At each grinding stage, the specimens were rotated by 90° to eliminate scratches from the previous stage. After each step, the specimens were rinsed with distilled water and dried.



Figure III.4: Buehler Metaserv Grinder-Polisher used for mechanical grinding and polishing (Heat treatment Laboratory, University of Tebessa).

III.5.2 Polishing

Final polishing was performed using a 6 µm diamond paste applied on a soft polishing cloth, until a mirror-like surface finish was achieved. The specimens were cleaned with distilled water and dried after each polishing step.



Figure III.5: (a) grinding papers. (b) diamond polishing compound (6 µm), (Heat Treatment Laboratory, University of Tebessa).

III.5.3 Chemical Etching

Chemical etching was necessary to reveal the grain boundaries and microstructural features of the aluminum specimens under the optical microscope. One etching solution was used in this study:

- Solution: Poulton's reagent:

$$24 \text{ ml } HCl + 12 \text{ ml } HNO_3 + 2 \text{ ml } HF + 2 \text{ ml } H_2O$$

Applied for approximately 10 seconds. This reagent produced the most clearly defined grain boundaries and was therefore selected for all subsequent metallographic observations.

The specimens were immersed in Poulton's reagent for approximately 10 seconds, then immediately rinsed with distilled water and dried.



Figure III.6: Reagents used for chemical etching: distilled water, nitric acid (HNO_3 65%), hydrochloric acid (HCl 37%), and hydrofluoric acid (HF 40%) (Heat treatment Laboratory, University of Tebessa).

III.6 Characterization Techniques

III.6.1 Mechanical Testing

III.6.1.1 Tensile Testing

Tensile tests were carried out at room temperature using a universal tensile testing machine available at the Materials Science Laboratory of the University of Tebessa (figure III.8). The tests were performed at a constant crosshead displacement rate of 2 mm/min. For each wire diameter, specimens were tested in the as-drawn condition and after each heat treatment (recovery and recrystallisation).

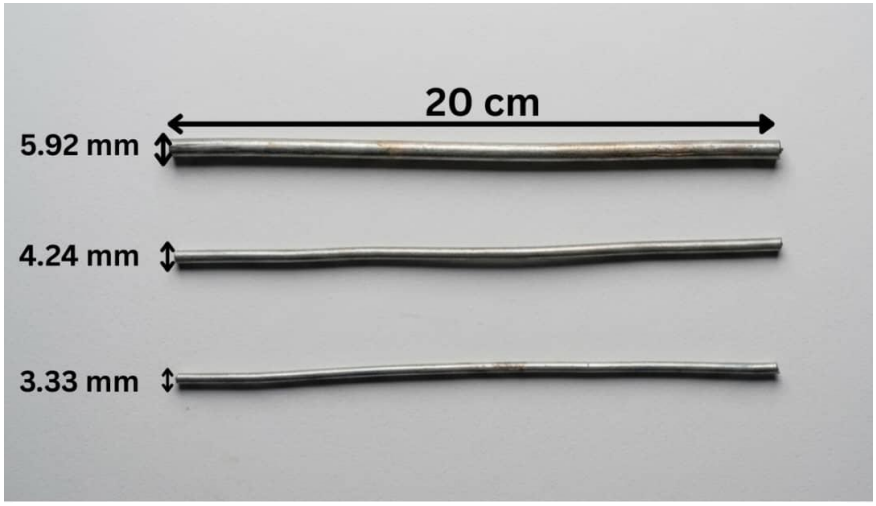


Figure III.7: Tensile test specimens of cold-drawn aluminum wires with diameters of 5.92 mm, 4.24 mm, and 3.33 mm (total length: 200 mm).

The specimens were prepared with a total length of 200 mm, as described in Section III.3. For each tested specimen, the machine automatically generated a stress-strain curve, from which the following mechanical parameters were extracted:

- Ultimate tensile strength (Rm, MPa)
- Upper yield and Lower strength (ReL, ReH, MPa)
- Elongation at fracture (A, %)

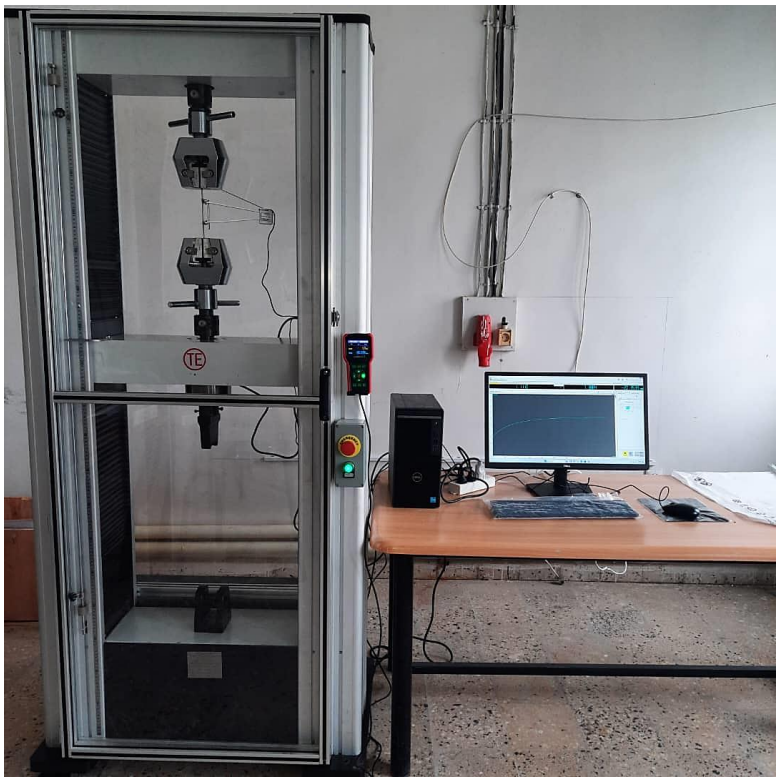


Figure III.8: Universal tensile testing machine (Materials Science Laboratory, University of Tebessa).

III.6.1.2 Microhardness Analysis

Vickers microhardness measurements were performed using a Vickers hardness testing machine available at the Materials Science Laboratory of the University of Tebessa (figure III.9). The hardness was measured on longitudinally polished surfaces of the mounted specimens.

A load of 500 gf was applied for a dwell time of 13 seconds (HV0.5/13). For each specimen, a minimum of three indentations were made, and the average value was recorded. The Vickers hardness number (HV) was calculated using the following equation:

$$HV = \frac{1.8544 \times F}{d^2} \qquad \text{[III.2]}$$

F is the applied load (gf) and d is the arithmetic mean of the two diagonal lengths of the indentation (µm).

Hardness measurements were carried out on all wire diameters, including the as-received machine wire (9.5 mm), in all three conditions: as-drawn, recovery-annealed, and recrystallisation-annealed. This allowed a systematic follow-up of the evolution of mechanical properties throughout the cold drawing and annealing sequence.



Figure III.9: KB 250 universal hardness testing machine (Materials Science Laboratory, University of Tebessa).

III.6.2 Optical Microscopy

Microstructural observations were carried out using an optical microscope available at the Heat treatment Laboratory of the University of Tebessa (figure III.10). The microscope is equipped with multiple objective lenses, allowing observations at various magnifications. Images were captured using a digital camera mounted on the microscope, enabling the documentation of microstructural features at each stage of the study.

This technique was applied to all wire diameters in their three conditions: as-drawn, recovery annealed, and recrystallisation annealed, as well as to the as received machine wire (9.5 mm) as a reference state. The observations focused on the evolution of grain morphology, the degree of deformation, and the progress of recovery and recrystallisation as a function of wire diameter and annealing condition.

All specimens were examined on longitudinally polished and chemically etched surfaces, prepared according to the procedure described in Section III.5.



Figure III. 10: Optical microscope (Heat treatment Laboratory, University of Tebessa).

Chapter IV: Results & Discussion

IV.1 Introduction

This chapter presents and discusses the experimental results obtained from the mechanical testing and microstructural characterization of commercially pure aluminum wires in different conditions: as-drawn, recovery-annealed at 160℃ for 90 minutes, and recrystallisation-annealed at 290 ℃ for 60 minutes. Three wire diameters were investigated 5.92 mm, 4.24 mm, and 3.33 mm corresponding to area reduction ratios of 61.17 %, 80.08%, and 87.72 %, respectively. The as-received machine wire (9.5 mm) was also included as a reference state. The results are organized into two main sections: tensile testing and Vickers hardness measurements, followed by microstructural observations by optical microscopy. The discussion aims to establish a clear correlation between the degree of cold deformation, the applied heat treatment, and the resulting mechanical and microstructural evolution.

IV.2 Mechanical Testing

IV.2.1 Tensile Testing

IV.2.1.1 As-Drawn Condition

The stress-strain curves of the cold-drawn wire diameters in the as-drawn condition are presented in figure IV.1. The results reveal a clear influence of the reduction ratio on the tensile behaviour of commercially pure aluminum wires. The wire of 3.33 mm diameter, which underwent the highest reduction ratio of 87.72%, exhibits the greatest ultimate tensile strength of 356 MPa, with an elongation at fracture of 8.0%. This elevated strength is a direct consequence of the intense work hardening introduced during cold drawing, which generates a high density of dislocations that mutually interact, impede further plastic deformation, and restrict dislocation motion throughout the metallic lattice. The wire of 4.24 mm diameter, corresponding to a reduction ratio of 80.08%, shows an ultimate tensile strength of 340 MPa, with an elongation of 8.5%.

The wire of 5.92 mm diameter, corresponding to a reduction ratio of 61.17%, shows an ultimate tensile strength of 332 MPa, with an elongation of 6.5%. The lower dislocation density compared to the 3.33 mm wire accounts for the slightly reduced strength level. The stress-strain curves further show that as the reduction ratio increases, the plastic region becomes increasingly flat, reflecting the reduced capacity for further strain hardening in heavily deformed wires. This behaviour is consistent with the saturation of dislocation density at high deformation levels, as widely reported for cold-worked face-centred cubic metals. The tensile test results for the as-drawn condition are summarised in Table IV.1.

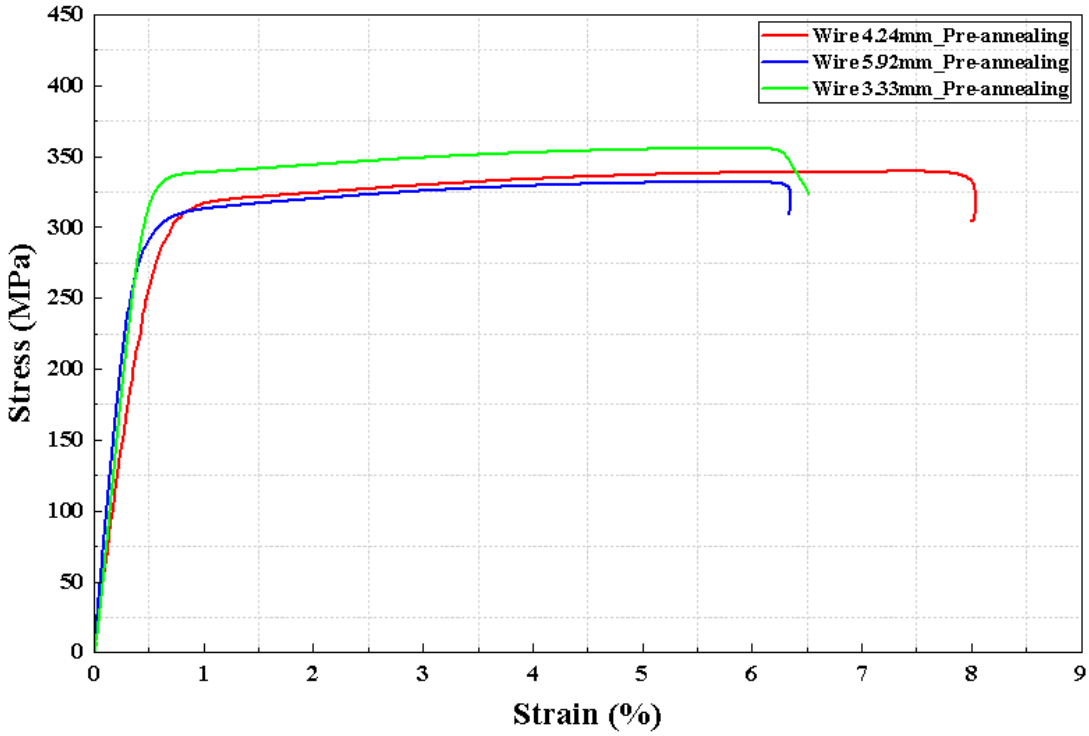


Figure IV. 1: Stress-strain curves of cold-drawn aluminum wires (5.92 mm, 4.24 mm, and 3.33 mm) before heat treatment.

Table IV.1: Tensile properties of cold-drawn aluminum wires in the as-drawn condition.

ε (%)	σ_y (MPa)	σ_{Uts} (MPa)	E (GPa)	A (%)
87.72	333	356	77	8
80.08	306	340	52	8.5
61.17	297	332	79	6.5

IV.2.1.2 Recovery-Annealed Condition

The stress-strain curves of the three wire diameters after recovery annealing at 160°C for 90 minutes are presented in figure IV.2. A significant reduction in tensile strength is observed for all wire diameters compared to the as-drawn condition, while the elongation remains relatively limited.

The 3.33 mm wire, which carries the highest stored deformation energy, exhibits a tensile strength of 248 MPa, with an elongation of 2.5%. The 4.24 mm wire shows a tensile strength of 252 MPa, with an elongation of 2.5%. The 5.92 mm wire exhibits an ultimate tensile strength of 223 MPa, with an elongation of 3.0%.

The reduction in strength observed after recovery annealing is attributed to the rearrangement and partial annihilation of dislocations, which reduces the internal stress state of the material without triggering the formation of new strain-free grains. At this temperature, thermally activated processes allow dislocations to rearrange into lower-energy configurations such as sub-grain boundaries, a phenomenon known as polygonisation.

However, since the grain structure remains essentially unchanged, the elongation values do not recover significantly, confirming that the material is still in a work-hardened state with only partial stress relief. The test results are summarised in Table IV.2.

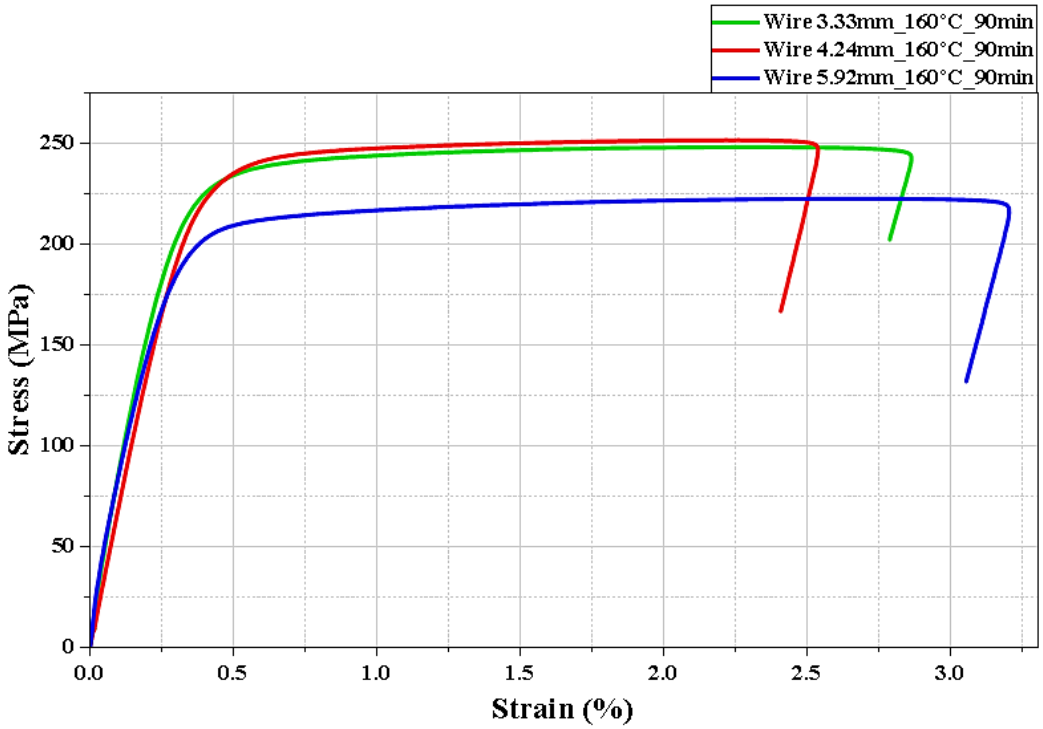


Figure IV. 2: Stress-strain curves of cold-drawn aluminum wires (5.92 mm, 4.24 mm, and 3.33 mm) after recovery annealing at 160°C for 90 minutes.

Table IV. 2: Tensile properties of cold-drawn aluminum wires after recovery annealing (160°C / 90 min).

ε (%)	σ_y (MPa)	σ_{Uts} (MPa)	E (GPa)	A (%)
87.72	235	248	71	2.5
80.08	239	252	66	2.5
61.17	209	223	63	3

IV.2.1.3 Recrystallisation-Annealed Condition

The stress-strain curves after recrystallisation annealing at 290°C for 60 minutes are presented in figure IV.3. A dramatic reduction in tensile strength is observed for all wire

diameters, accompanied by a substantial increase in elongation at fracture, indicating that full or near-complete recrystallisation has taken place.

The 3.33 mm wire, despite carrying the highest prior deformation, exhibits a tensile strength of 128 MPa, with an elongation of 16.5%. The 4.24 mm wire shows a tensile strength of 124 MPa, with an elongation of 22.0%.The 5.92 mm wire exhibits an ultimate tensile strength of only 107 MPa, with a markedly increased elongation of 20.5%.

These results confirm that recrystallisation annealing at 290°C is sufficient to promote the nucleation and growth of new strain-free equiaxed grains, effectively eliminating the dislocation substructure accumulated during cold drawing. The near-complete elimination of work hardening explains the dramatic drop in strength values to levels approaching those of the annealed machine wire. The higher elongation values recorded for the 5.92 mm and 4.24 mm wires compared to the 3.33 mm wire may be related to differences in the recrystallized grain size, where lower prior deformation tends to produce coarser recrystallized grains with greater capacity for uniform plastic deformation. The observation that the 3.33 mm wire retains a slightly higher strength after recrystallisation may suggest that the recrystallisation process is more complete in the more heavily deformed wires due to the greater availability of nucleation sites, resulting in a finer recrystallized grain structure with slightly higher strength but reduced elongation.

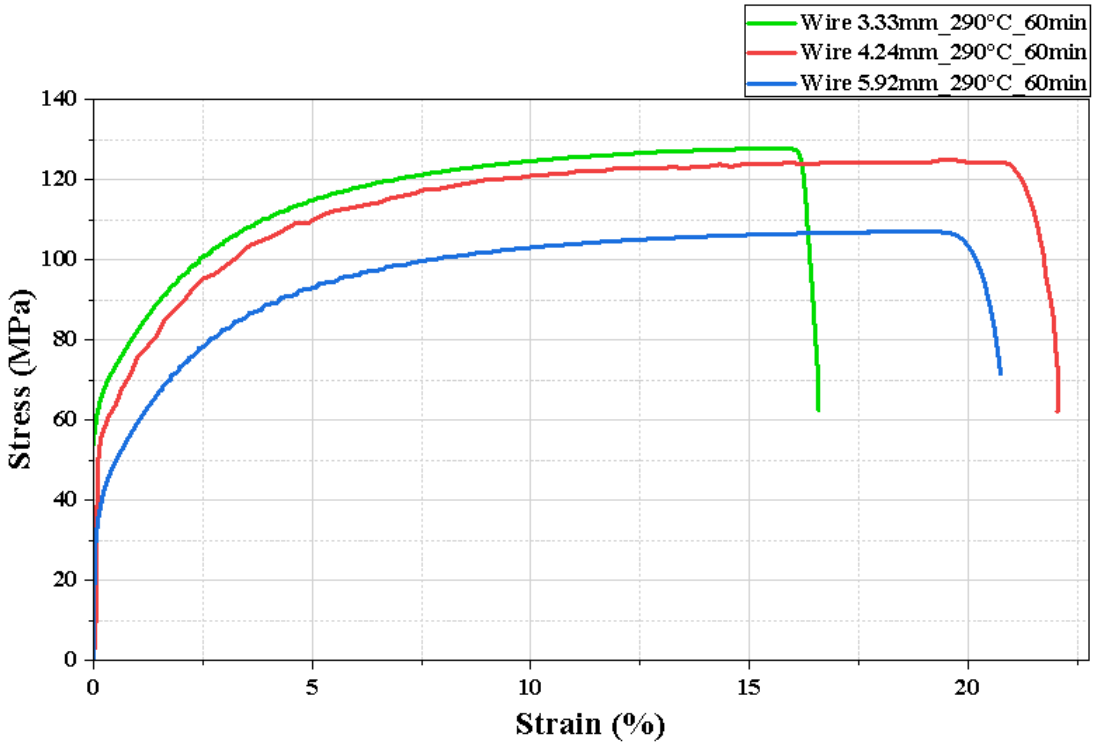


Figure IV. 3: Stress-strain curves of cold-drawn aluminum wires (5.92 mm, 4.24 mm, and 3.33 mm) after recrystallisation annealing at 290°C for 60 minutes.

Table IV.3: Tensile properties of cold-drawn aluminum wires after recrystallisation annealing (290°C / 60 min).

ε (%)	σ_y (MPa)	σ_{Uts} (MPa)	E (GPa)	A (%)
87.72	72	128	8	16.5
80.08	68	124	11	22
61.17	65	107	2	20.5

IV.2.1.4 Comparative Analysis

The comparative evolution of ultimate tensile strength and elongation at fracture as a function of area reduction ratio for all annealing conditions are presented in figures IV.4 and IV.5 respectively.

The Rm vs reduction ratio plot clearly shows three well-separated curves, confirming that each thermal condition produces a distinctly different strength level across all wire diameters. The as-drawn curve maintains the highest strength values, ranging from 332 MPa to 356 MPa, while the recovery-annealed curve occupies an intermediate position between 223 and 252 MPa, and the recrystallisation-annealed curve remains consistently low between 107 and 128 MPa.

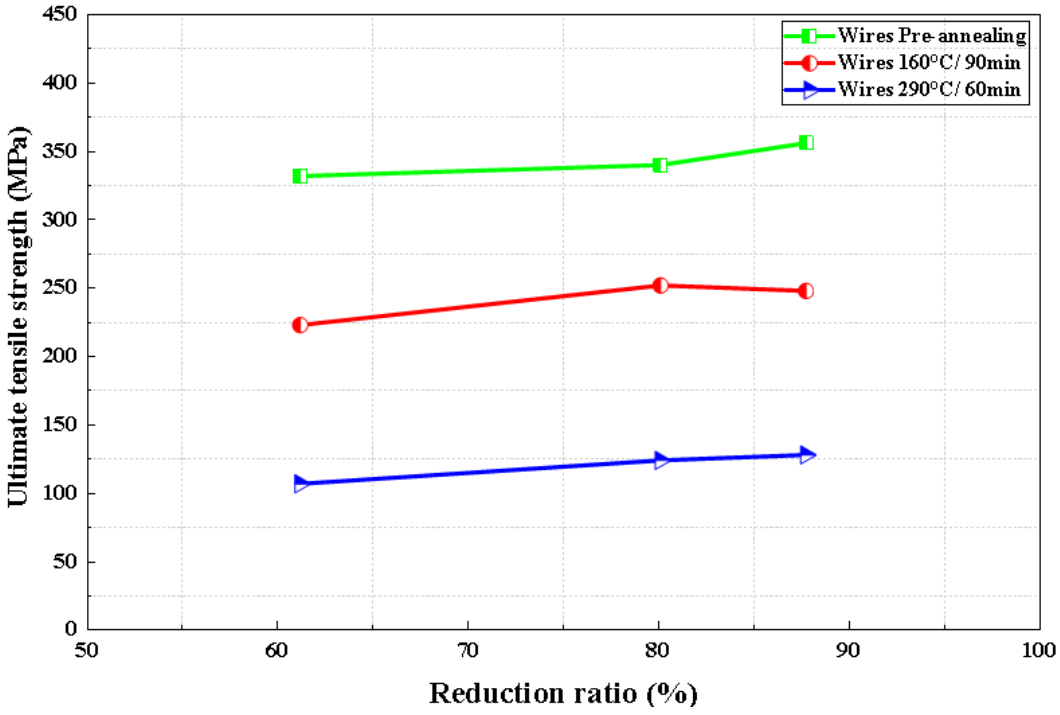


Figure IV. 4: Evolution of ultimate tensile strength as a function of area reduction ratio for all annealing conditions.

Overall, the results demonstrate the dramatic impact of heat treatment on the mechanical behaviour of cold-drawn aluminum wires. The ultimate tensile strength dropped from a maximum of 356 MPa in the as-drawn condition to as low as 107 MPa after recrystallisation annealing, representing a reduction of approximately 70%. Conversely, the elongation at fracture evolved from a maximum of 22.0% after recrystallisation annealing to as low as 2.5% after recovery annealing, highlighting the inverse relationship between strength and ductility governed by the annealing condition applied.

IV.2.2 Hardness Testing

IV.2.2.1 Hardness As-Drawn Wires Condition

All the Vickers hardness measurements tests were performed under an applied load of 500 g and dwell time of 13 s. The evolution of Vickers hardness as a function of the area reduction ratio in the as-drawn condition is presented in figure IV.6. The results demonstrate a pronounced and monotonic increase in hardness with increasing reduction ratio, which is in full agreement with the classical theory of work hardening in face-centred cubic metals.

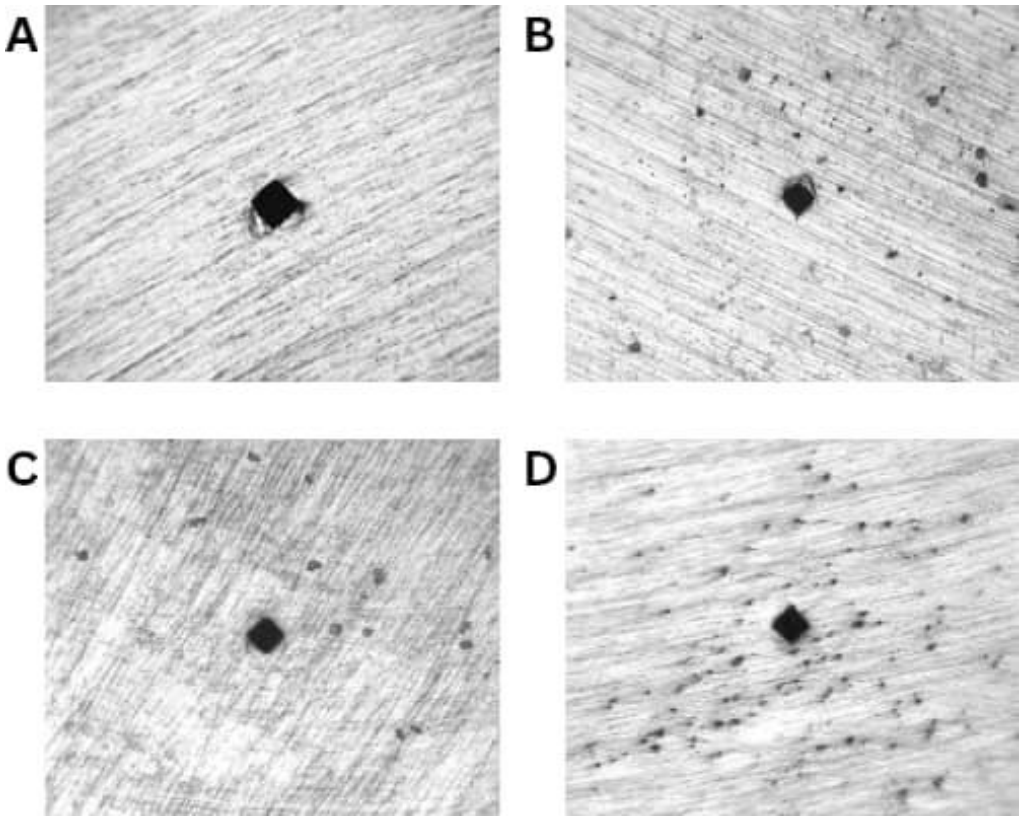


Figure IV. 5: Vickers hardness indentations on cold-drawn aluminum wire surfaces in the as-drawn condition: (A) 9.5 mm machine wire, (B) 5.92 mm, (C) 4.24 mm, (D) 3.33 mm.

The as-received machine wire (9.5 mm, ε = 0%) exhibits a hardness of only 25.5 HV, reflecting the softened, strain-free state of the material prior to cold drawing. Upon cold drawing to 5.92 mm (ε = 61.17%), the hardness rises sharply to 94.5 HV, representing an

increase of approximately 270% relative to the machine wire. Further drawing to 4.24 mm (ε = 80.08%) and 3.33 mm (ε = 87.72%) yields hardness values of 100 HV and 99.7 HV respectively, indicating a progressive saturation of the hardening response at high deformation levels. This saturation behaviour reflects the equilibrium between dislocation multiplication and dynamic recovery processes, which limit the net accumulation of dislocation density beyond a critical deformation level.

Table IV. 4: Vickers hardness of cold-drawn aluminum wires in the as-drawn condition.

ε (%)	**0 (Machine wire)**	**61.17**	**80.08**	**87.72**
HV	25.5	94.5	100	99.7

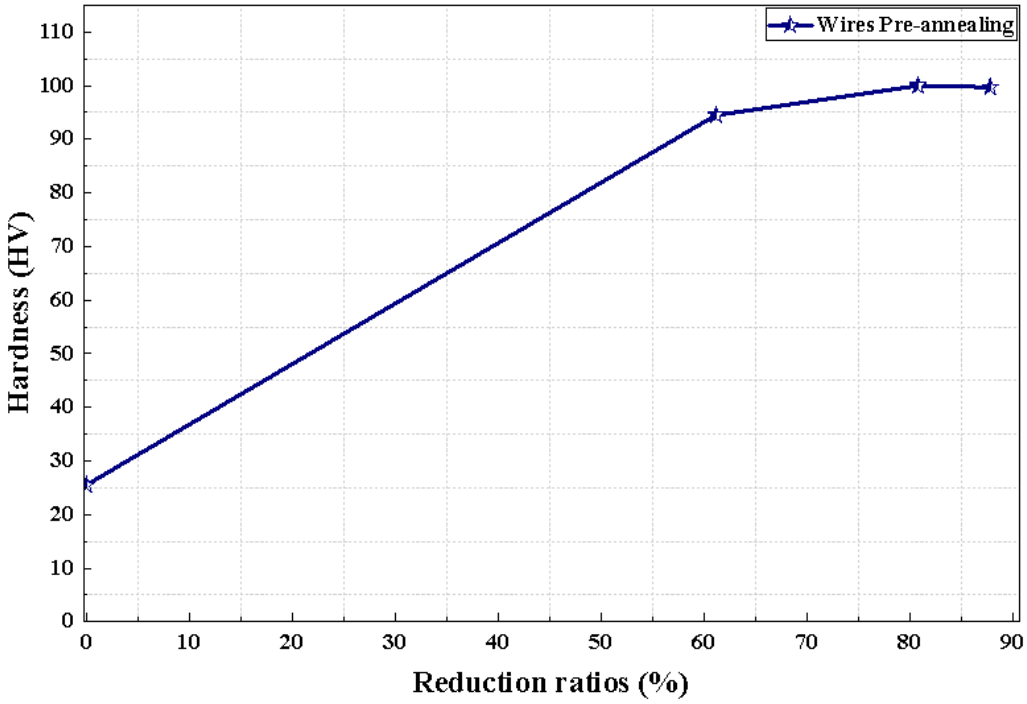


Figure IV. 6: Evolution of Vickers hardness as a function of area reduction ratio for cold-drawn aluminum wires in the as-drawn condition.

IV.2.2.2 Hardness of Recovery-Annealed Wires

After recovery annealing at 160°C for 90 minutes, a moderate reduction in hardness is observed for all wire diameters, as shown in figure IV.8. The 5.92 mm wire shows a hardness of 74.1 HV, the 4.24 mm wire 81.0 HV, and the 3.33 mm wire 77.5 HV, compared to their respective as-drawn values of 94.5, 100.0, and 99.7 HV.

The reduction in hardness at this relatively low annealing temperature is attributed to thermally activated recovery mechanisms, primarily the rearrangement of dislocations into lower-energy configurations such as low-angle sub-grain boundaries through the process of

polygonisation, and the partial annihilation of oppositely signed dislocations. These processes reduce the total dislocation density and the associated long-range internal stress fields, thereby lowering the resistance to plastic deformation.

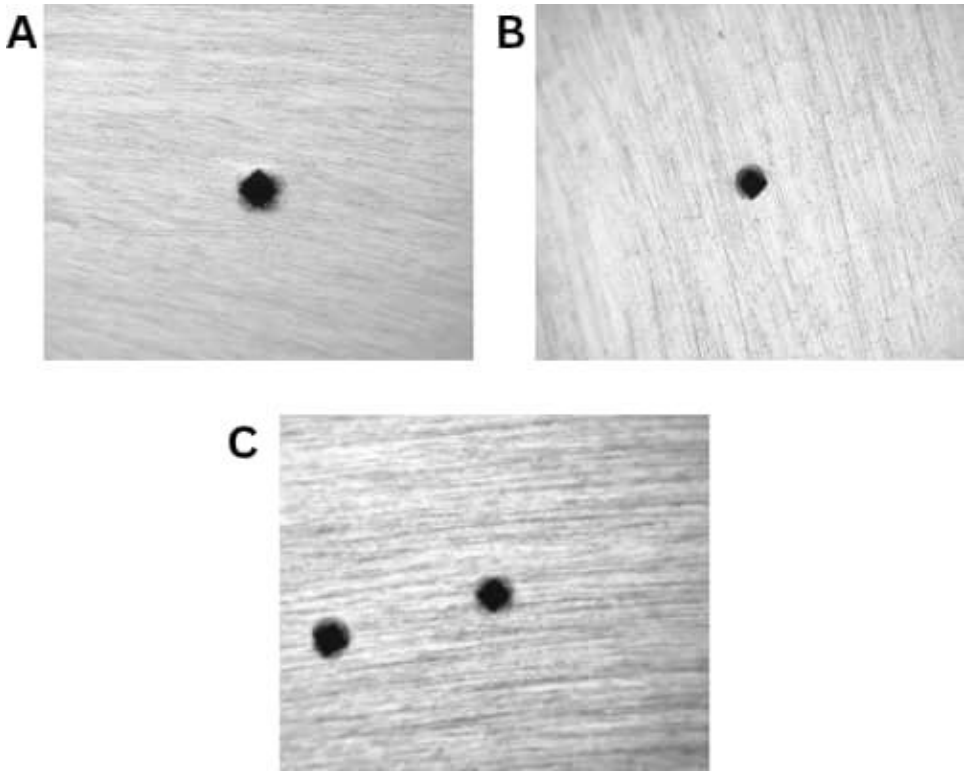


Figure IV. 7: Vickers hardness indentations on cold-drawn aluminum wire surfaces after recovery annealing at 160°C for 90 minutes: (A) 5.92 mm, (B) 4.24 mm, (C) 3.33 mm.

However, since the overall grain morphology remains unchanged and a substantial dislocation substructure is retained, the hardness values remain significantly above those of the fully recrystallised state, confirming that recovery alone is insufficient to restore the original mechanical properties of the material.

Table IV. 5: Vickers hardness of cold-drawn aluminum wires after recovery annealing (160°C / 90 min).

ε (%)	**61.17**	**80.08**	**87.72**
HV	74.1	81	77.5

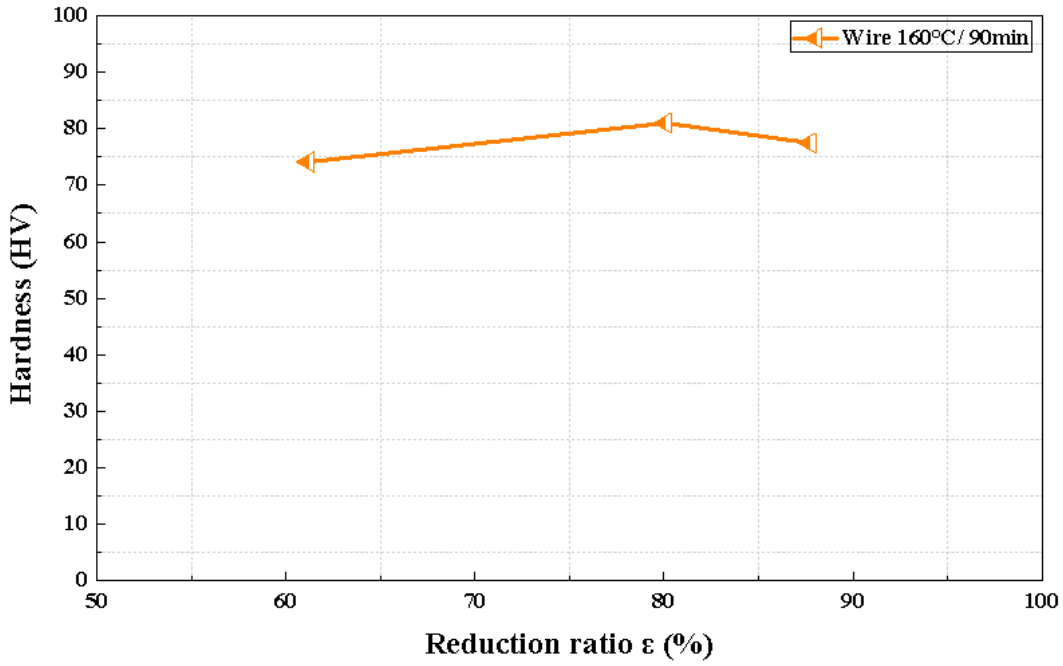


Figure IV. 8: Evolution of Vickers hardness as a function of area reduction ratio after recovery annealing at 160°C for 90 minutes.

IV.2.2.3 Hardness of Recrystallisation-Annealed Wires

The most dramatic reduction in hardness is observed after recrystallisation annealing at 290°C for 60 minutes, as illustrated in figure IV.10. The hardness values drop to 31.1 HV, 33.1 HV, and 35.2 HV for the 5.92 mm, 4.24 mm, and 3.33 mm wires respectively, approaching the hardness of the as-received machine wire (25.5 HV). This near-complete restoration of the original softness confirms that recrystallisation has occurred in all three wire diameters.

The dramatic drop in hardness is directly attributable to the elimination of the work-hardened dislocation substructure through the nucleation and growth of new strain-free equiaxed grains. The driving force for recrystallisation is the stored elastic energy associated with the high dislocation density accumulated during cold drawing. As new grains consume the deformed matrix, the dislocation density falls to near-equilibrium levels, and the hardness approaches that of the annealed state. A slight but consistent increase in hardness with increasing reduction ratio is observed even after recrystallisation: 31.1 HV for $\varepsilon = 61.17\%$, 33.1 HV for $\varepsilon = 80.08\%$, and 35.2 HV for $\varepsilon = 87.72\%$. This trend is consistent with the Hall-Petch relationship, whereby more heavily deformed wires provide a greater number of recrystallisation nucleation sites, resulting in a finer recrystallised grain structure with slightly higher hardness due to increased grain boundary strengthening.

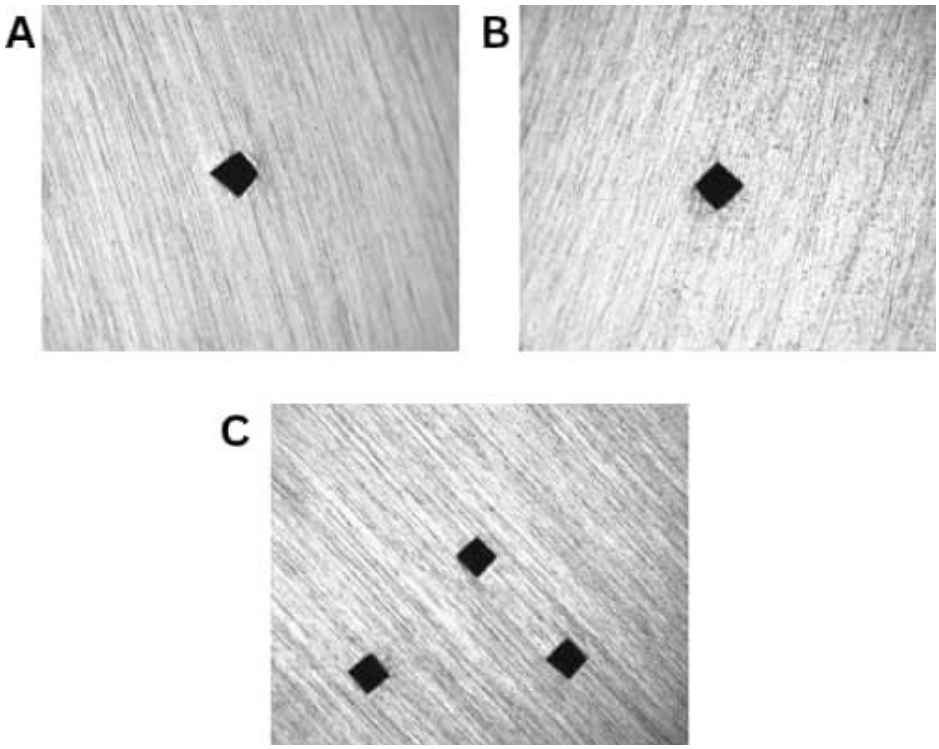


Figure IV. 9: Vickers hardness indentations on cold-drawn aluminum wire surfaces after recrystallisation annealing at 290°C for 60 minutes: (A) 5.92 mm, (B) 4.24 mm, (C) 3.33 mm.

Table IV. 6: Vickers hardness of cold-drawn aluminum wires after recrystallisation annealing (290°C / 60 min).

ε (%)	**61.17**	**80.08**	**87.72**
HV	31.1	33.1	35.2

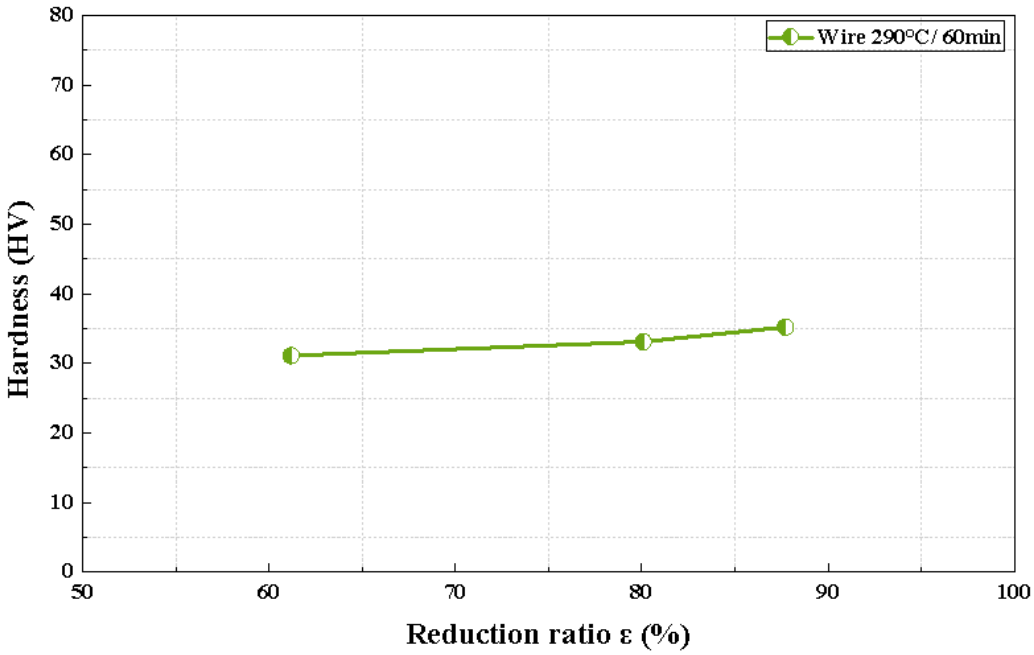


Figure IV. 10: Evolution of Vickers hardness as a function of area reduction ratio after recrystallisation annealing at 290°C for 60 minutes.

IV.2.2.4 Comparative Analysis

The superimposition of the three hardness evolution curves, presented in figure IV.11, provides a clear and comprehensive picture of the influence of heat treatment on the mechanical behaviour of cold-drawn commercially pure aluminum wires. The three curves are well separated across the entire range of reduction ratios investigated, confirming that each thermal condition produces a distinctly different hardness level. The as-drawn curve maintains the highest hardness values with a saturation plateau above 95 HV, the recovery curve occupies an intermediate position between 74 and 81 HV, and the recrystallisation curve remains consistently low between 31 and 35 HV. The progressive downward shift of the hardness level from as-drawn to recovery to recrystallisation reflects the successive elimination of the stored deformation energy and the associated dislocation substructure, demonstrating that thermal annealing is an effective means of controlling the mechanical properties of cold-drawn aluminum wires.

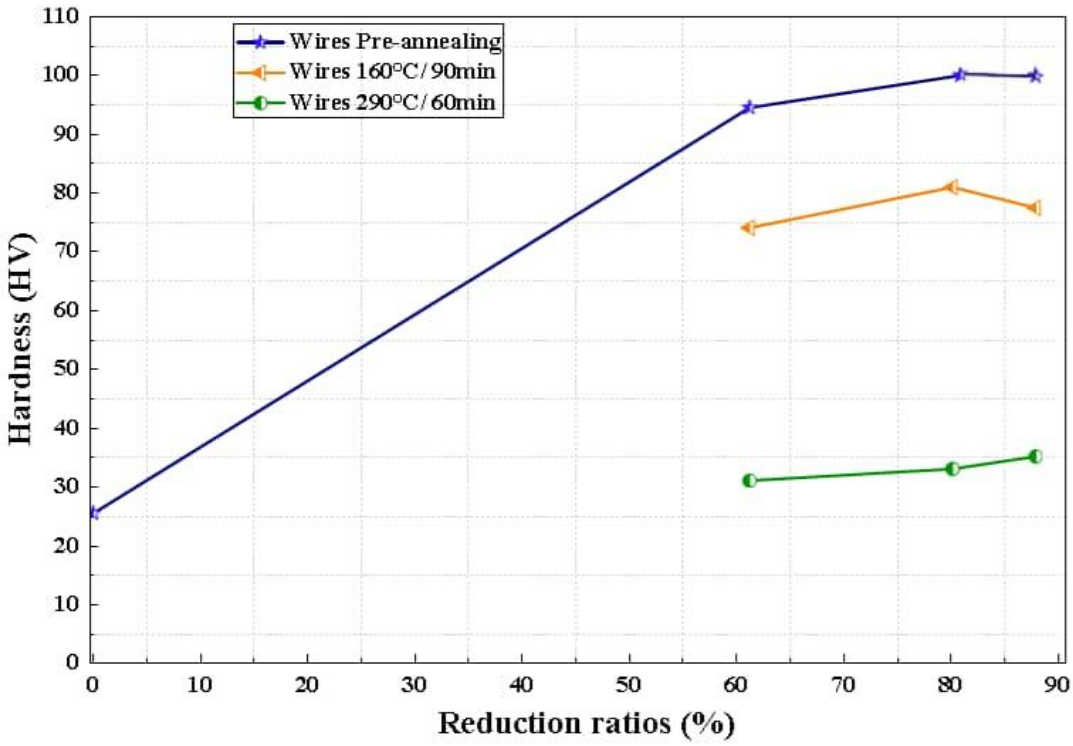


Figure IV. 11: Comparative evolution of Vickers hardness as a function of area reduction ratio for all annealing conditions.

IV.3 Micrographic Analysis

IV.3.1 As-Drawn Condition

The optical micrographs of the transverse sections of cold-drawn aluminium wire specimens in the as-drawn condition are presented in Figure IV.12 (A–D). The initial 9.5 mm machine wire exhibits a coarse and heterogeneous grain structure. As the drawing strain

increases to ε = 61.17%, 80.08%, and 87.72%, the microstructure becomes progressively finer and more homogeneous due to severe plastic deformation. This evolution is attributed to the accumulation of dislocations, grain subdivision, and the formation of deformation-induced subgrain structures. At the highest strain level (ε = 87.72%), the microstructure appears highly refined, indicating an advanced work-hardened state of the material.

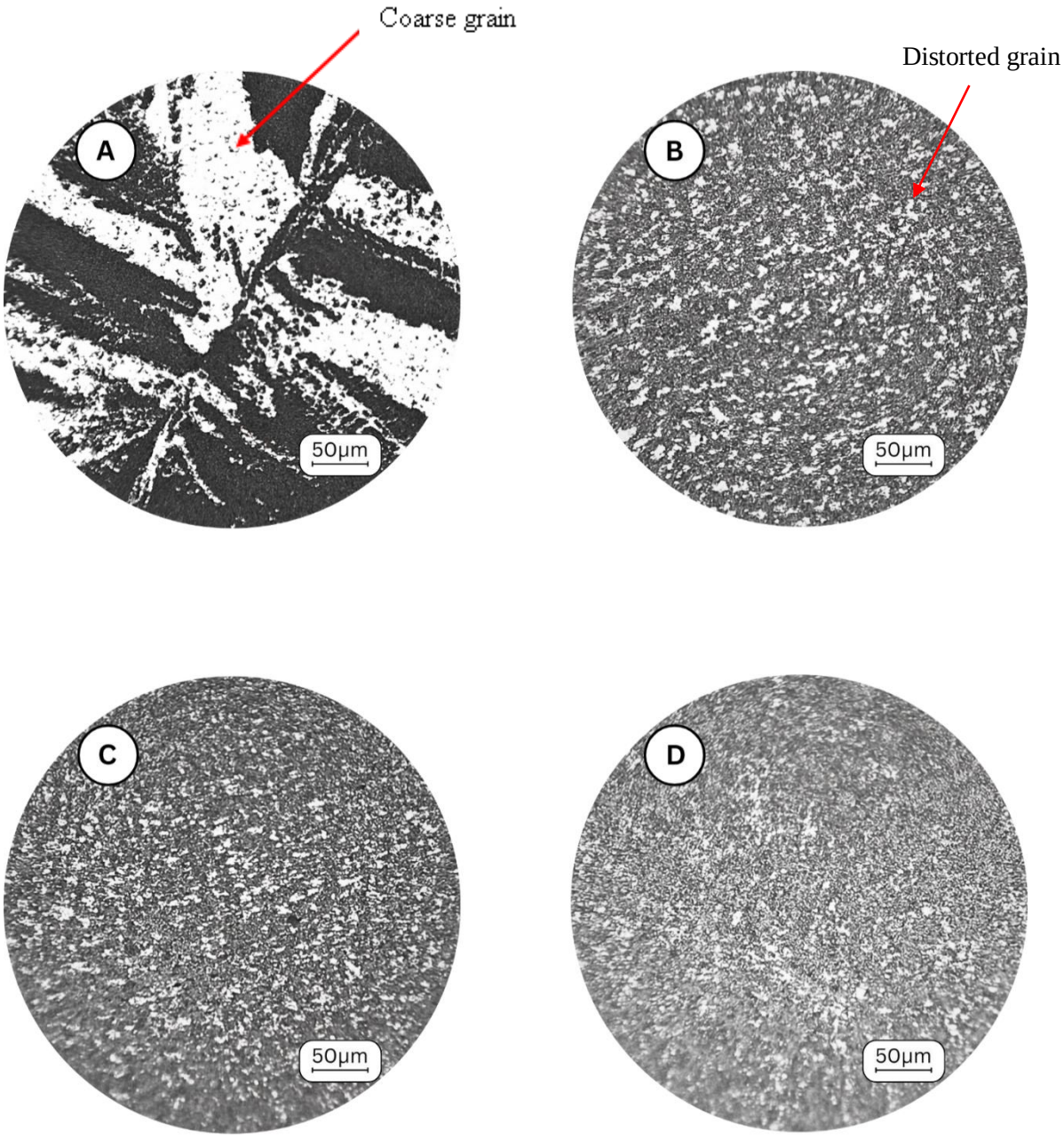


Figure IV. 12: Optical micrographs of cold-drawn aluminum wire specimens in the as-drawn condition: (A) 9.5 mm machine wire, (B) ε = 61.17%, (C) ε = 80.08%, (D) ε = 87.72%.

IV.3.2 Effect of Recovery Annealing

The optical micrographs of the cold-drawn aluminum wire specimens after recovery annealing at 160°C for 90 minutes are presented in Figure IV.13 (E–G). As the prior deformation increases from ε = 61.17% to ε = 87.72%, the microstructure becomes progressively more homogeneous due to the rearrangement and partial annihilation of dislocations. The deformation-induced substructure remains visible, indicating that recovery is the dominant restoration mechanism. Although the specimen with ε = 87.72% exhibits the highest degree of structural uniformity, no clear evidence of complete recrystallisation is observed, suggesting that the annealing treatment primarily relieves internal stresses while preserving much of the work-hardened microstructure.

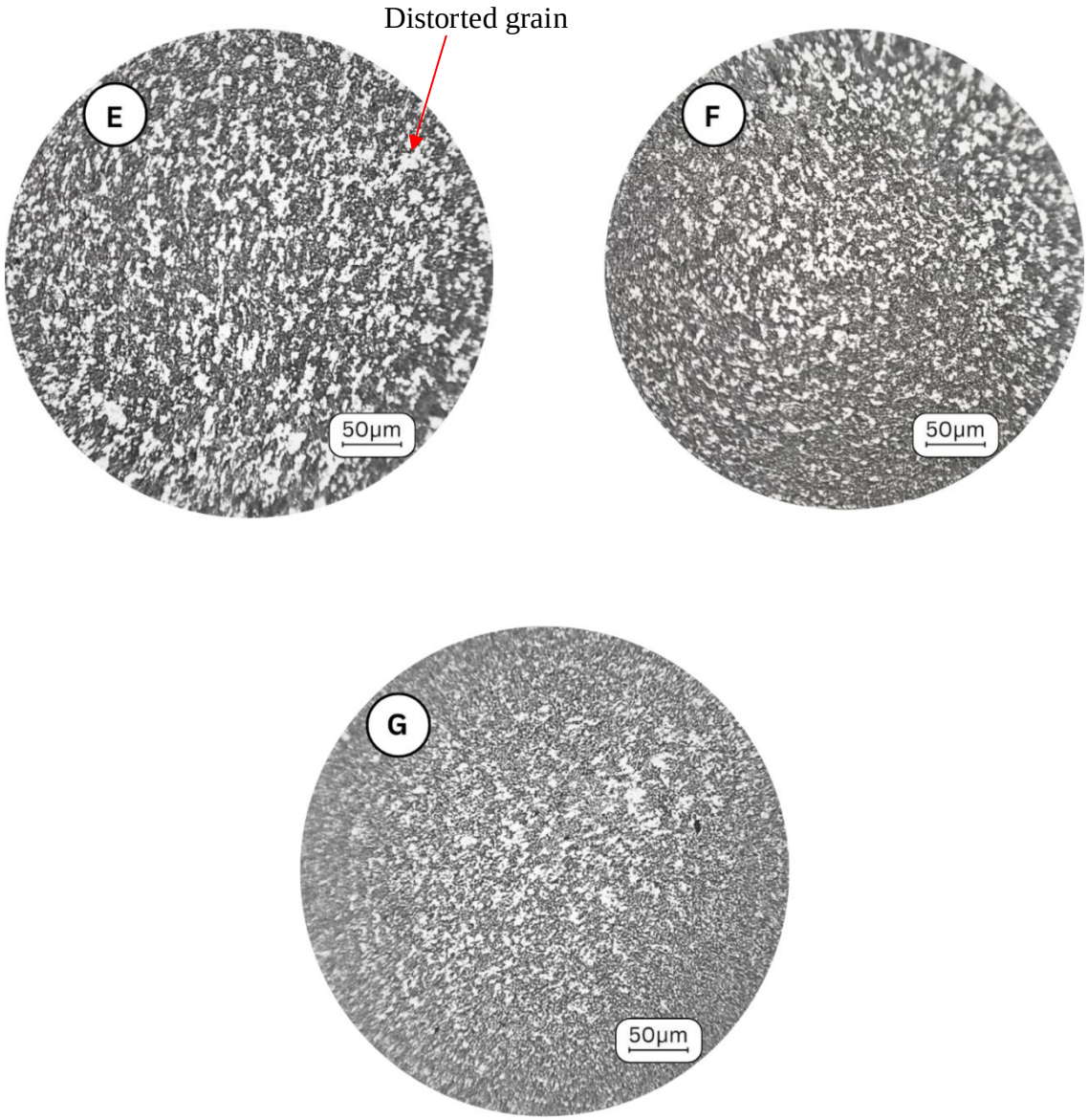


Figure IV. 13: Optical micrographs of cold-drawn aluminum wire specimens after recovery annealing at 160°C for 90 minutes: (E) ε = 61.17%, (F) ε = 80.08% and (G) ε = 87.72%

IV.3.3 Effect of Recrystallisation Annealing

The optical micrographs of the cold-drawn aluminum wire specimens after recrystallisation annealing at 290°C for 60 minutes are presented in Figure IV.14 (H–J). The deformed microstructure presents after drawing and recovery annealing is replaced by a new population of equiaxed, strain-free grains. As the prior drawing strain increases from ε = 61.17% to ε = 87.72%, the recrystallised grain size decreases and the microstructure becomes progressively more homogeneous. This behaviour is attributed to the higher stored deformation energy associated with larger drawing strains, which increases the density of recrystallisation nuclei and promotes the formation of a finer recrystallised grain structure. Specimen J (ε = 87.72%) exhibits the finest and most uniform microstructure, indicating the most effective recrystallisation response.

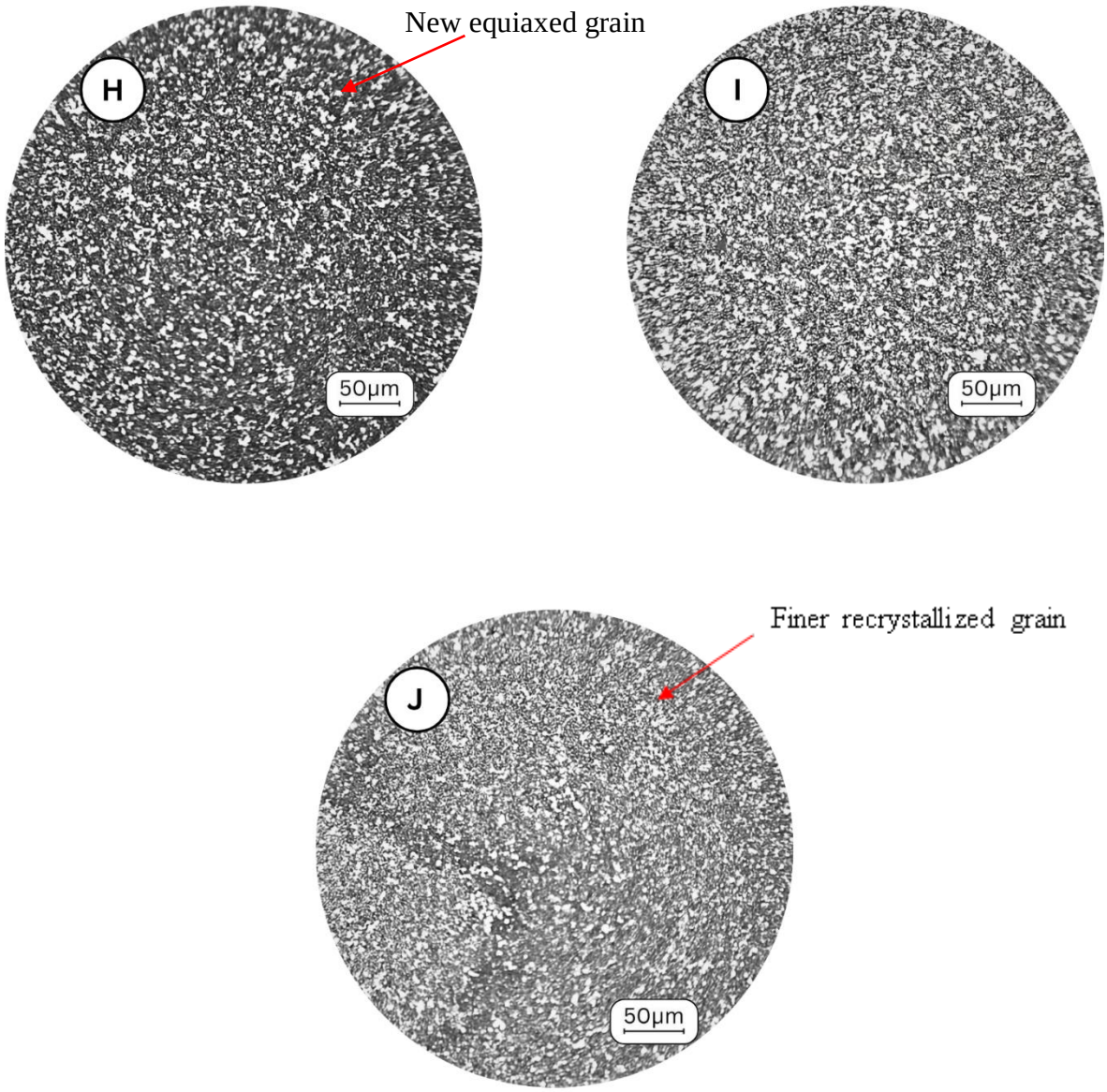


Figure IV. 14: Optical micrographs of cold-drawn aluminum wire specimens after recrystallisation annealing at 290°C for 60 minutes: (H) ε = 61.17%, (I) ε = 80.08% and (J) ε = 87.72%

IV.4 Conclusion

The experimental results presented in this chapter demonstrate a clear and consistent influence of both cold drawing and subsequent heat treatment on the mechanical properties and microstructure of commercially pure aluminum wires.

Cold drawing produced a significant increase in hardness and tensile strength with increasing reduction ratio, reaching approximately 100 HV and 356 MPa, respectively, at $\varepsilon = 87.72\%$, as a direct consequence of dislocation accumulation and work hardening. Optical microscopy confirmed the progressive elongation and refinement of the grain structure with increasing drawing strain.

Recovery annealing at 160°C for 90 minutes resulted in a moderate reduction in strength and hardness through dislocation rearrangement and partial annihilation, without altering the deformed grain morphology or significantly restoring ductility. The work-hardened microstructure was essentially preserved at this temperature.

Recrystallisation annealing at 290°C for 60 minutes caused a dramatic softening, with hardness and tensile strength dropping by approximately 65–70% relative to the as-drawn condition, accompanied by a marked increase in elongation. Optical microscopy confirmed the formation of new equiaxed strain-free grains distributed uniformly across the entire cross-section, with a finer grain size observed in more heavily deformed wires.

Taken together, these results confirm that annealing temperature is the primary parameter controlling the balance between strength and ductility in cold-drawn commercially pure aluminum wires.

General Conclusion

This study investigated the influence of heat treatment on the recovery and recrystallisation behaviour of cold-drawn commercially pure aluminum wires, produced by EN.I.CA.B, Biskra. Three wire diameters were examined: 5.92 mm, 4.24 mm, and 3.33 mm, corresponding to area reduction ratios of 61.17%, 80.08%, and 87.72% respectively, alongside the as-received machine wire (9.5 mm) as a reference state. Two annealing treatments were applied: a recovery annealing at 160°C for 90 minutes, and a recrystallisation annealing at 290°C for 60 minutes. The characterisation was carried out through tensile testing, Vickers hardness measurements, and optical microscopy. The main findings of this work can be summarized as follows:

Effect of cold drawing on mechanical properties and microstructure:

Cold drawing was found to exert a significant and progressive influence on both the mechanical properties and the microstructure of commercially pure aluminum wires. As the area reduction ratio increased from 0% (machine wire) to 87.72%, the Vickers hardness has increased significantly from 25.5 HV to approximately 100 HV, representing an increase of nearly 270 %. This pronounced hardening is a direct consequence of the accumulation of a high dislocation density within the metallic lattice during plastic deformation, which impedes further dislocation motion and restricts plastic flow. The ultimate tensile strength followed a similar trend, increasing from 332 MPa for the wire ($\varepsilon = 61.17\%$) and reaching 356 MPa for the most deformed wire ($\varepsilon = 87.72\%$). The ultimate tensile strength followed a similar trend, reaching 356 MPa for the most heavily deformed wire ($\varepsilon = 87.72\%$), compared to 332 MPa for the 5.92 mm wire ($\varepsilon = 61.17\%$). Optical microscopy confirmed these observations, revealing a progressive elongation and alignment of grains along the drawing direction with increasing reduction ratio, and a near-complete loss of the original equiaxed grain morphology in the most heavily deformed wires.

Effect of recovery annealing (160°C / 90 min):

Recovery annealing at 160°C for 90 minutes produced a moderate but consistent reduction in hardness across all wire diameters, with HV values decreasing from the as-drawn range of 94.5–100 HV to 74.1–81.0 HV. A corresponding reduction in tensile strength was also observed, with Rm values decreasing to 223–252 MPa. However, the elongation at fracture remained low (2.5–3.0%), indicating that the ductility of the material was not significantly restored at this annealing temperature. These results are consistent with the

occurrence of thermally activated recovery mechanisms, primarily the rearrangement and partial annihilation of dislocations, which reduce the internal stresses and lattice microstrains within the material without triggering the nucleation of new strain-free grains. Optical microscopy confirmed that the deformed, elongated grain morphology was fully preserved after recovery annealing, with no evidence of new grain formation across all three wire diameters.

Effect of recrystallisation annealing (290°C / 60 min):

Recrystallisation annealing at 290°C for 60 minutes produced a dramatic transformation in both the mechanical properties and the microstructure of all wire diameters. The Vickers hardness dropped sharply to values in the range of 31.1–35.2 HV, approaching the hardness of the as-received machine wire (25.5 HV), and representing a reduction of approximately 65% relative to the as-drawn condition. The ultimate tensile strength fell to values between 107 and 128 MPa, a reduction of approximately 70% compared to the as-drawn state. In contrast, the elongation at fracture increased markedly to values between 16.5% and 22.0%, confirming the near-complete restoration of ductility. These results provide clear evidence that recrystallisation annealing at 290°C for 60 minutes is sufficient to initiate and complete primary recrystallisation in commercially pure aluminum wires, regardless of the prior deformation level. The driving force for this transformation is the high stored elastic energy associated with the dense dislocation substructure accumulated during cold drawing. Optical microscopy revealed the formation of new, small, equiaxed grains distributed uniformly across the entire cross-section of the specimens, including both the peripheral and core regions, confirming that recrystallisation proceeded homogeneously throughout the full volume of the material.

Influence of reduction ratio on recrystallisation behaviour: A consistent trend was observed across all characterisation techniques: even after full recrystallisation annealing, a slight but systematic increase in hardness and tensile strength with increasing reduction ratio was noted, with HV values of 31.1, 33.1, and 35.2 for ε = 61.17%, 80.08%, and 87.72% respectively, and corresponding maximal strength values of 107, 118, and 128 MPa. This behaviour is attributed to the finer recrystallised grain size produced in more heavily deformed wires.

A lower elongation is also observed for the 3.33 mm wire after recrystallisation annealing (A = 16.5%) compared to the 5.92 mm wire (A = 20.5%) and the 4.24 mm wire (A = 22.0%).

Perspective for future work:

It is proposed to extend this study in several key directions.

- Firstly, it would be important to extend the heat treatment to higher temperatures (exceeding 350°C) and longer durations to investigate the phenomena of grain growth or even secondary recrystallisation, and to understand their impact on the final properties and particularly the thermal stability of the microstructure.
- Secondly, performing electrical conductivity measurements after each heat treatment would be of great importance, given that the primary objective of recrystallisation in this type of product is to enhance electrical conductivity alongside the restoration of ductility.
- Thirdly, this work will focus on the application of X-ray diffraction (XRD) technique to quantify the evolution of density dislocations and lattice distortion (microstrain). Also to gain a deeper understanding of recrystallization mechanism occurring in cold drawn wire.